A Spectroscopic Study of Planetary Nebulae in the Magellanic Clouds

A thesis submitted by

David James Monk

to the

University of London

for the degree of Doctor of Philosophy

University College London

October 1986

ERRATA

On the advice of the examiners.

Page 36, paragraph 3, line 5. 'This additional.... ....image tube chain.'. Replace with new sentence 'This additional reduction in flux at short wavelengths is attributable to the narrower slit used for the medium resolution spectra.'.

Page 61, paragraph 3, line 1. Replace 'for each level' with 'for each transition'.

Page 67, Section 3.3. Add 'Following the work of Peimbert and Torres-Peimbert (1971) the effects of collisional excitations on He I line intensities are ignored.'.

Page 120, paragraph 2, line 6. Replace 'If a particular model predicts a larger value for this ratio than is observed,' with 'The predicted ratio assumes that all photons shortward of 504 Å are absorbed by helium. However, if the He^+/H^+ ratio derived from the observations is equal to 0.1 or larger,'.

Chapter 5 (pp 132-150).

The unreliable nature of the [N II](6548+6585)/5755 Å flux ratio as an electron temperature diagnostic is clearly seen in Fig. 5.4, and is really more suitable, in this case, as an electron density diagnostic. In fact its shorter wavelength range makes it less sensitive to any errors in the reddening correction and therefore a better density diagnostic than the [O II]3727/7325 Å flux ratio. A guide to the electron temperature can be obtained from the [O III](4959+5007)/4363 Å flux ratio, where the upper limit to [O III]4363 Å is used to obtain a T_e upper limit. The derived value of this ratio (>95.3) combined with the [N II] ratio yields an electron temperature of <12100 K and an electron density of $> 5.3 \times 10^4$ cm^{-3}.

The ionic and elemental abundances of LMC N25 have been recalculated for this electron temperature and density, and for an electron temperature of 10000 K with a corresponding density of 1×10^5 cm^{-3}. The new abundances are presented in the table below, which replace Table 5.2. The helium abundance is not listed as the lower T_e values decrease the estimated helium abundance by factors of 3% and 6% only (for 12100 K and 10000 K respectively), and the ionised helium abundances given in Chapter 5 are correct within the errors given.

It should be noted that the elemental abundances of LMC N25 are increased significantly at the lower T_e values, particularly the oxygen abundance ($1 - 4 \times 10^{-4}$), which is within the range found about the mean LMC PN oxygen abundance (3.1×10^{-4}).

LMC N25 is therefore probably a low-excitation, normal abundance nebula and not a low-oxygen nebula, and the above analysis also makes the 'low-oxygen' description of the other LMC and SMC PN in Table 3.9 doubtful. For this reason the electron temperatures for these objects (given in Table 2.1) have been bracketed and their abundances (Tables 3.4,3.5,3.6 and 3.9) have been flagged as uncertain (::). It is also noted that the discussion of the elemental abundances of LMC N25 on page 142 is now irrelevant.

The lower electron temperature for LMC N25 also leads to a lower nebular continuum (decreases of 22% and 43% in the nebular continuum at 4500 Å for T_e equals 12100 K and 10000 K respectively) and therefore a slightly higher stellar continuum (the nebular continuum level at 4500 Å being 32% and 24% of the total continuum for T_e equals 12100 K and 10000 K respectively). The best fit model to this new stellar continuum level is a Mihalas 40000 K, log g 3.5, model, giving a stellar luminosity of 12000 ± 1000 L$\odot$, a core mass of 0.685 ± 0.015 M$\odot$, a stellar radius of 2.3 ± 0.1 R$\odot$, and a predicted log g of 3.5 ± 0.1. This new Zanstra temperature of 40000 ± 5000 K could be consistent with a significant neutral helium abundance if it was at the lower end of its allowed range. The new O^+/O ratio (0.85 - 0.90) does indicate a large neutral helium content (Torres-Peimbert and Peimbert, 1977). Similarly, the upper limit on the [Ne III]3868 Å flux of <2.3 is probably inconsistent with a high temperature central star. It should be noted that in this effective temperature range the derived stellar luminosity depends mainly on the absolute nebular Hβ flux, which for LMC N25 is significantly larger than the average.

The motivation for the discussion in Chapter 5 of the primordial helium abundance was the previous, incorrect, derived low oxygen abundance, the high central star Zanstra temperature, and the low ionised helium abundance. Since the oxygen abundance is now shown to be normal for LMC PN, and the O^+/O ratio indicates a substantial neutral helium content, the primordial helium abundance discussion (pp 147 - 150) is therefore no longer relevant, and the references to the oxygen abundance of LMC N25 within it are no longer correct.

Table 5.2 Ionic and elemental abundances for LMC N25.

Ion	λ(Å)	$\frac{n(ion)}{n(H^+)}$ T_e=12100 K	$\frac{n(ion)}{n(H^+)}$ T_e=10000 K	Element	Elemental T_e=12100 K	Abundance T_e=10000 K
N^+	6548+6584	1.04×10^{-5}	2.30×10^{-5}	N	1.23×10^{-5}	2.53×10^{-5}
O"	6300	3.11×10^{-6}	6.03×10^{-6}			
O^+	3727	9.41×10^{-5}	3.68×10^{-4}			
O^+	7325	6.49×10^{-5}	1.77×10^{-4}			
O^{++}	5007+4959	1.41×10^{-5}	2.75×10^{-5}	O	1.11×10^{-4}	4.02×10^{-4}
Ne^{++}	3868	$< 9.22 \times 10^{-7}$	$< 1.88 \times 10^{-6}$	Ne	$< 6.12 \times 10^{-6}$	$< 2.05 \times 10^{-5}$
S^+	4068+4076	1.69×10^{-7}	2.59×10^{-7}			
S^{++}	6312	9.10×10^{-7}	1.73×10^{-6}	S	1.08×10^{-6}	1.99×10^{-6}
Ar^{++}	7135	1.29×10^{-7}	1.97×10^{-7}	Ar	1.93×10^{-7}	2.95×10^{-7}

Page 140, Section 5.4. The equation for the calculation of the sulphur abundance should be replaced with,

$$ICF(S) = \left(1 - \left(1 - \frac{N(O^+)}{N(O)}\right)^3\right)^{-0.3}$$

where

$$S/H = (S^+ + S^{++})/H^+ \quad \times \quad ICF(S)$$

Page 152. Delete last paragraph on page.

Page 160, paragraph 5, last sentence. Replace last sentence with 'The weak nature of the [O II]3727 Å line may indicate a high nebular electron density'.

Page 173. Points 10, 11, and 12 are no longer relevant.

To my family and friends.

Acknowledgements

It is a pleasure to acknowledge Mike Barlow who has supervised this thesis, and thank him for the guidance, support, and dicussion throughout the course of the work.

I am grateful to Robin Clegg for providing supervision during Mike's stay at JILA, and for many fruitful discussions. I would also like to thank Robin and Ian Howarth for proof reading earlier versions of this thesis.

I acknowledge the SERC for financial support during the last three years, and thank University College London, through Prof. R Wilson, for the Perrin studentship award covering the final six months of the thesis work.

There are many people who deserve thanks for making the last three years at University College London so enjoyable, but special thanks should go to Paul, Tim, Raman, Pete, Janet, Keith, Tony, Linda, Terry (down under), Steve, Ian, David, Shashi, and John. Thanks also to the members of the IR group, Pat, Alistare, John, Chris, Brian, Murray, Chris, Melvyn, Bill, Ian, and Martin.

Finally, I dedicate this thesis to my family and friends, who will be glad to hear that my student days are over, and that my working life has begun.

Abstract

Spectroscopic data for 74 Planetary Nebulae (PN) in the Large and Small Magellanic Clouds (LMC and SMC) have been analysed. The optical line fluxes have been used to determine the nebular temperatures and densities, and the abundances of He, N, O, Ne, and Ar, relative to H. In the sample the analogues of Galactic PN are found: there are 5 (and possibly 10) He- and N-rich nebulae resembling Peimbert's Type I PN, 6 objects with low oxygen abundance, analogous to the PN of the Galactic Halo, 5 very-low-excitation (VLE) nebulae, and 5 PN central stars with Wolf-Rayet WC class features.

Mean abundances are calculated for each cloud, from the nebulae not in the Type I, 'low-oxygen', or VLE groups, and are compared with the average abundances for Galactic PN, and H II regions in the Galaxy, the LMC, and the SMC. The comparison shows a significant enhancement of He and N in the LMC and SMC PN, with respect to LMC and SMC H II regions, whilst oxygen, neon, and argon abundances are similar in PN and H II regions within each galaxy.

The central star luminosities and H I Zanstra temperatures are derived for 19 objects within the survey, and are compared to the evolutionary tracks for PN central stars of Schönberner (1979,1983). The comparison shows good agreement between theory and observation for most objects, although the high luminosity of LMC N201 (27502 $L_{\odot}$) places it a long way above the tracks.

Of the six MC PN with low oxygen abundances two, LMC N25 and LMC N199, also have very low ionic helium abundances, and central star temperatures at which only a small contribution from neutral helium would be expected (40000 - 45000 K). LMC N25 is studied in more detail through the analysis of recent IPCS spectra.

Contents

List of tables

Chapter 2

Chapter 3

Chapter 4

Chapter 5

Chapter 6

List of figures

Chapter 2

Chapter 3

Chapter 4

Chapter 5

Chapter 6

CHAPTER 1

Introduction

In this introductory chapter earlier theoretical and observational work will be reviewed to provide a background for this study, and the aims of the study will be defined.

In a survey of the size reported here (74 objects in two local galaxies) the analysis touches upon many different aspects of interest in current astrophysics research. To restrict the length of this introductory discussion, therefore, only those topics directly related to the main analysis will be included; that is, the elemental abundances and central star parameters of Magellanic Cloud planetary nebulae (MC PN).

The aims of this study are defined in the final section of this chapter, §1.4.

1.1 Distance, reddening, and gas phase elemental abundances of the Magellanic Clouds.

This section briefly reviews the recent determinations of distances to the Large and Small Magellanic Clouds (LMC and SMC), and outlines a method for the determination of interstellar extinction for individual objects in each galaxy, §1.1.1 and §1.1.2. This is followed in §1.1.3 by a discussion of the gas phase elemental abundances of both galaxies (as determined by H II region studies).

1.1.1 Distance determinations to the Magellanic Clouds.

The LMC and SMC are two 'Irregular' galaxies of the local group, usually considered

to be satellites of our own galaxy. Both the LMC and SMC are relatively nearby (within 60 kpc), and for this reason present the rare opportunity of observing individual objects within a galactic system at a different evolutionary phase to our own.

The main methods used for the determination of the distance to these nearby galaxies are the studies of the periods of RR Lyrae and Cepheid variables, where the period-luminosity relationship is used to derive absolute brightnesses, and thus distances to these objects. Observations of RR Lyrae stars have recently been used to determine the distance to the LMC by Reid and Strugnell (1986), who by comparison with distances determined from other methods (Cepheid stars, Main Sequence fitting, and OB stars) suggested a 'best bet' distance of 47.5 ± 2 kpc for the LMC, and, following a similar comparison, 57.5 ± 3 kpc for the SMC. The small errors on both of these distances, and the small additional error in assuming all objects in a galaxy to be at the same distance, is in contrast to the highly uncertain distance scales used for Galactic PN. One of the main advantages of observing PN in the Magellanic Clouds is that with accurate distances, reasonably accurate estimates of the luminosties of PN central stars (NPN) can be made. Coupled with a derived stellar temperature this allows the NPN to be directly compared to theoretical evolutionary tracks in the log L, log T_{eff} plane of the HR diagram (§1.2).

A recent complication to this situation was reported by Mathewson *et al.* (1986) who from a study of Cepheid variable stars in the SMC, determined a depth to the SMC of 32 kpc, with a range of distances from 43 kpc to 75 kpc, although the maximum concentration of objects was at 59 kpc in agreement with the Reid and Strugnell (1986) result. The uncertainty of assuming a single distance for all objects in the SMC is therefore $\pm 27\%$, and could have a significant effect on some objects although the mean value of parameters determined from a single distance should not be greatly affected.

1.1.2 Interstellar extinction to the LMC and SMC.

Another advantage of observing PN in the Magellanic Clouds, apart from the accurate distances, is the low interstellar extinction to the two galaxies, $E(B-V) = 0.074 \pm 0.007$ for the LMC, and $E(B-V) = 0.054 \pm 0.004$ for the SMC (Caldwell and

Coulson, 1985), values that do not vary by a great deal over the face of the two galaxies. The situation for the Galaxy is rather different and Galactic objects can have very large extinction along their line of sight, with individual values varying dramatically throughout the Galaxy (Burstein and Heiles, 1982). For PN, however, the optical spectra provide a straightforward method for determining this reddening, by correcting the flux ratio of the hydrogen Balmer series to the theoretical values (Brocklehurst, 1971) using a reddening law derived for galaxy in question. For the spectra analysed in this study, though, the large atmospheric dispersion affect (§2.3) meant that the individual reddening of the objects observed could not be derived by this method. Therefore, rather than adopt a single mean reddening for each galaxy, the reddening for each individual object was determined from the column density of neutral hydrogen, $N(HI)$, and relationships derived between it and the interstellar extinction as measured by $E(B-V)$.

To determine the extinction to individual objects, then, each object was assumed to have a known amount of Galactic foreground reddening, plus a reddening component local to the appropriate cloud. The Galactic foreground component was estimated from the maps of Burstein and Heiles (1982), which give contours of $E(B-V)$ in steps of 0.03, and only varied slightly from one object position to another. To determine the LMC or SMC contribution the following gas to dust ratios, determined from Lyman-α profile fitting (Bohlin, 1975), were adopted:

$$\frac{N(HI)}{E(B-V)} = 2 \times 10^{22} \quad (cm^{-2}mag^{-1}),$$

for the LMC (Koornneef, 1982); and

$$\frac{N(HI)}{E(B-V)} = 8.7 \times 10^{22} \quad (cm^{-2}mag^{-1}),$$

for the SMC (Fitzpatrick, 1985). By determing the column density of neutral hydrogen for the position of an individual object from the N(H I) maps of Rohlfs *et al.* (1984) for the LMC, and Hindman (1967) for the SMC, the Magellanic Cloud components of the total interstellar extinction are derived.

The results of this analysis are adopted for each object analysed in this survey, §4.3, although it is recognised that small scale variations in the dust to gas ratio, or

neutral hydrogen column density, will not be accounted for in this analysis, and that some objects will have an actual reddening significantly different to that adopted.

It is of interest to note here that the derived gas to dust ratios for the LMC and SMC are greater than that of the Galaxy ($4.8 \times 10^{21} cm^{-2} mag^{-1}$, Bohlin *et al.*, 1978) by factors of 4 an 18 respectively, and that both appear depleted in dust with respect to that in the Galaxy. The dust that is present in the LMC and SMC also appears to differ in extinction properties to the Galaxy, with the distinctive bump at 2200 Å seen in the extinction curve of our own galaxy barely present in that of the LMC, and not discernable in the extinction curve of the SMC (Nandy, 1984; Howarth, 1983). These differences in extinction curves are marked in the ultraviolet region, with the optical part of all three curves being remarkably similar. From the point of view of correcting an optical spectrum the reddening curves are essentially identical.

In terms of element abundance, Nandy (1984), using the grain size distribution of Mathis *et al.* (1977), was able to fit the extinction curve of the LMC with a graphite contribution 35% of that used in fitting the Galactic 2200 Å feature, and the SMC with a nil contribution from graphite. This result implies a depletion of graphite (assuming it to be responsible for the 2200 Å feature) from the Galaxy, to the LMC, and finally to the SMC. Similarly, the result can be seen as a depletion of carbon through the three galaxies, a suggestion that is further substantiated by an observed decrease in gas phase carbon (as measured by H II regions) across the three galaxies (Dufour *et al.*, 1982).

1.1.3 Gas phase elemental abundances in the Magellanic Clouds.

The trend of decreasing carbon abundance in H II regions from the Galaxy, to the LMC, and the SMC, is a recent result which reflects the general depletion of other elements through the three galaxies as reported in earlier studies of H II regions. A review of this work since 1974 is given by Dufour (1984) and brings together the work of four main groups (Peimbert *et al.*, Pagel *et al.*, Dufour *et al.*, and Aller *et al.*; see Dufour, 1984, for full references), and derives "recommended abundances" for He, C, N, O, Ne, S, Cl, and Ar in the LMC and the SMC based on the results of these groups. For each element the SMC abundance is significantly below that of the LMC, and, by comparison with mean elemental abundances of Galactic H II regions, the LMC is

significantly depleted with respect to the Galaxy in these elements (a good summary of these results is given in Table 3 of Dufour (1984)).

The importance of the H II region abundances is that they provide the gas phase elemental abundance from which, presumably, the PN were formed, and direct comparison of H II region elemental abundances with PN elemental abundances provides a measure of the enhancement (or otherwise) of each element during the lifetime of the PN progenitor. A comparison of this type is made for MC PN and MC H II regions in §3.4 using the elemental abundances derived in this study and the "recommended abundances" of Dufour (1984).

1.2 Elemental abundances and evolutionary theory for Galactic PN.

In this section the review of Galactic PN will be restricted to a discussion of the typical abundances of these objects, §1.2.1, and a short summary of the elemental abundances of Halo PN, §1.2.2. Subsection 1.2.3 presents a summary of the classification of 'Type I' PN, and of the 'dredge-up' processes thought to be responsible for the He and N enhancement in these objects. Finally, in §1.2.4, a short discussion of the problems involved in comparing the central star luminosities of Galactic PN with those predicted by PN evolutionary theory, is presented.

1.2.1 Elemental abundances of Galactic PN.

Decades of observations of Galactic PN have provided a mass of data which provide a consistent and thorough evaluation of elemental abundances in these objects. A recent survey of 41 Galactic PN by Aller and Czyzak (1983 a) provides a good example of the techniques used and typical errors involved in present day studies.

From these large surveys and from compilations of the work of many groups (see Kaler, 1985, and references therein) a pattern of elemental abundances for Galactic PN has begun to emerge, which can be summarised by considering three distinct groups of PN within the Galaxy. First, the PN with reasonably similar abundances which

can be used as 'typical values' (by far the vast majority of PN), second, the elemental abundances of 'low-Z' or 'Halo' PN, and last the elemental abundances of 'Type I' PN (those enriched in He and N).

The 'typical' PN give a reasonably consistent picture of elemental abundance, with nitrogen, oxygen, neon, sulphur, chlorine, and argon having mean abundances by number of 8.26, 8.64, 8.03, 7.00, 5.22, and 6.43 respectively ($12 + \log X/H$; Aller and Czyzak, 1983 a). The helium abundance of these Galactic PN, excluding objects where there is a large fraction of neutral helium, provides a remarkably consistent value of 0.110. Compared to Galactic H II regions (see Table 3.7(a)) He, N, and C are enhanced, whilst the other elements remain approximately unchanged.

1.2.2 Elemental abundances of 'Halo' PN.

A small number of PN observed in the Halo of the Galaxy display remarkably low elemental abundances compared to typical PN and Solar abundances. Table 3.9 presents the abundances of four of these 'Halo' PN (K648, H4-1, BB-1, and DDDM-1) taken from the studies of Torres-Peimbert *et al.* (1981) and Barker (1980,1983). They are depleted, with respect to typical Galactic PN, in N, O, Ne, S, and Ar by approximate factors of 4, 7, 9, 100, and 100 respectively, although important variations do occur from object to object (Clegg *et al.*, 1986).

1.2.3 Galactic 'Type I' PN.

A third distinct group of Galactic PN (in terms of elemental abundances) are those which display enhancements of He and N (or N/O) compared to typical PN abundances, the 'Type I' class of PN defined by Peimbert and co-workers (see Peimbert and Torres-Peimbert, 1983) from the following criteria;

$$\mathrm{He/H} \geq 0.125 \quad \text{and} \quad \log \mathrm{N/O} \geq -0.3.$$

These 'Type I' PN tend to be bi-polar nebular and show pronounced filamentary structure in the nebula, and are believed to evolve from the higher mass end of the initial mass range for PN. The enhancement of He and N in these objects is thought to be due to the second 'dredge-up' process (see below) occuring on the Asymptotic Giant Branch (AGB) phase of their evolution.

The three 'dredge-up' processes, thought to occur when the base of the convective envelope extends inwards (in mass) to regions rich in material processed by stellar nucleosynthesis, are fully reviewed by Iben and Renzini (1983), and only a summary of the changes to the surface abundances will be given here.

(1) On becoming Red Giants for the first time (following exhaustion of central hydrogen), the star experiences the first dredge up phase, which alters the surface elemental abundances of nitrogen (roughly doubled), helium (slight increase), and carbon (reduced by 30%), with oxygen staying roughly the same.

(2) Following the exhaustion of central helium, and the formation of an electron-degenerate core, the most massive AGB stars undergo a second dredge-up where up to 1 $M_{\odot}$ of He rich material can be added to the convective envelope. This dredge up of material from a hydrogen depleted zone further enriches the surface nitrogen and helium abundances, and depletes the surface carbon abundance. The detailed changes vary with initial mass and metalicity, and are given in Becker and Iben (1979).

(3) The third 'dredge-up' phase occurs during the final stages of AGB evolution and is a combination of several mixing episodes. In each case, following a helium shell flash (thermal pulse), significant amounts of He and C are added to the convective envelope, giving a further increase in helium surface abundances, and an increase in the surface carbon abundances following the decrease of the earlier to 'dredge-up' phases.

The correlation between increasing helium abundance and increasing nitrogen abundance for 'Type I' PN is thought to be a consequence of the second 'dredge-up', and the final dredge-up of carbon provides an explanation for the grouping of M, S, and C stars up the AGB (Iben and Renzini, 1983; Wood *et al.*, 1983). The difficulties with the Galactic PN distance scale, however, does not allow accurate determination of NPN luminosities and masses, which severely hinders comparison with the 'dredge-up' theory.

1.2.4 Observations of Galactic PN central stars.

The Galactic PN distance scale problem also causes many difficulties when comparisons are made with NPN evolution theory, as, although it is generally accepted that PN form the evolutionary link between Red Giants and White Dwarfs, the uncertainty in the derived luminosities of Galactic NPN hinders direct comparison with evolutionary

theory (which follows the star from Red Giant to White Dwarf), in the log L, log T_{eff} plane of the HR diagram.

The standard theoretical work of PN central star evolution is that of Schönberner (1979,1981,1983), following earlier work by Paczyński (1971,1975). The Schönberner models take various intermediate mass AGB stars that are in the thermal pulse phase of evolution, and evolve them into NPN during an interpulse period. Steady mass loss is included in the models but does not explain the total removal of the hydrogen rich envelope (Schönberner, 1979). The timing of the onset of the PN phase in the interpulse period produces models that cross the HR diagram and move down to the White Dwarf region in times comparable with the derived age of PN (30000 - 40000 yrs.; Schönberner, 1983). Some models of lower core mass have been calculated for higher mass loss rates, and for a final thermal pulse after PN ejection (Schönberner, 1983). The main conclusions from this work are that only 20% of post-AGB stars will undergo a thermal pulse, and that the lower limit for the luminosity and mass of the central stars of PN are 2500 $L_{\odot}$ and 0.55 $M_{\odot}$ respectively.

The NPN evolutionary tracks were calculated for two pairs of core masses, 0.64 $M_{\odot}$ and 0.60 $M_{\odot}$ (Schönberner, 1979) and 0.565 $M_{\odot}$ and 0.546 $M_{\odot}$ (Schönberner, 1983). The main features of the tracks are the near horizontal (constant luminosity) evolution of the central star across the HR diagram from the tip of the AGB, followed by a sudden drop in luminosity and slow decrease in temperature towards the White Dwarf region (occuring at $\sim$ 100000 K). The luminosity of the 'horizontal' part of each track is directly associated with the core mass and interpolation between the tracks to derive core masses between the tracks can be done with reasonable accuracy, as shown by the extrapolated low core mass tracks of Schönberner (1981) and the calculated low core mass tracks of Schönberner (1983) In this study they are used for comparison with derived NPN luminosity and temperature in an HR diagram (Fig. 4.3).

For Galactic PN Pottasch (1983) has shown that some measure of agreement exists between the NPN evolutionary theory (Paczyński, 1971) and derived stellar luminosities and temperatures, by using only the PN which have reasonably well determined distances. However, all but a few NPN lie below the 0.60 $M_{\odot}$ track of Paczyński (1971), and no high mass, high luminosity PN are found in the sample of 50. Additionally, of the NPN nearest to, but below, the 0.60 $M_{\odot}$ track, 3 are classified as 'Type I' PN by

Peimbert and Torres-Peimbert (1983), NGC 6751, NGC 6629, and NGC 7008, a further 'Type I' PN lies just above the 0.60 $M_{\odot}$ track, NGC 6537. These positions are odd as the central stars of 'Type I' PN should evolve from the higher mass end of the PN progenitor mass range, and form NPN with core masses at the higher end of the range, *i.e.* $\sim$ 0.8 M$\odot$ (Iben and Renzini, 1983). Assuming the 'Type I' PN to be wrongly placed by $\sim$ 0.2 $M_{\odot}$ in Fig. 6 of Pottasch (1983), it is easy to visualise moving the entire sample of 50 PN up in luminosity by a factor of 3 or so, to fall around the 0.6 $M_{\odot}$ track with a few PN near the 0.8 $M_{\odot}$ track (including the 'Type I' PN mentioned above). It seems possible, therefore, that the distances adopted by Pottasch for these PN are still not correct, a suggestion that is further supported by the fact that many of the NPN have derived luminosities below the lower limit of 2500 $L_{\odot}$ suggested by Schönberner (1983). The importance of studying MC PN, where accurate distances are available, is evident for comparisons of this type.

1.3 Previous studies of MC PN.

In this section previous observations of Magellanic Cloud PN are reviewed; §1.3.1 summarises the early surveys that identified MC PN, whilst §1.3.2 reviews the studies whose aim was to derive MC PN elemental abundances. The final subsection, §1.3.3, summarises the observations of MC PN central stars.

1.3.1 Early surveys of MC PN.

Early surveys of MC PN concentrated on the identification of these objects through their emission line spectra and low stellar continuum level in the optical. Surveys of MC PN (mainly with objective prisms) have been carried out by Lindsay (1955, 1956, 1961), Koelbloed (1956), Henize and Westerlund (1963), Sanduleak, MacConnell, and Philip (1978), Jacoby (1980), Sanduleak and Pesch (1981), and Sanduleak (1984). Succesive surveys have eliminated misidentified compact H II regions and emission line stars from earlier surveys, as well as steadily increasing the number of known PN in the

two galaxies. The most reliable listing of MC PN to date is given by Sanduleak *et al.* (1978), with additional LMC PN from Sanduleak (1984).

1.3.2 Elemental abundance studies of MC PN.

Detailed chemical abundance studies of MC PN were not possible until 1976 when Osmer (using a photoelectric scanner) observed 3 LMC PN (WS 7, WS 8, and WS 40; or N97, N24, and LM1-61 in the nomenclature of this study) and 3 SMC PN (N2, N54, and N67), although an objective prism study by Sanduleak *et al.* (1972) did indicate a general nitrogen deficiency in the LMC and SMC PN.

The study by Osmer (1976) reported evidence for an overabundance of helium by $\sim$ 40% and an underabundance of oxygen by a factor of 10 in the SMC and 3 in the LMC. The N/O ratio was found to be similar to that of Galactic PN.

Dufour and Killen (1977) (using photographic image-tube techniques) also observed SMC N67 and LMC N97, along with LMC N153 and 3 H II regions. They found SMC N67 to have a high helium abundance, in agreement with Osmer (1976), but that the two LMC PN had normal helium abundances with respect to Galactic PN. Additionally, the oxygen abundances displayed the same trend as those reported by Osmer (1976), and the N/O ratio was found to be significantly larger than that measured in MC H II regions.

More recently, Aller and his co-workers have observed 7 SMC PN (N2, N5, N43, N54, N70, and N87; Aller *et al.*, 1981), and 8 LMC PN (N184, N97, N24, N102, N153, N178, N201, and LM1-61; Aller, 1983; Maran *et al.*, 1982; Aller and Czyzak, 1983 b).

For the LMC PN, Aller (1983) concluded that the helium abundance was greater than in the LMC H II regions and comparable with the Galactic PN abundance, except that N97, N201, and N178 were all helium rich. Two LMC PN were found to be nitrogen rich, N24 and N201, but the other objects displayed nitrogen abundances greater than LMC H II regions and less than Galactic PN. Oxygen was found to be strongly depleted in N97, N102, and N201, but was comparable to LMC H II regions in the other objects.

Similar results were found by Aller *et al.* (1981) for the SMC PN, with He and N showing enhancements compared to H II regions, and deficiencies compared to Galactic

PN. Whilst the oxygen abundance was comparable with SMC H II regions but less than that of Galactic PN.

More recent work by this group (Maran *et al.*, 1982; Stecher *et al.*, 1982) reports the ultraviolet spectra of 3 MC PN, presenting nebular carbon abundances, stellar luminosities, and core masses. This small, but important, study was extended to 12 MC PN (6 LMC and 6 SMC) by Gull *et al.* (1986) who revised the central star luminosities reported earlier by Stecher *et al.* (1982) downwards by factors of 6-12. The conclusions of this series of ultraviolet observations, summarised by Gull *et al.* (1986), are that carbon and nitrogen are enhanced by factors of 10 in the SMC and 4 in the LMC compared to H II regions, and that elements other than carbon are deficient in MC PN compared to Galactic PN.

From the results of the Gull *et al.* (1986) survey, the mean carbon abundance of LMC PN, excluding possible 'Type I' objects (N97, N102, and N201), is 8.56 (12 + log X/H). For SMC PN, excluding N67, the mean carbon abundance is 8.65. In each galaxy, excluding possible 'Type I' objects, the PN have C/O > 1. The 'Type I' candidate MC PN all showed lower carbon abundances (7.34, 7.49, 7.27, and 6.27 for LMC N97, LMC N102, LMC N201, and SMC N67 respectively), possibly showing a strong depletion of carbon during the second 'dredge-up' phase.

Compared to the mean carbon abundance of Galactic PN (Aller and Keyes, 1986) and LMC and SMC H II regions (8.71, 7.9 and 7.16 respectively (Dufour *et al.*, 1982)), the 'normal' He/N abundance MC PN reflect the same pattern for carbon abundance as the other elements, falling between Galactic PN and MC PN H II region values. The difference between the Galactic PN and MC PN abundances is not very large, however, whilst the differences between PN and H II region carbon abundances in the Galaxy, the LMC and the SMC are 0.25 dex, 0.66 dex, and 1.49 dex, respectively. This indicates a strong correlation between increasing carbon abundance enhancement during AGB/PN evolution and decreasing metalicity and could be a reflection of a strong metalicity dependence for the third 'dredge-up' process (Iben and Renzini, 1983), linking in strongly with the increasing C to M star ratio found with decreasing metalicity (Iben, 1984, and references therein). These remarks are obviously based on the derived carbon abundances and it should be noted that errors of a factor of 2 would not be unusual

for such determinations, and any conclusions drawn should be weighed against these uncertainties.

1.3.3 Central star studies of MC PN.

Despite the importance of observing MC PN central stars, for comparison with theoretical models of NPN evolution, very little work has previously been carried out in this area, due to the difficulty of detecting the stellar continuum at the distance of the Magellanic Clouds with present day instruments. At the temperatures of the majority of NPN the stellar continuum is brightest in the ultraviolet, but to detect it requires long exposures ($\sim$ 4 hours) with *IUE*. Observations of the stellar continuum in the optical are feasible (see Chapter 4 of this study) but only sample those PN with lower stellar temperatures (25000 - 50000 K).

Only one ultraviolet survey of MC PN central stars has been reported: Gull *et al.* (1986, and references therein). This has provided an indication of the possibilities in this field, although the recent revision by this group of their derived stellar luminosities also reflects the problems involved and the care needed in the analysis. The final stellar luminosities and masses derived for the central stars in the survey of Gull *et al.* (1986) fall within the range 3500 - 11200 $L_{\odot}$ and 0.58 - 0.71 $M_{\odot}$ respectively, in good agreement with the NPN evolutionary tracks of Schönberner (1979,1983), although no direct comparison was made by the authors.

1.4 The main aims of this study.

Based on this brief review of earlier Galactic and Magellanic Cloud PN studies, which have only been able to determine mean elemental abundances for a small sample of objects, the aims of this study are defined as:

(1) The determination of elemental abundances for individual Magellanic Cloud planetary nebulae not previously studied, and confirmation of elemental abundances for the small number of MC PN previously investigated.

(2) The determination of mean He, N, O, Ne, and Ar abundances for LMC and SMC PN from a large sample of objects (but excluding anomalous abundance PN), for direct comparison with mean elemental abundances of Galactic PN and Magellanic Cloud H II regions.

(3) The determination of elemental abundances for MC PN defined as 'Type I', for comparison with Galactic 'Type I' PN and with theoretical predictions.

(4) The derivation, where possible, of stellar temperatures and luminosities for MC PN central stars, for direct comparison with the theoretical NPN evolutionary tracks of Schönberner (1979,1983).

CHAPTER 2

Observations and Calibration

In this chapter the basic details of the observations are presented (§ 2.1), and are followed by a discussion of the technique used to deconvolve the important emission line blends of the spectra (§2.2). The final section (§2.3) discusses atmospheric dispersion and its correction in this data set, and includes, in Tables 2.1 (a) to (d), the corrected relative line intensities for the 74 objects studied in this survey.

2.1 Observations

The observations were made by E. J. Wampler with the 3.9 m Anglo-Australian Telescope (AAT) at Siding Spring Observatory during the nights of 27/28 November 1975 (low resolution data), and 4/5, 5/6, 6/7, and 7/8 February 1976 (medium resolution data), using the Boller and Chivens Spectrograph and Image Dissector Scanner (IDS) (Robinson and Wampler, 1972), at the F/15 focus. The low resolution spectra were obtained with a 300 line/mm grating, giving a noise-limited useful wavelength range from 3600 Å to 7400 Å , at a resolution of $\sim$ 25 Å FWHM. The medium resolution spectra were obtained with a 600 line/mm grating, giving a useful coverage of 3600 Å to 7100 Å , at a resolution of $\sim$ 12 Å FWHM. The low and medium resolution spectra were obtained with entrance slots of 1 x 2 mm and 1 x 1 mm respectively, which gave projected areas on the sky of 3.6 x 7.2 arc sec and 3.6 x 3.6 arc sec. Each object was observed for two minutes in each of the slots having a projected separation on the sky

of 20 arc sec. The object spectra were then summed and the sky spectra, which had been recorded simultaneously in the alternative slots, were subtracted in order to yield net spectra. All of the low-resolution spectra were obtained on the night of November 27/28 1975, when the PN were observed in essentially Right Ascension order. The same order of observation applied on the nights of the medium-resolution observations. The medium-resolution observations of the SMC PN N6, L239, L302, and L305 were obtained on February 7/8, while the remaining SMC medium-resolution data were obtained on February 5/6.

The spectra were wavelength calibrated with respect to comparison exposures of a He-Ne arc, and were calibrated spectrophotometrically by observations of white dwarf stars from the list of Oke (1974), using the SDRSYS reduction routine at the AAO (Straede, 1980). The subsequent analysis of the calibrated spectra was carried out at the UCL *STARLINK* node, using the *DIPSO* package of routines (Howarth and Maslen, 1984) to measure line intensities.

2.2 Deconvolution of major emission line blends.

Several groups of lines were only partially resolved in both series of spectra, most importantly the [N II] 6548 Å , 6584 Å and Hα lines, and the Hγ and [O III] 4363 Å lines, which are used either for the determination of interstellar extinction and atmospheric dispersion, or as temperature diagnostics. To deconvolve these lines into their respective components the *DIPSO* routine *ELF* written by Dr. P. J. Storey was used. The routine provides a multi-component fit, with either gaussian or user-defined profiles, where each component, n, is of the form;

$$i_n p_n(x)$$

for a peak intensity i_n, and where (for gaussian profiles)

$$p_n(x) = exp - \left(\left(\frac{x - c_n}{0.601 w_n} \right)^2 \right).$$

Where c_n is the position of line centre, and w_n is the full width half maximum, measured in either wavelength or velocity space.

To deconvolve the blend the routine performs a least squares fit to the observed data by minimising the function

$$F = \sum_m \left(\sum_n i_n p_n(x_m) - f_{obs}(x_m) \right)^2$$

where f_{obs} is the observed flux at point x_m, the sum n is over the number of components, and the sum m is over the number of observed points.

For all blend deconvolutions gaussian profiles were adopted and the fit procedure was carried out in wavelength space. The constraints to the fit were the theoretical line centres (in terms of the wavelength differences from the strongest line in the blend), and, for the (N II 6548 Å ,6584 Å : Hα) blend, a relative intensity ratio of 3:1 for the nitrogen lines, from the ratio of their transition probabilities (as they both originate from the same excited level). The value of the FWHM was not constrained in the procedure, except that the FWHM of similar components should be equal, but fits were only accepted for FWHM's within $\sim$ 3 Å of the FWHM of the unblended lines of the spectrum.

The fitting was made more complicated by the presence of broad wings on the stronger lines (those with intensity $\geq$ 100 relative to Hβ for a typical PN), which are a feature of the instrument itself, and whose width increased with increasing line intensity. However, the full profile (including the broad wings) of the strongest, unblended line, Hβ, could not be satisfactorily scaled up to fit the line profiles of the N II , Hα blend, as the strong broad component was far more prominent in the N II , Hα blend than in the Hβ line It was necessary, therefore, to estimate the FWHM of this broad component from the (unblended) Hβ line, and fit both a narrow and broad component to the strong lines within the blends. Another technique would have been to use the Hβ profile as a standard profile and to deconvolve the blends with this rather than a gaussian shape. The main drawback to this technique is that the width of the broad wings varied with the line intensity, so that the Hβ profile would only match in shape a line of similar intensity. Examples of the multi-component gaussian fits for the [N II], Hα blend and for the Hγ, [O III] blend, for both the low and the medium resolution spectra, are given in Figs 2.1 and 2.2.

In the medium resolution spectra the [N II], Hα blend and the Hγ, [O III] blend are almost resolved by the instrument, and the estimated errors for the intensities are in

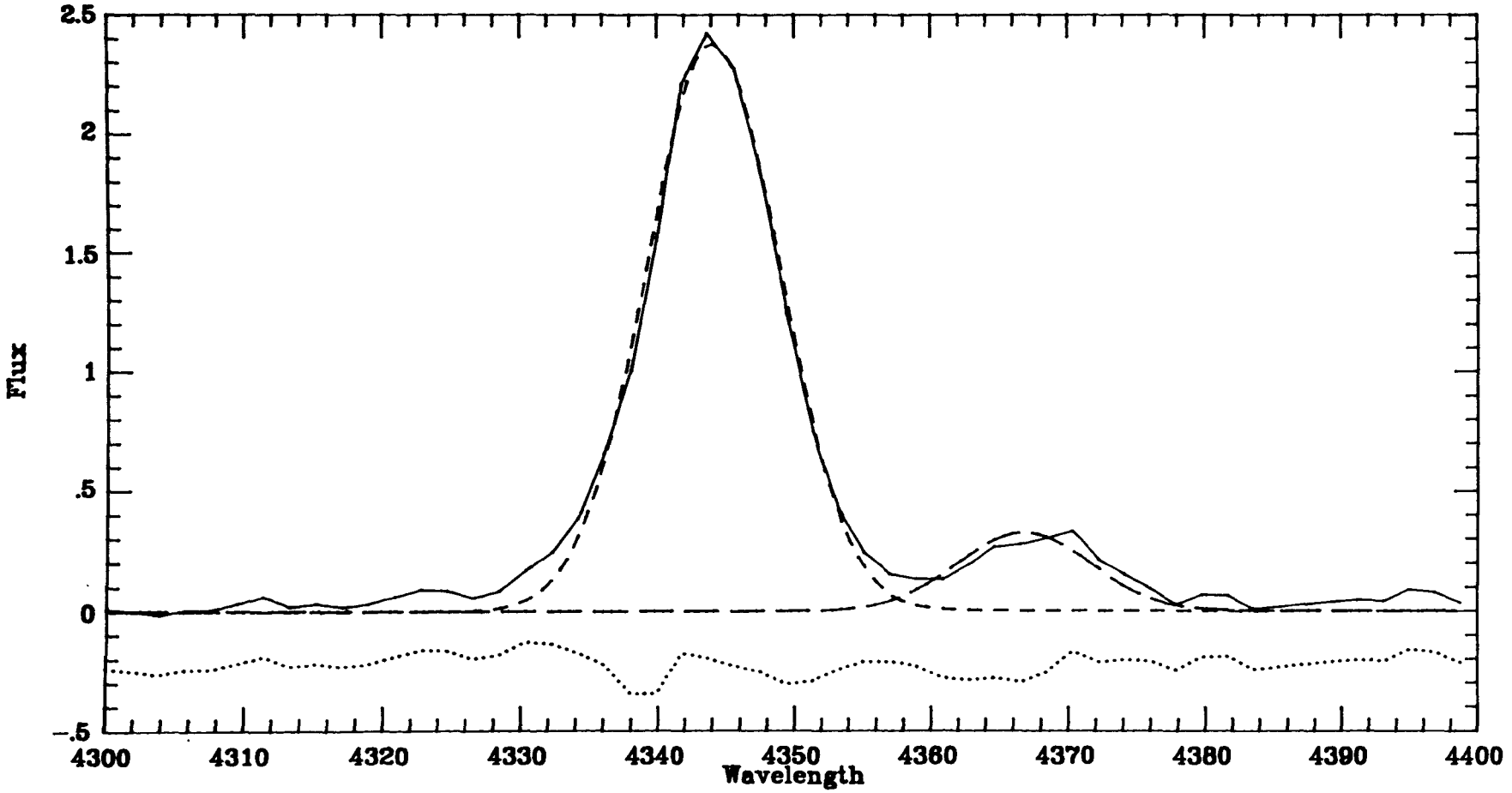

Figure 2.1(a). *Example of a multicomponent gaussian fit to the Hγ,[O III]4363 Å blend for a medium resolution spectrum. (Flux units of 10^{-14} ergs cm^{-2} sec^{-1}).*

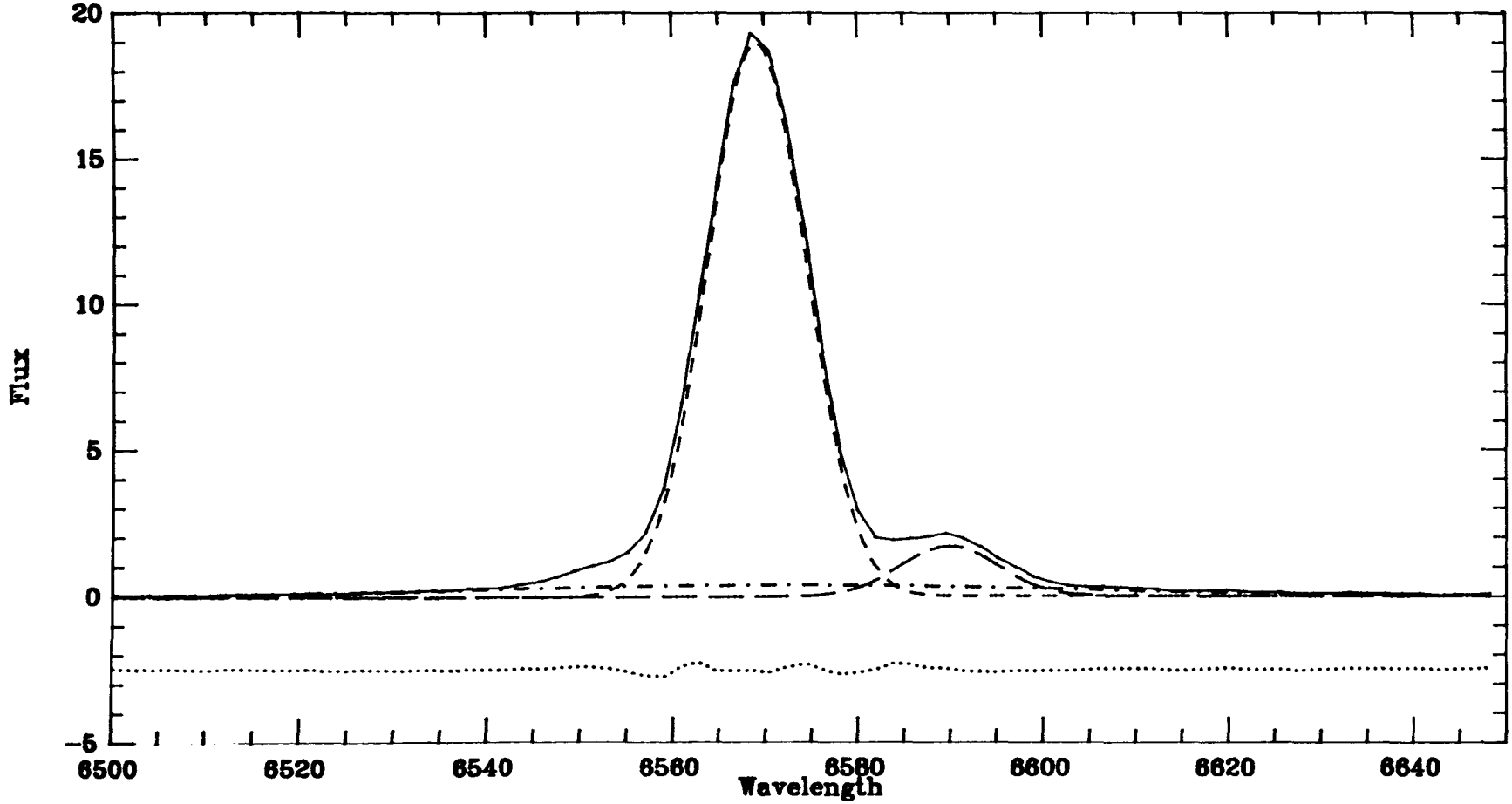

Figure 2.1(b). *Example of a multicomponent gaussian fit to the Hα,[N II]6548,6584 Å blend for a medium resolution spectrum. (Flux units of 10^{-13} ergs cm^{-2} sec^{-1}).*

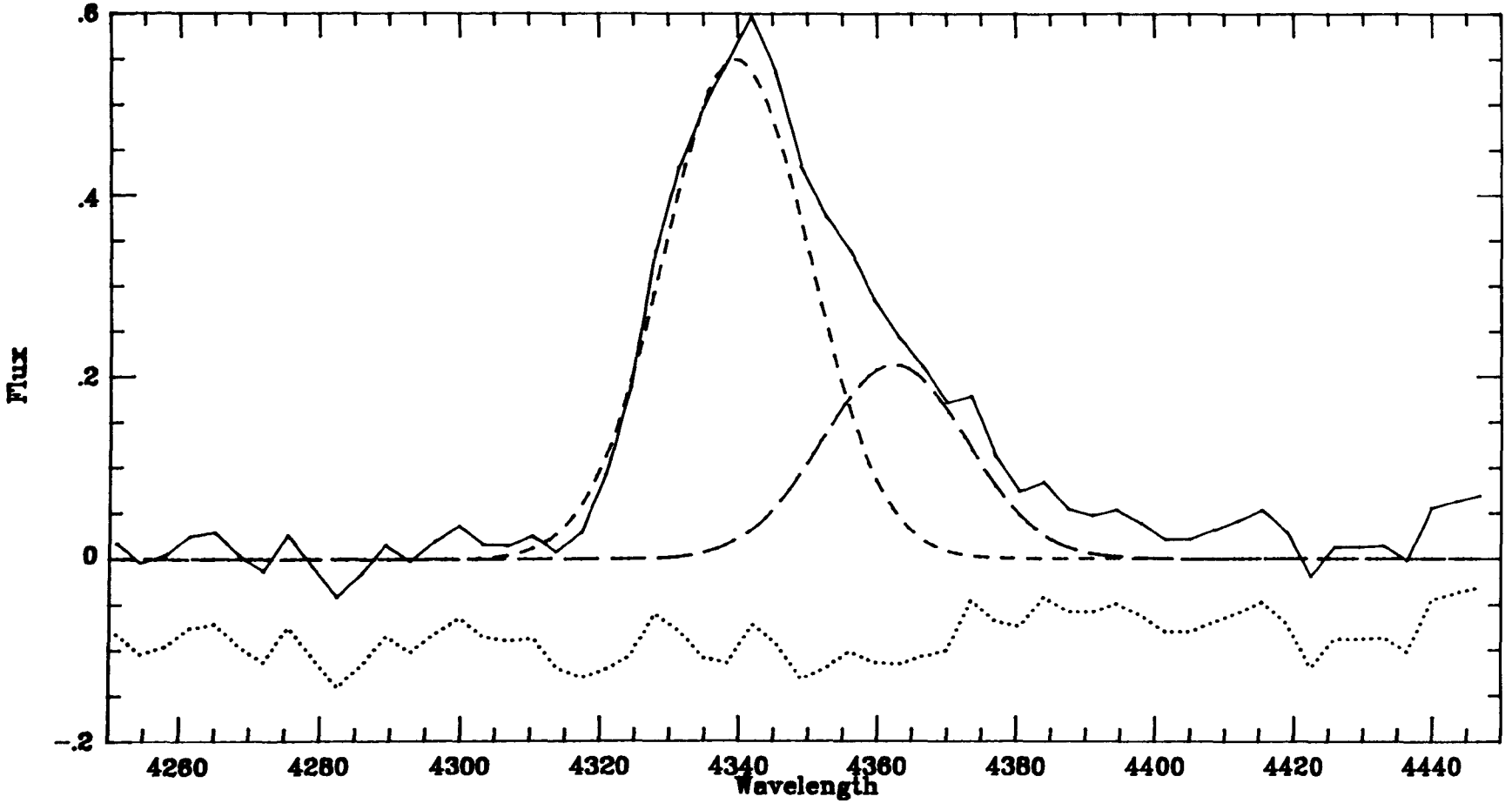

Figure 2.2(a). *Example of a multicomponent gaussian fit to the Hγ,[O III]4363 Å blend for a low resolution spectrum. (Flux units of 10^{-15} ergs cm^{-2} sec^{-1}).*

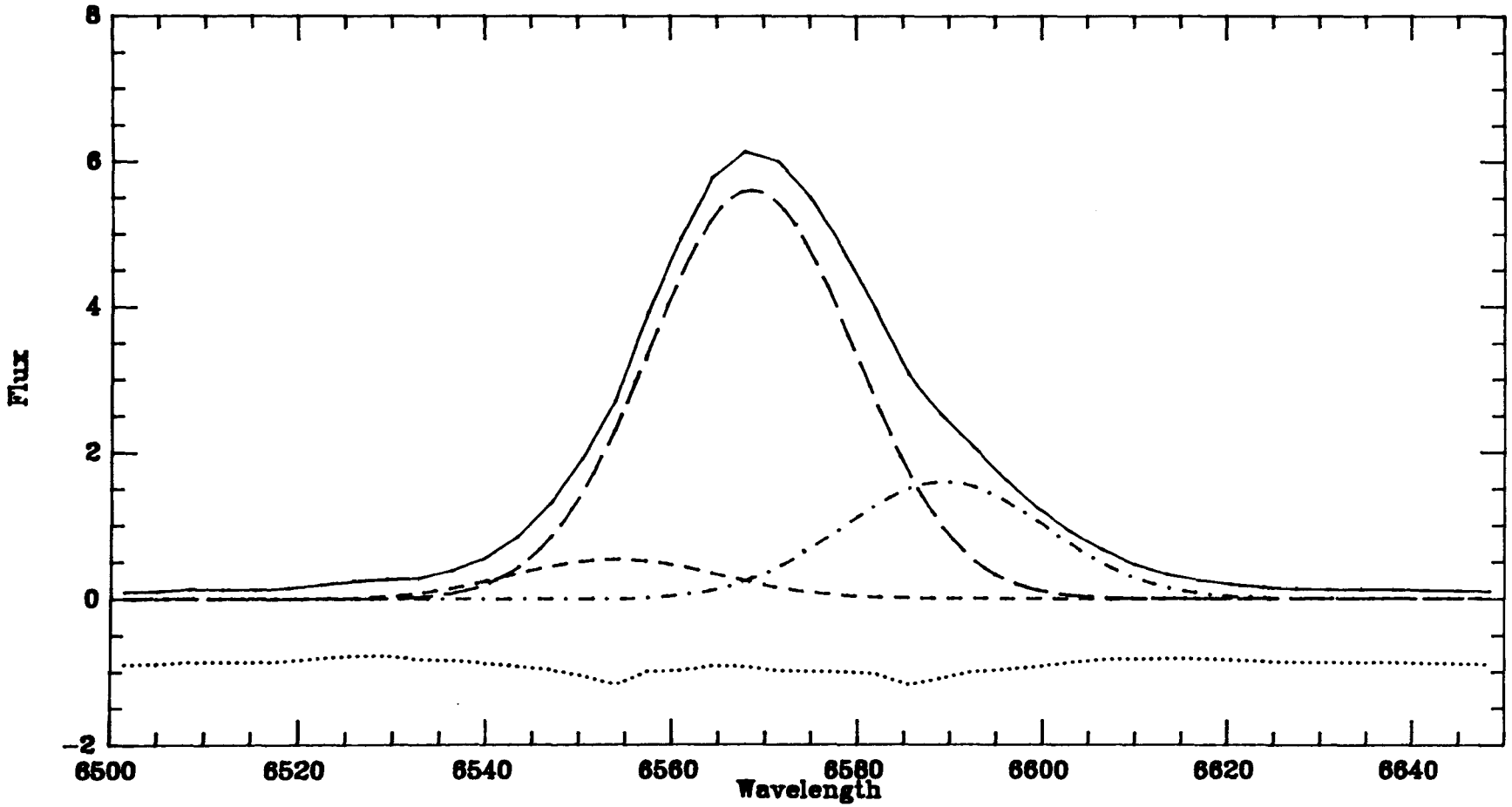

Figure 2.2(b). *Example of a multicomponent gaussian fit to the Hα,[N II]6548,6584 Å blend for a low resolution spectrum. (Flux units of 10^{-14} ergs cm^{-2} sec^{-1}).*

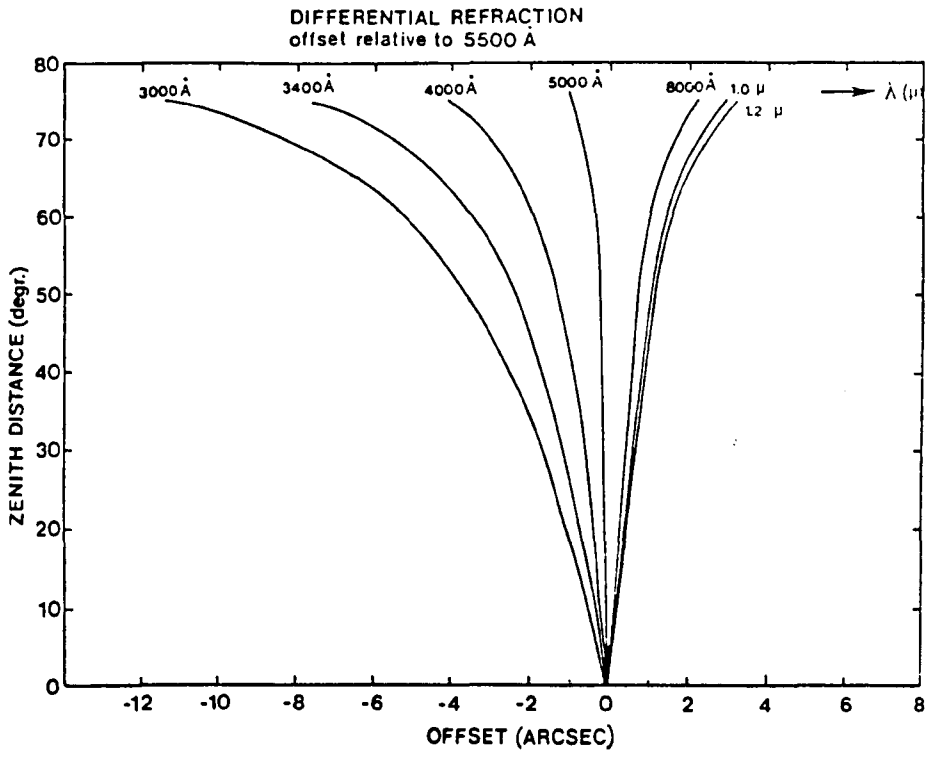

Figure 2.3

Atmospheric dispersion curves: showing the offset relative to 5500 Å for a range of wavelengths from 3000 Å to 8000 Å

the range 5% to 15% , depending on the relative strengths of the components involved. There was more significant blending, however, in the low resolution spectra, and errors of about 10% to 30% are estimated. It should be noted that the Hγ, [O III] blending was particularly pronounced in the low resolution spectra, and the weakest [O III] 4363 Å relative line intensities have the highest associated errors.

2.3 Atmospheric dispersion and interstellar extinction corrections

The effect of atmospheric dispersion can be seen in Fig. 2.3, where the differential refraction, offset relative to 5500 Å , is plotted against zenith distance for a range of wavelengths from 3000 Å to 1.2μ (from a diagram by David Hanes, AAT Observers Guide, 1976). It is clear from Fig. 2.3 that for large zenith distances (*i.e.* greater than

about 40 degrees) the image is offset by more than 1 arc sec for wavelengths less than $\sim$ 4500 Å , and less than 1 arc sec for wavelengths between 5500 Å and 7000 Å . For large entrance apertures, and good 'seeing' conditions, these offsets have a negligible effect, as the image is still fully within the aperture for all wavelengths. However, when a narrow entrance aperture is in use, and the 'seeing' is of the order of the aperture size (as was generally true for all spectra in this data set) any image offset will lead to a loss of flux, and will be worse at shorter wavelengths, as an increasingly large proportion of the image at these wavelengths falls outside of the aperture. The effect under these conditions is not disimilar to that of interstellar extinction, in as much as the differential offset is greater at the blueward end of the spectrum, leading to an overall reddening of the spectrum.

The magnitude of the effect is dependent on the exact zenith distance, the entrance aperture (*i.e.* slit width), and the 'seeing' at the time of the observation, and for this data set it could only be corrected for empirically. To do this it was assumed that there would be a reasonably linear relationship between the flux 'extinction' and wavelength for the atmospheric dispersion and that it would follow a similar trend to the interstellar extinction between 3500 Å and 7000 Å . Following a single, combined, correction for both atmospheric dispersion and interstellar extinction, using the reddening law of Howarth (1983), any deviations from the above assumption are corrected for empirically by comparison between the flux intensities of PN in this data set with those in data sets not as greatly affected by atmospheric dispersion.

All spectra were, therefore, first corrected to the theoretical Hα:Hβ intensity ratio (Brocklehurst, 1971), using a galactic reddening law curve (Howarth, 1983) with a suitable value for the logarithmic constant (c' in Tables 2.1(a) to 2.1(d)). The galactic law was used for the total dereddening rather than seperate curves for the LMC, SMC, and our own galaxy, as the various extinction laws of the three galaxies longward 3500 Å are almost identical (Howarth, 1983; Nandy, 1984), and any of them would serve as an estimate to the true extinction. It should be noted here also that, because of the effect of atmospheric dispersion, c' does not represent a value for the true interstellar extinction suffered by each object, but should be an upper limit to the logarithmic extinction constant.

Following this correction, the effects of atmospheric dispersion were, as expected, most pronounced at the blue end of the spectra and further corrections were found to be necessary to the fluxes of the lines shortwards of 4400 Å . In order to estimate the magnitude of the corrections needed, two types of comparison were made. First the corrected relative intensities of [O II]3727 Å and [Ne III]3868 Å , were compared with the dereddened relative intensities for these lines from Aller *et al.* (1981), Aller (1983), and Barlow (1986), for the nebulae in common. The relevant line fluxes are listed in Tables 2.3(a) (LMC PN), and 2.3(b) (SMC PN). A summary of the mean ratios of the IDS intensities to the other intensities is presented in Table 2.4. Secondly, the corrected Hγ:Hβ and Hδ:Hβ ratios obtained from the IDS spectra were compared to the theoretical ratios for $T_e = 10^4$ K and $N_e = 10^4$ cm^{-3}, 0.469 and 0.259, respectively (Brocklehurst, 1971). A comparison between the observed mean ratios and theoretical ratios is also included in Table 2.4.

Inspection of the various ratios in Table 2.4, for the low resolution spectra of both the SMC and LMC PN, indicates that the corrections needed for the [O II], [Ne III], Hδ, Hγ fluxes are similar. The weighted mean of all 93 low resolution ratios (IDS divided by other) is 0.89. All low resolution line fluxes between 3700 Å and 4400 Å have therefore been multiplied by a factor of 1/0.89 (= 1.12). The corrected low resolution line fluxes listed in Tables 2.1(b) and 2.1(d) are thus the result of the dereddening of all fluxes by c′, followed by multiplication by a factor of 1.12 for those lines with $\lambda < 4400$ Å .

In the case of the medium resolution spectra, the dereddened to intrinsic Balmer line ratios in Table 2.4 indicate that a correction factor of 1/0.89 (= 1.12) is again appropriate for Hδ and Hγ, for both the SMC and LMC PN. However, in the case of the [O II] and [Ne III] lines, the ratio of the medium resolution IDS to others is significantly lower than 0.89. This additional reduction in flux at short wavelengths was attributed not to atmospheric dispersion, but to the fact that these lines fall close to the detector edge in the medium resolution spectra, and the sensitivity of the detector in its outer regions is significantly lower than in the central regions due to pincushion distortion in the electrostatically-focussed image tube chain. On the basis of Table 2.4, medium resolution spectra correction factors of 1/0.70 (= 1.43) for lines with 3700 Å $< \lambda <$ 4000 Å , and 1/0.89 (= 1.12) for lines with 4000 Å $< \lambda <$ 4400 Å were adopted. The corrected medium resolution line fluxes listed in Tables 2.1(a) and 2.1(c) are thus

Table 2.2 Estimated errors in line intensity measurements due to uncertainty in the continuum level caused by noise.

Relative Intensity	Wavelength Range (Angstroms)			
(Hβ=100)	< 3900	3900-4200	4200-6000	6000-7000
3-5	> 50 %	> 50 %	40 %	30 %
5-15	"	30-40 %	20-30 %	20 %
15-35	"	25 %	10-15 %	10 %
> 35	> 30 %	10 %	10 %	10 %

the result of the dereddening of all fluxes by c', followed by multiplication of the above correction factors.

The final corrected relative line intensities (on a scale where Hβ = 100) are presented separately for the medium and low resolution spectra of the LMC PN (Tables 2.1(a) and 2.1(b), respectively), and the SMC PN (Tables 2.1(c) and 2.1(d), respectively). The estimated errors of measurement of the relative line intensities are listed in Table 2.2, and are a function of (a) the wavelength, (b) the line intensity (relative to Hβ), and (c) the overall strength of the signal. These effects will combine to produce a specific signal-to-noise ratio for an individual line within a spectrum, and the estimated errors are the uncertainty due to the noise over the various wavelength regions. Figs. 2.4 (a), (b), and (c) show example spectra from the dataset to illustrate the signal-to-noise ratio variations over the wavelength range analysed. Spectra with a weak overall signal have higher associated uncertainties, and these spectra have been labelled by an asterisk next to the object name in Tables 2.1(a) to 2.1(d). For these spectra, and for other spectra with non-detections of the important [O II]3727 Å and [Ne III]3868 Å lines, upper limits to the fluxes in these lines were measured. For some nebulae for which only upper limits for [O II]3727 Å or [Ne III]3868 Å could be derived, the relative intensities of the lines were available from the higher resolution IPCS data of Barlow (1986). In such cases, the relative intensities from the latter source are given in brackets following the upper limits derived from the IDS spectra (Tables 2.1(a) to 2.1(d)), and were used subsequently for the derivation of the O^+ and/or Ne^{++} abundances.

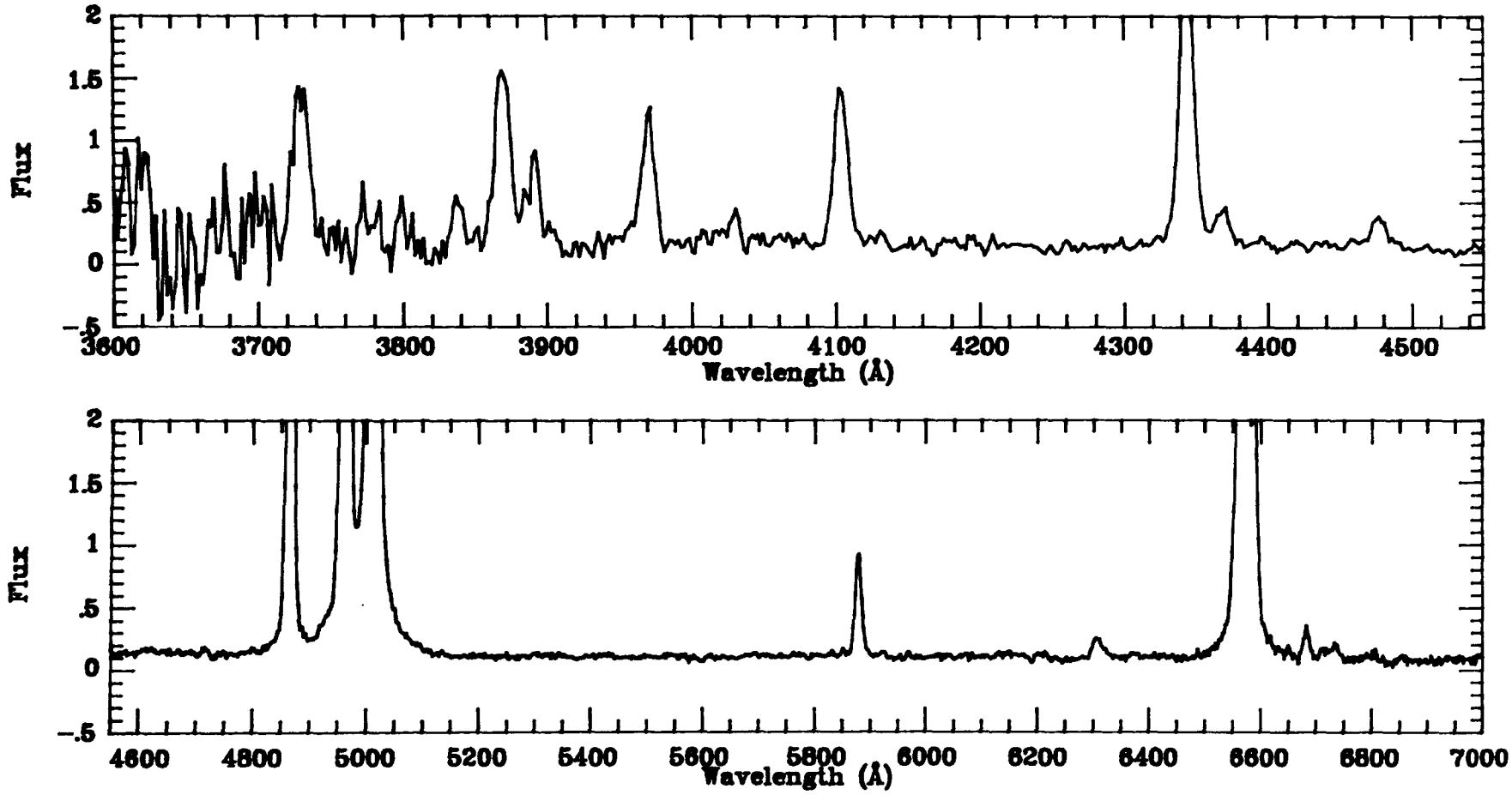

Figure 2.4(a). *An example IDS spectrum (for signal to noise comparison): LMC N123 (medium resolution).*

(Flux units of 10^{-15} ergs cm^{-2} sec^{-1}).

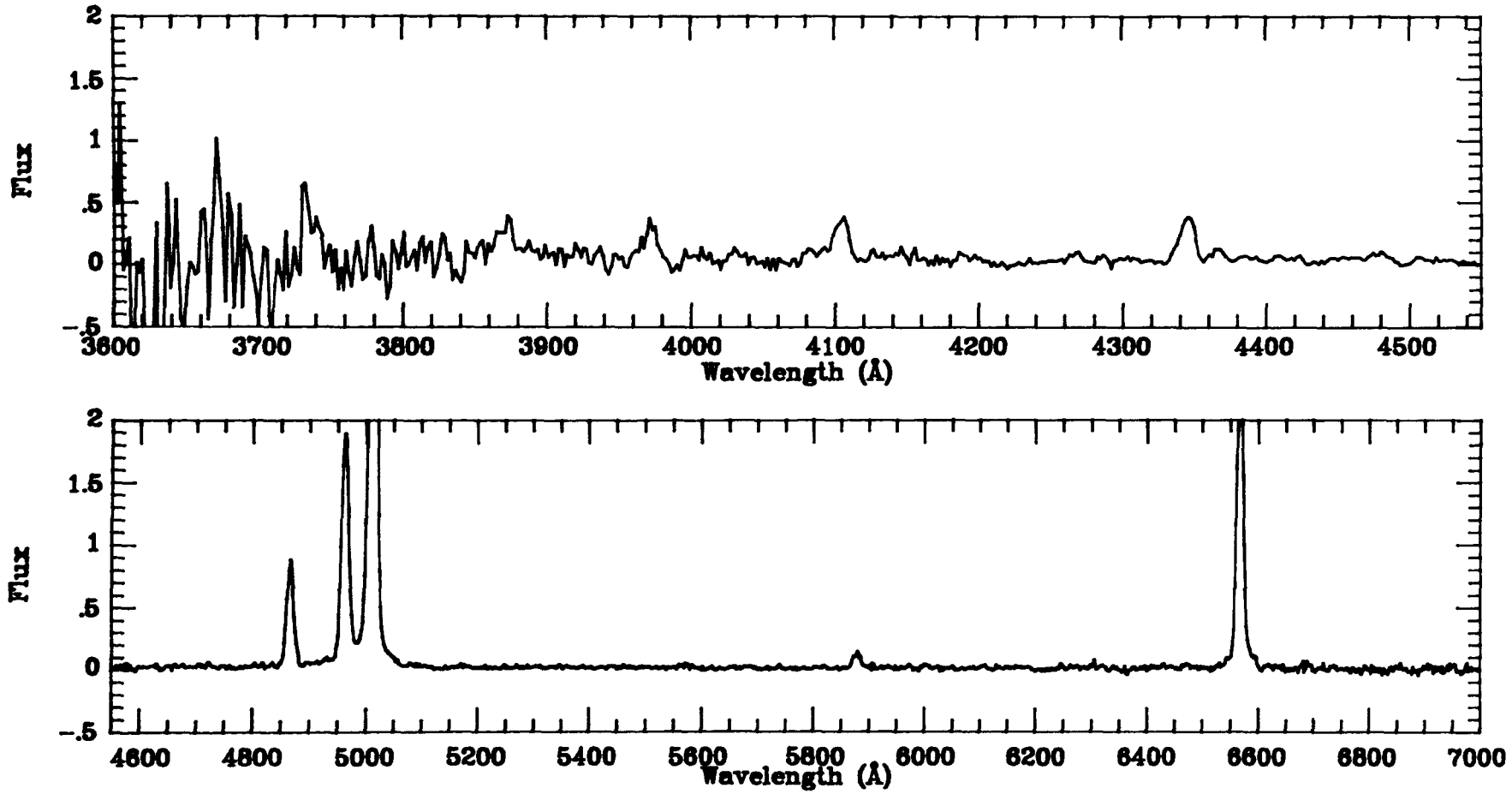

Figure 2.4(b). *An example IDS spectrum (for signal to noise comparison): LMC N212 (medium resolution).*
(Flux units of 10^{-15} ergs cm^{-2} sec^{-1}).

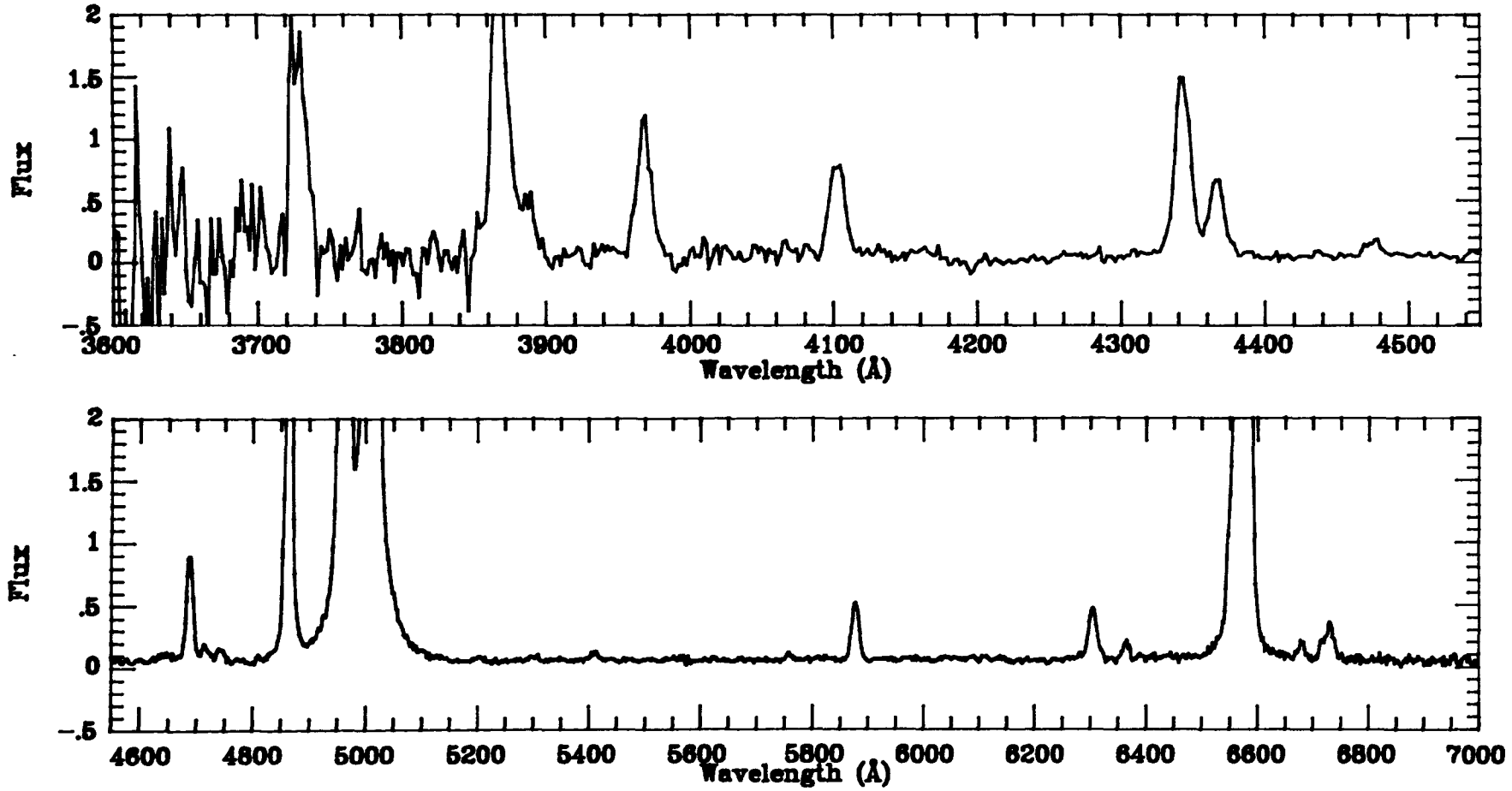

Figure 2.4(c). *An example IDS spectrum (for signal to noise comparison): LMC N208 (medium resolution).*
(Flux units of 10^{-15} ergs cm^{-2} sec^{-1}).

Table 2.1(a) Corrected relative line intensities for LMC PN : medium resolution

λ(Å)	ID	N1	N25	N42	N52	N60	N66
3727	[OII]	< 28.9	58.9	< 101.0	< 30.9	< 32.1	< 86.2(60.6)a
3868	[NeIII]	< 28.1	< 19.2	< 119.1	66.7	45.7	103.1(112.2)a
3889	HeI,H8		33.3::		22.6	22.8	
3969	[NeIII],Hε	18.0		< 64.8	42.5	19.2	15.4
4101	Hδ	27.2	31.5	30.4	20.4	24.8	27.5
4340	Hγ	44.1	48.7	39.8	52.5	47.8	49.3
4363	[OIII]	8.9	< 9.7	30.6	13.2	6.0	18.7
4471	HeI				4.8	4.5	
4542	HeII						
4686	HeII				23.8		60.2
4712	HeI,[ArIV]				5.8		15.0
4740	[ArIV]				5.3		8.7
4861	Hβ	100.0	100.0	100.0	100.0	100.0	100.0
4959	[OIII]	128.6	17.4	448.3	418.0	222.4	319.0
5007	[OIII]	398.0	47.7	1403.8	1238.3	647.2	973.8
5200	[NI]						
5411	HeII						5.8
5755	[NII]		3.2				2.6
5876	HeI	13.5	4.9	15.8	11.1	13.4	7.7
6300	[OI],[SIII]	1.5	2.5	11.9		2.8	10.0
6363	[OI]	0.9					3.5
6548	[NII]	1.6	17.1	21.9	0.6	4.3	40.0
6563	Hα	282.3	282.8	282.6	282.7	282.4	282.2
6584	[NII]	4.6	49.8	63.8	1.6	12.7	117.0
6678	HeI	3.8		4.4	4.3	3.4	
6717	[SII]						5.8
6731	[SII]			6.9		1.8	8.0
	OIII RATIO:	59.1	6.7	60.6	125.2	145.7	69.0
	NII RATIO:		21.1				59.7
	TEMP(OIII):	(16000)		15750	11750	11250	15000
	TEMP (NII):		(21000)				11000
	c′ :	0.45	0.88	0.64	−0.03	0.68	0.50

Table 2.1(a). *-continued*

λ(Å)	ID	N77F	N78	N101	N102	N104A	N110
3727	[OII]	279.4	28.6	53.5	55.8	< 206.2	72.7
3868	[NeIII]	87.3	38.2	29.2	99.3	100.6	83.9
3889	HeI,H8						28.5
3969	[NeIII],Hε	26.1	22.2		30.5	36.2::	50.0
4101	Hδ	18.9	25.7	23.6	22.7	11.5	25.2
4340	Hγ	45.4	45.8	51.5	47.6	52.1	42.7
4363	[OIII]	31.4	1.6		45.7	25.1	9.8
4471	HeI		7.2		5.2		4.6
4542	HeII						
4686	HeII	68.1			75.3	39.1	
4712	HeI,[ArIV]				12.3		
4740	[ArIV]				17.5		
4861	Hβ	100.0	100.0	100.0	100.0	100.0	100.0
4959	[OIII]	453.5	186.5		380.0	525.0	429.9
5007	[OIII]	1382.8	549.1	2.3	1124.8	1545.9	1198.3
5200	[NI]	10.5			12.7		
5411	HeII	9.5			5.7		
5755	[NII]	14.4		2.9	9.0		
5876	HeI	6.6	14.8	1.2	11.8	9.9	15.2
6300	[OI],[SIII]	30.6	2.5	3.2	26.8	11.9	13.7
6363	[OI]					1.8	3.7
6548	[NII]	156.3	6.5	29.7	117.5	28.7	14.1
6563	Hα	283.4	281.2	282.3	282.8	283.0	282.8
6584	[NII]	460.9	18.9	87.0	342.8	83.1	41.2
6678	HeI		4.5				5.4
6717	[SII]	14.4	2.8			6.1	
6731	[SII]				30.4	12.5	4.5
	OIII RATIO:	58.4	456.1		32.9	82.6	166.0
	NII RATIO:	42.8		40.4	51.4		
	TEMP(OIII):	16000	(10000)		23250	13750	10500
	TEMP (NII):	13000		13500	12000		(6250)
	c′ :	−0.27	0.80	0.40	0.67	1.18	0.26
			0.33				

Table 2.1(a). *–continued*

λ(Å)	ID	N122	N123	N124	N125	N133	N141
3727	[OII]	52.6	37.5	34.8	38.5::	< 25.4(6.6)a	22.0
3868	[NeIII]	125.8	38.5	67.0	40.3::	51.8::(37.8)a	41.6
3889	HeI,H8	22.8	15.5	17.0			10.6
3969	[NeIII],Hε	50.0	24.5	36.7	22.8::	53.2	28.1
4101	Hδ	26.4	25.2	18.1	21.5	26.2	18.9
4340	Hγ	45.7	44.5	46.4	48.2	47.6	37.4
4363	[OIII]	19.0	6.1	21.8	11.3	11.2	8.0
4471	HeI	5.1	4.6	3.6	4.3	4.4	4.4
4542	HeII	2.4					
4686	HeII	42.0		23.1			
4712	HeI,[ArIV]	6.3	0.9	4.4			
4740	[ArIV]	9.3		3.0			
4861	Hβ	100.0	100.0	100.0	100.0	100.0	100.0
4959	[OIII]	367.9	229.1	521.6	341.9	251.1	344.7
5007	[OIII]	1066.0	684.6	1512.6	1004.9	701.2	976.1
5200	[NI]	1.9					
5411	HeII	3.2		1.5			
5755	[NII]	8.3					
5876	HeI	15.3	13.3	10.6	14.8	13.2	13.4
6300	[OI],[SIII]	13.0	3.7	5.2	2.4	4.3	2.6
6363	[OI]	3.6		1.0			0.8
6548	[NII]	85.2	7.8	7.0	4.8	1.8	6.2
6563	Hα	282.0	282.1	282.9	281.7	282.9	282.6
6584	[NII]	250.6	22.9	20.5	14.0	5.1	18.1
6678	HeI		3.2	3.6	5.2	2.8	3.6
6717	[SII]						
6731	[SII]	13.1	3.1	5.3	3.8		3.2
	OIII RATIO:	75.3	148.6	93.3	119.2	85.1	164.9
	NII RATIO:	40.7					
	TEMP(OIII):	14400	11000	13000	12000	13250	10750
	TEMP (NII):	13800					
	c′ :	0.02	0.29	0.30	1.10	0.26	0.54

Table 2.1(a). *-continued*

λ(Å)	ID	N151	N153	N170	N178	N181	N182
3727	[OII]	< 38.3	55.6	67.5	59.5	373.2	34.3
3868	[NeIII]	73.0	99.1	94.2	84.6	92.8	50.5
3889	HeI,H8		29.5	34.0	20.7		11.8
3969	[NeIII],Hε	47.3	35.1	33.2	42.1		35.3
4101	Hδ	22.9	31.1	20.2	26.8		24.0
4340	Hγ	43.2	43.1	41.3	38.8	36.1	44.7
4363	[OIII]	9.9	20.6	17.1	15.5	7.2	7.1
4471	HeI	4.9	4.0	4.2	2.9	5.8	4.0
4542	HeII						
4686	HeII		30.7	32.1	9.7	55.4	
4712	HeI,[ArIV]		3.9	3.7	2.7		2.5
4740	[ArIV]		4.5	5.9	2.9		
4861	Hβ	100.0	100.0	100.0	100.0	100.0	100.0
4959	[OIII]	331.2	478.9	499.4	463.8	160.8	262.8
5007	[OIII]	946.2	1444.6	1481.5	1394.8	472.4	799.0
5200	[NI]					31.9	
5411	HeII		3.3	3.0	1.6	4.1	
5755	[NII]					32.2	
5876	HeI	13.9	9.7	10.3	12.1	9.8	14.4
6300	[OI],[SIII]	4.3	9.2	16.4	7.0	75.6	3.7
6363	[OI]		2.3	4.1	2.3	23.3	0.9
6548	[NII]	6.6	13.5	17.0	9.6	511.1	4.8
6563	Hα	281.3	283.3	282.1	281.1	281.8	282.3
6584	[NII]	19.2	39.4	49.7	28.3	1493.0	14.2
6678	HeI	4.8	2.8	4.8	2.4		3.4
6717	[SII]		1.3		1.1		
6731	[SII]		4.3	11.4	3.9	113.2	
	OIII RATIO:	128.6	93.2	115.8	119.6	87.5	148.8
	NII RATIO:					62.2	
	TEMP(OIII):	11500	13100	12000	11900	13500	11000
	TEMP (NII):					10750	
	c′ :	0.49	0.54	0.68	0.12	0.58	−0.11
							0.25

Table 2.1(a). *-continued*

λ(Å)	ID	N184	N199	N201	N203	N207	N208
3727	[OII]	56.3	78.7	35.9	< 79.7(70.8)a	82.4	76.8
3868	[NeIII]	110.5	< 8.0	67.5	47.2	105.3	126.8
3889	HeI,H8			17.9			13.9
3969	[NeIII],Hε	32.5	30.3	38.3		35.3	43.8
4101	Hδ	15.5	28.4	23.8	13.5	26.3	25.7
4340	Hγ	38.8	37.7	45.6	39.9	44.7	47.5
4363	[OIII]	18.5	3.6	25.0	5.5	18.0	20.7
4471	HeI	3.7	4.3	2.9		5.2	4.0
4542	HeII						
4686	HeII	45.7		25.3		43.1	25.3
4712	HeI,[ArIV]			5.8		2.5	4.8
4740	[ArIV]			7.4			3.5
4861	Hβ	100.0	100.0	100.0	100.0	100.0	100.0
4959	[OIII]	487.7	52.5	407.2	278.6	473.7	549.7
5007	[OIII]	1361.5	148.6	1144.7	800.0	1387.3	1556.6
5200	[NI]			0.8			0.9
5411	HeII	6.7		3.0		4.7	1.7
5755	[NII]		2.1::	0.8		1.5	1.1
5876	HeI	10.5	6.7	12.1	15.2	10.4	12.1
6300	[OI],[SIII]	9.7	3.0	7.6	3.3	14.5	11.3
6363	[OI]			1.5		4.9	3.0
6548	[NII]	9.1	28.0	11.4	7.7	25.8	16.2
6563	Hα	281.5	281.5	281.4	282.4	281.4	282.8
6584	[NII]	26.4	82.0	33.5	22.3	75.2	47.4
6678	HeI	4.2	2.5	3.4		3.4	3.0
6717	[SII]	3.5	1.0	2.1			1.4
6731	[SII]	3.9	1.7	5.5	5.3	15.3	6.3
	OIII RATIO:	100.1	55.2	62.0	194.9	103.3	101.9
	NII RATIO:		51.7	59.1		67.8	57.9
	TEMP(OIII):	12750	(18250)	15500	10000	12500	12750
	TEMP (NII):		(11750)	11000		10500	11250
	c' :	0.74	0.29	0.43	1.07	0.80	0.42

Table 2.1(a). *-continued*

λ(Å)	ID	N209	N211	N212	N221 (WS42)	LM1-27 (WS17)	LM1-61 (WS40)
3727	[OII]	49.0	< 44.8	51.7	39.8	107.4	< 29.4(21.8)a
3868	[NeIII]	92.9	76.9::	37.0::	58.8	85.7	57.6
3889	HeI,H8	21.8					29.3
3969	[NeIII],Hε	57.4	50.0	44.2	35.3	44.6	33.8
4101	Hδ	17.3	22.7	33.1	15.0	16.9	16.0
4340	Hγ	46.1	40.6	41.6	41.2	36.6	43.7
4363	[OIII]	16.4	22.6	11.0	16.6	12.2	18.4
4471	HeI		4.4		3.6		2.2
4542	HeII	2.7					2.1
4686	HeII	23.5			20.4	12.3	66.0
4712	HeI,[ArIV]	4.6	3.4		3.0		10.3
4740	[ArIV]	4.6	4.5		2.0		6.1
4861	Hβ	100.0	100.0	100.0	100.0	100.0	100.0
4959	[OIII]	481.4	460.0	248.6	513.7	415.5	343.2
5007	[OIII]	1392.1	1337.5	768.0	1518.2	1224.8	993.8
5200	[NI]						
5411	HeII	1.5			1.8		5.8
5755	[NII]	0.6			2.0	2.3::	
5876	HeI	11.9	14.6	17.5::	11.4	10.6	4.0
6300	[OI],[SIII]	9.6	5.3		8.8	2.0	3.9
6363	[OI]	2.7			3.0	1.5	3.0
6548	[NII]	10.8	4.2	2.8	33.8	21.6	2.1
6563	Hα	281.9	283.3	281.0	281.8	282.1	281.3
6584	[NII]	31.4	12.2	8.3	99.0	63.0	6.3
6678	HeI	4.2	3.7		2.0		
6717	[SII]	2.4	0.9				
6731	[SII]	5.3	3.1	2.6	8.9	24.7	
	OIII RATIO:	114.2	79.6	92.7	122.0	134.7	72.7
	NII RATIO:	72.6			68.1	37.4	
	TEMP(OIII):	12000	14000	13250	11750	11250	14500
	TEMP (NII):	10250			10500	(14000)	
	c′ :	0.66	0.89	0.03	0.16	0.92	0.05
					0.64		0.68

Table 2.1(a). *–continued*

λ(Å)	ID	LM1-62 (WS41)	S1	N16 (VLE)	N47 (VLE)	N99 (VLE)
3727	[OII]	42.1	201.5	749.1	394.9	769.3
3868	[NeIII]	120.6	< 39.1			14.3::
3889	HeI,H8					
3969	[NeIII],Hε	41.6				
4101	Hδ	24.9	27.5			32.2
4340	Hγ	47.8	47.8			43.2
4363	[OIII]	20.9	10.0			
4471	HeI	4.0				
4542	HeII					
4686	HeII	15.0				
4712	HeI,[ArIV]	3.0				
4740	[ArIV]	3.0				
4861	Hβ	100.0	100.0		100.0	100.0
4959	[OIII]	529.2	91.5	8.7::		
5007	[OIII]	1523.8	273.2			7.0
5200	[NI]					
5411	HeII	1.4				
5755	[NII]					3.2
5876	HeI	13.1	13.4			2.0
6300	[OI],[SIII]	9.1			11.6	
6363	[OI]	1.7				
6548	[NII]	10.1	8.6	12.7	13.6	46.8
6563	Hα	282.6	282.5	282.0	281.0	282.5
6584	[NII]	29.5	25.2	37.0	38.0	136.9
6678	HeI	2.7				
6717	[SII]	5.5				
6731	[SII]			41.4	63.1	
	OIII RATIO:	98.4	36.3			
	NII RATIO:					56.9
	TEMP(OIII):	12750	(21000)	(10000)	(10000)	
	TEMP (NII):					11250
	c' :	0.47	0.06	0.33	0.50	0.50
		1.11				

Table 2.1(b) Corrected relative line intensities for LMC PN : low resolution

λ(Å)	ID	N24	N28	N39	N42	N66	N97
3727	[OII]	28.8	105.3	19.9	89.8	75.7(60.6)a	112.0
3868	[NeIII]	44.9	71.3	73.0	110.7	81.8(112.2)a	111.6
3969	NeIII,Hε	27.3	37.9	37.0	59.0	27.1	37.9
4101	Hδ	24.0	35.9	27.2	26.5	28.8	19.8
4340	Hγ	44.2	42.5	41.5	36.7	53.2	43.4
4363	[OIII]	9.5	18.4	16.1	26.1	23.6	35.4
4471	HeI	5.1	2.8	1.8	3.4		3.4
4640	NIII		6.6				
4686	HeII		46.8	18.1		66.0	59.5
4740	[ArIV]		7.7			17.5	8.1
4861	Hβ	100.0	100.0	100.0	100.0	100.0	100.0
4959	[OIII]	271.6	398.4	351.2	403.0	296.9	351.5
5007	[OIII]	782.8	1131.2	1024.9	1162.7	842.8	1004.4
5200	[NI]						28.5
5411	HeII		4.1			8.7	4.6
5755	[NII]		3.8			3.2	11.4
5876	HeI	12.2	9.0	12.0	11.6	5.4	11.4
6300	[OI],[SIII]	1.1	12.6	3.2	9.7	6.0	
6363	[OI]		5.1		4.0		18.7
6548	[NII]		60.4	2.5	11.4	43.0	175.5
6563	Hα	282.0	281.4	282.6	281.6	282.6	283.1
6584	[NII]		176.9	7.2	33.2	126.1	522.0
6678	HeI		2.1	2.5	3.8		
6725	[SII]		13.1	3.0	9.2	19.4	46.1
7065	HeI	4.3	6.7	6.5	6.1	4.0	4.0
7135	[ArIII]	8.9	11.7	4.7	7.5	10.9	14.2
7325	[OII]		16.6	3.2	7.2	9.6	14.0
	OIII RATIO:	111.0	83.3	85.4	60.1	48.2	38.3
	NII RATIO:		61.6			52.5	61.1
	TEMP(OIII):	12250	13750	13500	16000	17750	20500
	TEMP (NII):		10750			11750	11000
	c' :	0.29	0.31	0.35	0.47	0.13	0.34

Table 2.1(b). *-continued*

λ(Å)	ID	N102	N104A	N107	N184	N186A	N188
3727	[OII]	69.1	174.5	< 36.6	71.2	97.4	156.9
3868	[NeIII]	107.6	90.2	141.3	83.1	117.6	69.9
3969	NeIII,Hε	49.3	63.0		36.3	40.1	29.9
4101	Hδ	30.6	23.1	13.6	22.0	32.0	22.1
4340	Hγ	41.4	46.5	30.5	44.8	45.1	45.2
4363	[OIII]	32.4	17.0	26.2	18.7	11.5	17.4
4471	HeI	4.9			3.8	2.6	
4640	NIII	5.4					
4686	HeII	67.1	38.6	37.6	40.7	27.1	34.6
4740	[ArIV]	15.4			3.1		5.4
4861	Hβ	100.0	100.0	100.0	100.0	100.0	100.0
4959	[OIII]	352.8	444.4	519.3	436.7	426.1	442.9
5007	[OIII]	975.5	1223.6	1474.6	1166.1	1197.0	1254.2
5200	[NI]	8.0					
5411	HeII	4.4	3.2		1.3		1.5
5755	[NII]	11.2					
5876	HeI	11.0	8.8	14.6::	8.8	11.2	7.6
6300	[OI],[SIII]	23.7	12.3	9.0	7.9	10.6	12.2
6363	[OI]	9.2		2.8	2.2	3.6	4.3
6548	[NII]	119.9	22.7	10.1	5.0	10.7	20.9
6563	Hα	282.6	282.3	282.8	282.8	281.1	281.8
6584	[NII]	350.9	66.3	29.3	14.7	31.3	61.0
6678	HeI	3.5	3.1		2.3	1.6	2.2
6725	[SII]	28.3	17.3		6.2	8.6	21.0
7065	HeI	6.4	2.7	9.4	3.1	3.8	3.6
7135	[ArIII]	17.1	9.5	13.0	7.5	9.8	10.4
7325	[OII]	12.6	14.4	14.3	8.1	8.7	16.6
	OIII RATIO:	41.0	98.2	76.2	85.6	141.3	97.8
	NII RATIO:	41.9					
	TEMP(OIII):	19250	12750	14500	13500	11500	13000
	TEMP (NII):	13250					
	c' :	0.43	0.57	1.45	0.49	0.58	0.50

Table 2.1(b). *-continued*

λ(Å)	ID	N192	LM1-9 (WS 4)	LM1-27 (WS17)	WS12	WS16
3727	[OII]	80.7	48.6::	176.4	103.1	265.3
3868	[NeIII]	74.8	62.7	103.6	89.6	90.6
3969	NeIII,Hε	33.5	39.0	31.6	37.3	57.8
4101	Hδ	17.1	19.7	17.1	36.0	24.6
4340	Hγ	46.6	44.9	42.2	44.5	33.0
4363	[OIII]	18.1	18.2	23.3	13.0	12.3
4471	HeI				3.2	
4640	NIII		3.3			
4686	HeII	62.2	30.5	14.6	19.0	54.4
4740	[ArIV]	7.3	5.9	16.5		
4861	Hβ	100.0	100.0	100.0	100.0	100.0
4959	[OIII]	435.1	372.5	406.5	437.0	367.0
5007	[OIII]	1119.5	1077.4	1169.0	1196.7	1039.2
5200	[NI]					
5411	HeII	4.5				
5755	[NII]					
5876	HeI	6.2	9.2	11.8	9.0	10.6
6300	[OI],[SIII]	9.4	4.4	10.8	6.8	19.5
6363	[OI]					12.4
6548	[NII]	5.0	3.9	23.4	10.6	36.8
6563	Hα	281.2	281.3	282.6	281.8	282.3
6584	[NII]	14.7	11.4	68.3	31.1	107.7
6678	HeI	2.5	3.3	3.7		
6725	[SII]	10.6	4.6	24.6	4.8	31.1
7065	HeI	3.4	2.5	2.7	4.1	
7135	[ArIII]	7.9	5.2	14.3	9.1	17.5
7325	[OII]	5.6	5.3		4.0	9.4
	OIII RATIO:	86.0	79.7	67.5	125.7	114.7
	NII RATIO:					
	TEMP(OIII):	13500	14000	15000	11750	12000
	TEMP (NII):					
	c′ :	0.47	0.53	0.55	0.41	0.40

Table 2.1(c) Corrected relative line intensities for SMC PN : medium resolution

λ(Å)	ID	N1	N4	N6	N70
3727	[OII]	36.0	< 62.1(13.9)a	< 31.6(12.5)a	27.6::(85.6)a
3868	[NeIII]	< 15.9	26.2::(37.8)a	< 90.5(68.8)a	13.8::(26.1)a
3889	HeI,H8				
3969	[NeIII],Hε	31.1	41.7	< 46.6	24.5
4101	Hδ	29.7	30.4	18.9::	24.2
4340	Hγ	45.0	44.7	47.8	50.8
4363	[OIII]	2.7	9.9	14.8	6.0
4471	HeI	5.7		6.6	8.2
4542	HeII				
4686	HeII		8.7		
4712	HeI,[ArIV]				
4740	[ArIV]				
4861	Hβ	100.0	100.0	100.0	100.0
4959	[OIII]	64.8	277.1	270.6	154.9
5007	[OIII]	200.0	924.7	762.8	457.0
5200	[NI]				
5411	HeII				
5755	[NII]				
5876	HeI	8.8	18.6	15.5	12.4
6300	[OI],[SIII]				1.6
6363	[OI]				
6548	[NII]	5.5	1.2	7.9	5.0
6563	Hα	282.0	282.6	280.7	281.5
6584	[NII]	16.1	3.7	23.0	14.7
6678	HeI	3.7		4.9	2.6
6717	[SII]				1.8
6731	[SII]				
	OIII RATIO:	97.7	121.4	69.9	101.7
	NII RATIO:				
	TEMP(OIII):	(12750)	12000	14500	10900
	TEMP (NII):				
	c′ :	0.20	−0.07	0.77	0.23

Table 2.1(c). *-continued*

λ(Å)	ID	N87	L66	L239	L305
3727	[OII]	< 38.4(16.9)a	< 100.9(84.9)a	71.3::(32.4)a	< 517.7(29.9)a
3868	[NeIII]	41.1(31.2)a	< 101.7(53.7)a	62.2(70.2)a	< 310.3(82.6)a
3889	HeI,H8	15.6			
3969	[NeIII],Hε	20.9	49.0	39.2	123.4
4101	Hδ	25.6	36.6	27.8	15.2
4340	Hγ	47.4	56.6	47.8	50.5
4363	[OIII]	8.7	10.3	17.9	
4471	HeI	3.1	(2.5)a	3.7	
4542	HeII				
4686	HeII		70.9	49.8	40.9
4712	HeI,[ArIV]	2.7			
4740	[ArIV]				
4861	Hβ	100.0	100.0	100.0	100.0
4959	[OIII]	203.3	348.8	321.7	204.3
5007	[OIII]	617.1	1062.4	955.0	642.7
5200	[NI]				
5411	HeII				
5755	[NII]				
5876	HeI	15.6		10.3	11.6
6300	[OI],[SIII]	2.0		5.1	
6363	[OI]				
6548	[NII]	1.4	11.0	4.0	40.2
6563	Hα	281.5	281.7	281.6	281.4
6584	[NII]	4.2	32.5	7.3	117.2
6678	HeI	3.9		3.2	14.0
6717	[SII]				
6731	[SII]				
	OIII RATIO:	94.8	136.8	71.2	
	NII RATIO:				
	TEMP(OIII):	13000	11750	12700	18200
	TEMP (NII):				
	c' :	0.09	−0.14	−0.02	0.79
				0.65	

Table 2.1(c). *-continued*

λ(Å)	ID	L536	L302 (VLE)	N8 (VLE)
3727	[OII]	66.3::(29.0)a	272.7	484.3
3868	[NeIII]	< 111.8(66.7)a		
3889	HeI,H8			
3969	[NeIII],Hε			
4101	Hδ	11.9	22.7	63.2
4340	Hγ	46.3	51.1	52.8
4363	[OIII]	12.8		
4471	HeI			
4542	HeII			
4686	HeII	52.1		
4712	HeI,[ArIV]	12.8		
4740	[ArIV]	6.5		
4861	Hβ	100.0	100.0	100.0
4959	[OIII]	82.8	23.2	
5007	[OIII]	287.7	63.8	
5200	[NI]	3.7		
5411	HeII			
5755	[NII]	7.2		
5876	HeI	18.6		
6300	[OI],[SIII]			
6363	[OI]			
6548	[NII]	52.8	35.3	14.7
6563	Hα	282.5	283.2	281.9
6584	[NII]	154.9	103.5	42.9
6678	HeI	5.4		
6717	[SII]	11.1		32.1
6731	[SII]			
	OIII RATIO:	28.8		
	NII RATIO:	29.0		
	TEMP(OIII):	24600	10000	10000
	TEMP (NII):	17200		
	c′ :	0.16	0.33	0.63

Table 2.1(d) Corrected Relative Line Intensities for SMC PN : Low Resolution

λ(Å)	ID	N1	N2	N5	N6	N7
3727	[OII]	33.8	7.9	66.0	< 21.6(12.5)a	10.7
3868	[NeIII]	< 7.0	48.8	71.3	38.2(68.8)a	25.6
3969	NeIII,Hε	10.2	18.7	28.6	24.5	17.2
4101	Hδ	23.2	18.0	22.3	20.7	13.6
4340	Hγ	48.4	38.0	43.9	46.7	43.1
4363	[OIII]	3.9	12.8	18.6	17.7	8.1
4471	HeI	3.1	2.0	4.2	4.4	4.1
4640	NIII	1.0			1.6	
4686	HeII		25.4	40.0		
4740	[ArIV]					
4861	Hβ	100.0	100.0	100.0	100.0	100.0
4959	[OIII]	65.2	314.2	377.9	285.8	217.3
5007	[OIII]	188.8	862.7	1031.4	801.3	629.6
5200	[NI]					
5411	HeII		2.0	2.1		
5755	[NII]				1.9	
5876	HeI	9.5	9.8	8.6	12.9	12.8
6300	[OI],[SIII]	2.1	2.8	5.8	3.7	
6363	[OI]	1.1	1.8	1.9	1.2	
6548	[NII]	5.4		8.2	9.0	
6563	Hα	281.7	281.1	282.7	282.5	281.7
6584	[NII]	15.8		23.9	26.2	
6678	HeI	3.2		3.4	5.0	4.6
6725	[SII]		2.9	8.0	2.0	
7065	HeI	4.3	5.8	4.7	10.5	6.2
7135	[ArIII]	4.2	4.2	5.5	6.8	2.3
7325	[OII]	21.6	2.2	7.7	8.1	3.4
	OIII RATIO:	65.0	92.1	75.9	61.3	104.7
	NII RATIO:				18.2	
	TEMP(OIII):	(15250)	13250	14250	15250	12500
	TEMP (NII):					
	c′ :	0.38	0.40	0.34	0.74	0.49

Table 2.1(d). *-continued*

λ(Å)	ID	N18	N29	N38	N40
3727	[OII]	12.1::	210.9	36.2	57.8
3868	[NeIII]	34.4	< 53.5	65.9	83.3
3969	NeIII,Hε	27.5		34.6	30.7
4101	Hδ	29.9	19.6	26.7	27.9
4340	Hγ	52.4	52.1	46.4	44.6
4363	[OIII]	6.9		11.5	10.8
4471	HeI			3.6	
4640	NIII				2.7
4686	HeII				34.8
4740	[ArIV]				
4861	Hβ	100.0	100.0	100.0	100.0
4959	[OIII]	270.6	108.2	294.5	325.8
5007	[OIII]	766.7	310.9	825.9	911.5
5200	[NI]				
5411	HeII				
5755	[NII]		1.0		
5876	HeI	10.6	10.1	11.9	8.1
6300	[OI],[SIII]		5.1	3.0	2.5
6363	[OI]		1.1		
6548	[NII]				
6563	Hα	282.2	281.8	282.8	282.0
6584	[NII]				
6678	HeI			3.4	
6725	[SII]	5.3	7.9		
7065	HeI	3.7	6.0	8.5	
7135	[ArIII]	6.0	9.0	3.7	4.6
7325	[OII]		12.8	4.2	
	OIII RATIO:	149.6		97.0	114.8
	NII RATIO:				
	TEMP(OIII):	11000	10000	12750	12250
	TEMP (NII):				
	c' :	0.33	0.95	0.32	0.16

Table 2.1(d). *-continued*

λ(Å)	ID	N42	N43	N44	N47
3727	[OII]	145.1	12.5::(12.5)a	22.4	85.7
3868	[NeIII]	< 35.2	48.6	81.8	24.6
3969	NeIII,Hε		24.0	34.2	25.3
4101	Hδ	27.3	29.1	24.9	27.6
4340	Hγ	54.4	50.2	45.2	49.5
4363	[OIII]	5.5	9.4	10.8	2.4
4471	HeI		5.8	6.0	4.6
4640	NIII				
4686	HeII				
4740	[ArIV]				
4861	Hβ	100.0	100.0	100.0	100.0
4959	[OIII]	61.8	211.1	313.5	106.8
5007	[OIII]	158.2	617.6	881.4	293.7
5200	[NI]				
5411	HeII				
5755	[NII]				
5876	HeI	10.5	14.3	12.5	12.6
6300	[OI],[SIII]		2.5	2.3	3.4
6363	[OI]		1.2	1.1	
6548	[NII]	4.9			4.8
6563	Hα	281.1	281.3	282.6	283.0
6584	[NII]	14.5			14.0
6678	HeI		2.3	2.2	2.8
6725	[SII]		0.8		
7065	HeI	5.3	10.0	6.2	8.7
7135	[ArIII]		4.0	4.0	6.8
7325	[OII]	13.4	6.1		18.4
	OIII RATIO:	39.7	88.2	110.4	170.3
	NII RATIO:				
	TEMP(OIII):	(19750)	13250	12250	10500
	TEMP (NII):				
	c' :	0.51	0.63	0.32	0.51

Notes on Table 2.1 (a),(b),(c), and (d):

:: - Uncertain flux value.

a - Figures in brackets from Barlow (1986).

Table 2.3(a) Medium and low resolution spectra of LMC PN, corrected by c', compared to dereddened relative line intensities from Aller (1983), (or Maran *et al.* , 1982), and Barlow (1986).

		Relative Intensity (Hβ = 100)			
LMC	Line	Medium	Low	Aller (1983)	Barlow (1986)
N24	[OII]3727 Å	-	25.7	25.1	-
	[NeIII]3868 Å	-	40.1	42.9	-
N28	[OII]3727 Å	-	94.0	-	90.4
	[NeIII]3868 Å	-	63.7	-	92.6
N42	[OII]3727 Å	<70.6	80.2	-	-
	[NeIII]3868 Å	<83.3	98.8	-	-
N66	[OII]3727 Å	<60.3	67.6	-	60.5
	[NeIII]3868 Å	72.1	73.0	-	112.2
N97	[OII]3727 Å	-	100.0	116.4	101.0
	[NeIII]3868 Å	-	99.6	92.6	107.8
N102	[OII]3727 Å	39.0	61.7	7.2::	60.0
	[NeIII]3868 Å	69.5	96.1	85.5	129.4
N104	[OII]3727 Å	<144.2	155.8	-	-
	[NeIII]3868 Å	70.4	80.6	-	-
N110	[OII]3727 Å	50.8	-	-	57.1
	[NeIII]3868 Å	58.7	-	-	96.0
N133	[OII]3727 Å	26.2	-	-	6.6
	[NeIII]3868 Å	32.2	-	-	37.8
N141	[OII]3727 Å	15.4	-	-	30.9
	[NeIII]3868 Å	29.1	-	-	61.7
N153	[OII]3727 Å	38.9	-	65.0	-
	[NeIII]3868 Å	69.3	-	97.7	-
N178	[OII]3727 Å	41.6	-	49.4	-
	[NeIII]3868 Å	59.2	-	82.9	-
N184	[OII]3727 Å	39.3	63.5	71.3	80.3
	[NeIII]3868 Å	77.3	74.2	64.5	94.1
N201	[OII]3727 Å	25.1	-	-	36.7
	[NeIII]3868 Å	47.2	-	-	88.6
N203	[OII]3727 Å	55.9::	-	-	72.5
	[NeIII]3868 Å	33.0	-	-	40.9
LM1-27	[OII]3727 Å	75.1	157.5	-	-
	[NeIII]3868 Å	60.0	92.5	-	-
LM1-61	[OII]3727 Å	<20.6	-	22.0: (Maran)	21.8
	[NeIII]3868 Å	40.2	-	47.9 (Maran)	60.7

Table 2.3(b) Medium and low resolution spectra of SMC PN, corrected by c', compared to dereddened relative line intensities from Aller (1983), (or Maran *et al.* , 1982), and Barlow (1986).

SMC	Line	Relative Intensity (Hβ = 100) Medium	Low	Aller (1983)	Barlow (1986)
N1	[OII]3727 Å	25.1	30.2	-	-
	[NeIII]3868 Å	<11.1	<6.3	-	-
N2	[OII]3727 Å	-	7.1	24.5	27.9
	[NeIII]3868 Å	-	43.6	49.9	70.5
N4	[OII]3727 Å	<43.4	-	-	13.6
	[NeIII]3868 Å	18.3	-	-	37.0
N5	[OII]3727 Å	-	59.0	80.0	69.8
	[NeIII]3868 Å	-	63.7	87.0	75.6
N6	[OII]3727 Å	<22.1	<19.3	-	14.5
	[NeIII]3868 Å	<63.3	34.1	-	71.6
N8	[OII]3727 Å	338.7	-	-	446.1
	[NeIII]3868 Å	nd	-	-	3.5
N38	[OII]3727 Å	-	32.3	-	18.5
	[NeIII]3868 Å	-	58.8	-	49.9
N40	[OII]3727 Å	-	51.6	-	28.7
	[NeIII]3868 Å	-	74.4	-	66.2
N43	[OII]3727 Å	-	11.2::	14.4	12.5
	[NeIII]3868 Å	-	43.4	34.8	39.1
N44	[OII]3727 Å	-	20.0	25.5	20.5
	[NeIII]3868 Å	-	73.0	76.0	65.3
N70	[OII]3727 Å	19.3::	-	62.0	-
	[NeIII]3868 Å	9.6::	-	19.4	-
N87	[OII]3727 Å	<26.8	-	18.8	16.1
	[NeIII]3868 Å	28.8	-	27.5	31.2
L66	[OII]3727 Å	<70.6	-	-	102.8
	[NeIII]3868 Å	<71.1	-	-	63.7
L302	[OII]3727 Å	190.7	-	-	397.2
	[NeIII]3868 Å	nd	-	-	nd

Table 2.4 Comparison of IDS relative intensities (corrected by c' only) with other sources.

Compared Data Sets (see notes below)	Compared Lines	Mean Ratio
B86/AL81 (10 points in sample)	[OII]3727,[NeIII]3868	99.4±20%
SMC Low/(AL81 or BW86) (16 points in sample)	[OII]3727,[NeIII]3868	93.3±16%
SMC Low/Theory (13 points in sample)	$H\gamma/H\beta$	90.0±8.5%
SMC Low/Theory (13 points in sample)	$H\delta/H\beta$	82.6±17%
LMC Low/(AL83 or BW86) (17 points in sample)	[OII]3727,[NeIII]3868	93.0±16%
LMC Low/Theory (17 points in sample)	$H\gamma/H\beta$	81.2±10%
LMC Low/Theory (17 points in sample)	$H\delta/H\beta$	85.3±22%
SMC Med/(AL81 or BW86) (5 points in sample)	[OII]3727,[NeIII]3868	74.1±25%
SMC Med/Theory (11 points in sample)	$H\gamma/H\beta$	90.8±6.8%
SMC Med/Theory (11 points in sample)	$H\delta/H\beta$	93.4±50%
LMC Med/(AL83 or BW86) (22 points in sample)	[OII]3727,[NeIII]3868	67.0±15%
LMC Med/Theory (39 points in sample)	$H\gamma/H\beta$	84.4±8.3%
LMC Med/Theory (38 points in sample)	$H\delta/H\beta$	80.7±19%

Notes to Table 2.4.

BW86 : Barlow, 1986;
AL81 : Aller *et al.* , 1981;
AL83 : Aller, 1983;

Low : Low resolution data this paper
Med : Medium resolution data this paper
Theory : Brocklehurst, 1971

CHAPTER 3

Determination of Elemental Abundances

In this chapter the determination of the elemental abundances is dicussed. Sections 3.1 and 3.2 review the formation of recombination and collisionally excited lines, with a brief dicussion in §3.2 of the determination of electron density and electron temperature. In section 3.3 the ionic abundances and ionisation correction factors, are calculated, and the final elemental abundances are presented in Tables 3.5(c) and 3.6(c).

3.1 The recombination lines

In equilibrium, the temperature of a nebula is fixed by the balance between the heating caused by photoionisation, and the cooling by the collisionally excited emission lines and the nebular continua radiation. Following photoionisation of an H, or He atom, or an He^+ ion, the kinetic energy of the free electron is rapidly distributed by collisions with other ions before it finally recombines (similar, but less significant, heating is caused by the photoionisation of any species although it is not included here). The difference in energy between the electron immediately following photoionisation, and at the recombination is the net energy gain of the nebula per ionisation.

The ionisation structure of the nebula is determined by the assunmed ionisation equilibrium at each point in the nebula, that is, at all points the number of ionisations

equals the number of recombinations:

$$N_{X^{m+}} \int_{\nu_{X^{m+}}}^{\infty} \frac{4\pi J_\nu}{h\nu} a_\nu(X^{m^+})\, d\nu = N_e N_{X^{m+}} \alpha(X^{m^+}, T_e), \tag{3.1}$$

where J_ν is the mean intensity of the radiation field, $a_\nu(X^{m^+})$ is the photoionisation cross-section for the ion X^{m^+}, $m = 0, 1, 2$, etc, $\nu_{X^{m+}}$ is the threshold ionisation frequency, and $\alpha(X^{m^+}, T_e)$ is the total recombination coefficient.

It is convinient to adopt two forms of the total recombination coefficient, one for a nebula optically thin to Lyman continuum photons, Case A, and a second for a nebula optically thick to Lyman continuum photons, Case B. In the first case the total recombination coefficient, α_A , is over all levels. In the second case the radiative transitions to the ground level are exactly matched by upward transitions from the ground level, following the absorption of a Lyman photon. Thus the total recombination coefficient for Case B, α_B , is calculated excluding the ground state, ie

$$\begin{aligned} \alpha_B(X^{m^+}, T_e) &= \alpha_A(X^{m^+}, T_e) - \alpha_1(X^{m^+}, T_e) \\ &= \sum_{2}^{\infty} \alpha_n(X^{m^+}, T_e). \end{aligned} \tag{3.2}$$

Recombination coefficients for each level must also be calculated for each of the two cases, and are generally denoted as effective recombination coefficients, α^{eff} . For most nebulae,and all in this study, Case B applies, with the emission coefficient in the transition n to n' being given by

$$4\pi j_{n \to n'} = h\nu_{n \to n'} N_e N_{X^{m+}} \alpha^{eff}_{n \to n'}(X^{m^+}, T_e). \tag{3.3}$$

3.2 Collisionally excited line radiation, electron temperature, and electron density.

Radiative decay of collisionally excited lines of common ions is the most important cooling process in a nebula. Such ions as O^+ , O^{++} , and N^+ make an important contribution to cooling because they possess energy levels at potentials of the order of

kT. Also, the low lying excited levels of such ions arise from the same configuration as the ground level, and radiative transitions are forbidden between them and the ground level by the electric-dipole selection rules, but can occur by magnetic dipole, or electric quadrupole transitions. In practical terms this has the effect that a downward radiative transition from a low lying excited state emits a photon that is unlikely to be absorbed on its passage through the nebula, and, since the population of these levels is kept relatively high by the large number of collisional excitations, the energy lost through these emissions produces a significant cooling of the nebula.

Although many ions have more than two low lying energy levels, see for example the energy levels of O^{++} and N^{+} , Fig. 3.1, a simple treatment of a two level system can illustrate the major physical concepts involved. For a system of two levels, i and j , then, the cross-section for collisional excitation is given by

$$\sigma_{ij}(v_i) = \frac{\pi\hbar^2}{mv_i^2}\frac{\Omega_{ij}}{\omega_i} \tag{3.4}$$

and for collisional de-excitation by

$$\sigma_{ji}(v_j) = \frac{\pi\hbar^2}{mv_j^2}\frac{\Omega_{ij}}{\omega_j} \ , \tag{3.5}$$

where ω_i and ω_j are the statistical weights of the lower and upper levels respectively, $\Omega_{i,j}$ is the collision strength, and the velocities v_i and v_j are related by their kinetic energies and the energy difference of the two levels, χ_{ij}:

$$\frac{1}{2}mv_i^2 = \frac{1}{2}mv_j^2 + \chi_{ij}. \tag{3.6}$$

The transition rate for collisional de-excitation (per electron, per ion, per unit volume, per unit time) is given by

$$q_{ji} = \int_0^\infty v\sigma_{ji}(v)f(v)\,dv \tag{3.7}$$

and the collisional de-excitation rate (per unit volume, per unit time), for a Maxwellian velocity distribution, $f(v)$, is

$$N_eN_jq_{ji} = N_eN_j\frac{8.629\times10^{-6}}{T_e^{0.5}}\frac{\Upsilon_{ij}}{\omega_j}. \tag{3.8}$$

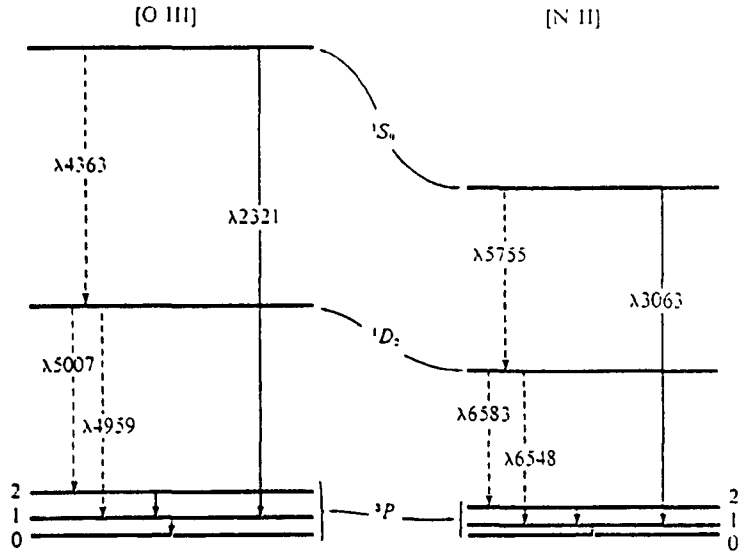

Figure 3.1

Energy level diagram for the lowest terms of O^{++}, all from the ground $2p^2$ configuration, and for N^+, of the same isoelectronic sequence (from Osterbrock, 1974).

Where Υ_{ij} is the mean collision strength given by

$$\Upsilon_{ij} = \int_0^\infty \Omega_{ij}(E_j) exp\left(\frac{-E_j}{kT}\right) d\left(\frac{E_j}{kT}\right), \quad \text{for} \quad E_j = \frac{1}{2} m v_j^2.$$

In collisional equilibrium the Boltzmann equation applies, and the ratio of the two populations is given by

$$\frac{N_j}{N_i} = \frac{\omega_j}{\omega_i} exp\left(\frac{-\chi_{ij}}{kT}\right) \tag{3.9}$$

where the ratio of the two transition rates is, similarly, given by

$$\frac{q_{ij}}{q_{ji}} = \frac{\omega_j}{\omega_i} exp\left(\frac{-\chi_{ij}}{kT}\right). \tag{3.10}$$

The collisional excitation rate (per unit volume, per unit time) is therefore given by

$$N_e N_i q_{ij} = N_e N_i q_{ji} \frac{\omega_j}{\omega_i} exp\left(\frac{-\chi_{ij}}{kT}\right). \tag{3.11}$$

In this simple model the collisional excitation rate equals the collisional de-excitation rate, plus the radiative de-excitation rate, ie

$$N_e N_i q_{ij} = N_e N_j q_{ji} + N_j A_{ji} \tag{3.12}$$

and with a constraint for the total number of ions, $N_{ion} = N_i + N_j$, equation 3.12 can be solved for the populations of both levels, and hence the emission rate for the radiative transition $j \rightarrow i$.

In a more general case collisional or radiative transitions could occur between any of the low lying levels, and the equilibrium equation for such a system is

$$\sum_{j \neq i} N_e N_j q_{ji} + \sum_{j>i} N_j A_{ji} = \sum_{j \neq i} N_e N_i q_{ij} + \sum_{j<i} N_i A_{ij} \tag{3.13}$$

which, with the normalising constraint that $\sum_i N_j = 1$, can be solved for the relative populations of all levels. The critical density where collisional de-excitations become dominant over radiative de-excitations is now given by

$$N_{crit}(j) = \sum_{j>i} A_{ji} \Big/ \sum_{j>i} q_{ji}. \tag{3.14}$$

From the solution of equation 3.13 for the population of any two levels i and k , the ratio of any two collisionally excited emission lines is

$$R = \frac{N_i \nu_{ij} A_{ij}}{N_k \nu_{kl} A_{kl}}. \tag{3.15}$$

In this study the program *EQUIB* (written by I.D.Howarth, UCL, and modified by S.Adams, UCL) was used to solve equation 3.13, with the transition probabilities and collision strengths listed in Table 3.1. The resulting population levels are used to calculate line intensity ratios, which, in general, will be a function of both T_e and N_e , and, by comparison with observed values, can be used as nebular diagnostics.

For ions that have two well seperated, low lying, energy levels, the ratio of the two emission lines produced by decays from these to lower energy levels provides a measure of the electron temperature, as the exponential term of equation 3.11 becomes dominant. The auroral-nebular (^{1}S,^{1}D) transition, and nebular (^{1}D,^{3}P) transitions of

Table 3.1 References for atomic data.

Ion	Transition Probability	Collision Strength
NII	Nussbaumer & Rusca, 1979.	Seaton, 1975.
OII	Zeippen ,1982.	Pradhan, 1976.
OIII	Nussbaumer & Storey, 1981.	Baluja, Burke & Kingston, 1980.
NeIII	Mendoza, 1983.	Butler & Mendoza, 1984.
SII	Mendoza & Zeippen, 1982.	Mendoza, 1983.
ArIII	Mendoza & Zeippen, 1983.	Krueger & Czyzak, 1970.
ArIV	Mendoza & Zeippen, 1982.	Krueger & Czyzak, 1970.

O III and N II (see Fig. 3.1) are good examples of decays between levels well seperated in energy and are used as the main T_e diagnostics for PN.

For other ions with two excited levels which are very close in energy, *e.g.* the $^2D_{\frac{3}{2}}$ and $^2D_{\frac{5}{2}}$ levels of O II (see Fig. 3.2), the ratio of the emission line intensities produced by decays from these levels to the ground level can be used as an electron density diagnostic, since the collisional excitation rate will now depend on the relative collision strengths involved (the exponential terms in equation 3.11 now cancelling). The ratio of the collisionally excited emission lines from two such levels has an upper and lower limit, determined by the ratio of the collision strengths at the low density limit, when collisional de-excitations are negligible, and by a Boltzmann distribution at the high density limit, where collisional de-excitations are dominant. The upper and lower limits for the O II ratio are 1.5 and 0.35 respectively, corresponding to density limits of ~100 and ~20000 cm^{-3}. Between these two limits the ratio depends upon the quantity $N_e/T_e^{0.5}$, and can be used as a density diagnostic.

The resolutions of the spectra in this study are not high enough to resolve the [O II] doublet; but, for 21 PN, data on the [O II] doublet were available from higher resolution AAT IPCS observations (Barlow, 1986). The derived electron densities, N_e(O II), are given in Table 3.2. For objects not included in this list a typical electron density of 5000 cm^{-3} was adopted.

An electron temperature, T_e(O III), was calculated from all but six of the medium resolution spectra by deconvolving the [O III]4363 Å line from Hγ (see § 2.2). The total error in the value of T_e(O III) is determined mainly by the error in the 4363 Å

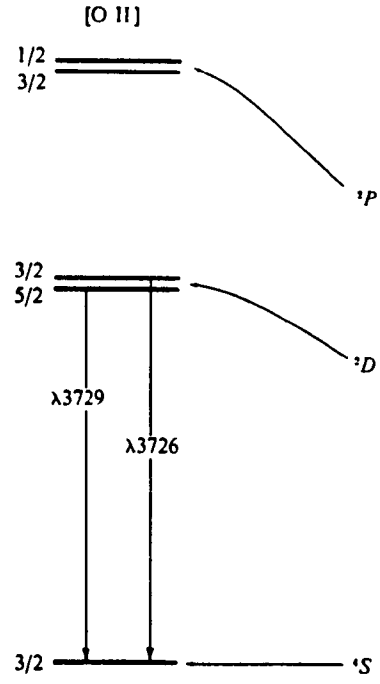

Figure 3.2

Energy level diagram of the $2p^2$ ground configuration of O^+ (from Osterbrock, 1974).

line intensity and more confidence can be placed in the temperatures derived from the medium resolution spectra than those from the low resolution spectra.

The electron temperature of the N^+ region , T_e(N II), was also calculated using lines which suffer some blending but in this case the overall error is determined mainly by the error in the 5755 Å line intensity. This line was absent in most spectra , but was clearly present in the spectra of the Type I LMC planetaries N28, N66, N77F, N97, N102, N122 and N181.

The calculated values of T_e(O III), T_e(N II) are given in Tables 2.1(a) - 2.1(d), at the bottom of the 'relative line intensity' column for each object. For the cases where no T_e(O III) or T_e(N II) value could be derived a temperature of 10000 K was adopted.

A check on the accuracy of the derived temperatures is provided by comparing the values obtained from the medium and low resolution spectra with those of Aller et al (1981), and Aller (1983); see Table 3.3. The comparison shows reasonable agreement between the data sets with a spread of $\sim$ 10 % about the derived mean values. To be self

Table 3.2 [O II] electron densities, from Barlow (1986)

LMC	[OII] Electron Density (cm^{-3})	SMC	[OII] Electron Density (cm^{-3})
N28	7900	N2	2850
N66	2600	N4	1850
N97	2400	N5	3900
N102	8100	N6	$\geq$26000
N110	$\geq$22000	N8	380
N122	2230	N38	7150
N133	$\geq$66000	N40	3250
N141	7700	N43	8800
N153	4580	N44	4600
N178	3960	N70	4200
N184	3500	N87	6600
N201	4800	L66	250
N203	$\geq$30000	L239	390
LM1-61	2000	L302	900
		L305	$\geq$40000
		L536	1930

consistent within this analysis it was decided to adopt the electron temperatures derived from the medium resolution spectra, where available (final column of Table 3.3), and again these adopted values are within $\sim$ 10 % of the derived mean value. This scatter of 10 % , though, is probably a lower limit on the overall accuracy, as it is derived from a comparison between the brighter objects in the sample, although the comparison of electron temperatures derived from low and medium resolution spectra does include some fainter PN.

3.3 Elemental abundances

The He^+ and He^{++} abundances relative to H^+ were derived from the equation;

$$\frac{N(He^{m+})}{N(H^+)} = \frac{I(\lambda)}{I(H\beta)} \frac{\alpha^{eff}_{H\beta}(N_e, T_e(H^+))}{\alpha^{eff}_{He^{m+}}(N_e, T_e(He^{m+}))} \frac{\lambda(\mathring{A})}{4861} \tag{3.16}$$

where the recombination coefficients, $\alpha^{eff}_{H\beta}, \alpha^{eff}_{He^{m+}}$ were taken from Brocklehurst (1971, 1972). The [O III] electron temperature was adopted for $T_e(H^+)$ and $T_e(He^{m+})$.

The ionic abundances derived from the He I 6678 Å , 4471 Å , and 5876 Å lines have significantly different errors associated with them, due mainly to the different intensities of the lines, and partly to the wavelength region in which they fall (see Table 2.2). The instrumental sensitivity is different for each wavelength region, with a high sensitivity at the central wavelengths and a gradual fall off towards the detector edges. This sensitivity variation is unimportant for the low resolution spectra since the three He I lines in question fall close to the central zone of the detector. For the medium resolution spectra, however, the 4471 Å and 6678 Å lines fall close to the outer, less sensitive, zones of the detector.

It was decided, therefore, to adopt He^+ abundances based on different procedures for the medium and low resolution spectra. The adopted He^+ abundance for the low resolution spectra is the weighted (1:3:1) mean of the abundances derived from the 4471 Å , 5876 Å , and 6678 Å lines respectively, as instrument sensitivity variations can be ignored, and the weighting applied is directly related to the signal to noise ratios of the three lines. For the medium resolution spectra the abundance was derived from the 5876 Å line alone due to its higher signal to noise ratio and its placement in the highest sensitivity region of the detector.

The ionic abundance of an ion X^{m+}, relative to H^+, for the collisionally excited lines is given by

$$\frac{N(X^{m+})}{N(H^+)} = \frac{\alpha^{eff}_{H\beta}}{N_i A_{ij}} \frac{\lambda}{4861} \frac{F(\lambda)}{F(H\beta)}, \tag{3.17}$$

where equation 3.13 is solved to obtain the relative population of the ith level, N_i . When only T_e(O III) was available it was adopted for $T_e(X_i)$ for all ions; if T_e(N II) was also available it was adopted for $T_e(X_i)$ for the O^+ , N^+ , and S^+ ions. The sources for the atomic data used are listed in Table 3.1.

The calculation of the elemental abundances was limited by the absence of optical lines from the higher ionic species of most elements. However, it is possible to make an empirical correction to the lower stage ionic abundances in order to give the total elemental abundances (Peimbert and Torres-Peimbert, 1971). Barker (1983) has recently discussed ionisation correction procedures for He, O, N, Ne, Ar, and S, and has found

a reasonable agreement between element abundances calculated from optical lines only (using the necessary ionization correction factors, ICF), and those derived using *IUE* observations of lines from higher ionic stages to supplement the optical data.

The ionisation correction procedures for He, O, N, Ne, and Ar used by Torres-Peimbert and Peimbert (1977), Barker (1983), and Barker (1980) are adopted here:

$$He/H = (He^{+}/H^{+}) + (He^{++}/H^{+})$$

$$O/H = ((O^{+}/H^{+}) + (O^{++}/H^{+})) \times ICF(O)$$

$$N/H = (N^{+}/H^{+}) \times ICF(N)$$

$$Ne/H = (Ne^{++}/H^{+}) \times ICF(Ne)$$

$$Ar/H = 1.5 \times (Ar^{++}/H^{+})$$

where

$$ICF(O) = (He^{+}+He^{++})/He^{+}$$

$$ICF(N) = O/O^{+}$$

$$ICF(Ne) = O/O^{++} .$$

The absence, or blending, of the 6312 Å [S III] line meant that no correction procedures could be applied for sulphur and therefore no total sulphur abundances could be derived from the S^{+} ionic abundances. The Ar^{++} and total Ar abundances could only be derived from the low-resolution spectra, since the wavelength coverage of the medium resolution spectra did not extend to [Ar III] 7135 Å .

The ionic and elemental abundances derived by the procedures outlined above are presented in Tables 3.4(a) to 3.4(c) for the eight objects with both medium and low resolution spectra. Tables 3.5(a) to 3.5(b) for the LMC PN, and Tables 3.6(a) to 3.6(b) for the SMC PN, present the ionic abundances of the objects with either a single low resolution or a single medium resolution spectra, and Tables 3.4(c) and 3.6(c) give the elemental abundances for all LMC and SMC objects in this survey.

From comparison of Tables 3.4(a, b, and c) it is possible to estimate the effects of the corrections applied to the medium resolution [O II]3727 Å and [Ne III]3868 Å line intensities (see § 2.3). The correction to the [O II] line will increase the derived oxygen abundance of each object by varying amounts depending on the contribution to the total oxygen abundance of the O^{+} ion relative to that of the O^{++} ion. In two cases, LMC

N99 and LMC N101, the O^+ ions make the dominant contribution and the abundance will increase in almost direct proportion to O^+ . For all other objects the correction for the derived oxygen abundance is less than 33% , and for the majority of these objects it is less than 6% .

Comparison of the O^+ abundances derived from the low and medium resolution spectra (Table 3.4(b)) shows agreement to within 30% for all objects except LMC LM1 27. For this case the [O II]3727 Å line intensity from the low-resolution spectra is probably the more reliable, and the low resolution values of the O^+ ionic abundance should be adopted for this PN. Comparison of the oxygen abundances (Table 3.4(c)) shows better agreement (within 20%) reflecting the small effect that the uncertainty in O^+ abundance has on this value for the majority of the PN studied.

Owing to the placement of [Ne III]3868 Å on a lower sensitivity region of the detector, neon abundances derived from the medium resolution spectra are significantly less reliable than those derived from the lower resolution spectra. Since O^{++} generally dominates over O^+, the ICF for Ne, and thus the derived Ne abundances, are not very sensitive to uncertainties in the O^+ abundance derived from [O II]3727 Å . From the comparison of ionic abundances, Table 3.4(b), it can be seen that there is agreement for Ne^{++} to within 30% for all objects. The agreement between low and medium resolution spectra for the derived Neon abundances, Table 3.4(c), is generally within 25% .

The total nitrogen abundances derived are inversely proportional to the [O II] 3727 Å line intensity, since the latter affects the nitrogen ICF in a linear manner (the nitrogen ICF of LMC N99 and LMC N101 being unaltered overall). Comparison of N^+ ionic abundances from the low and medium resolution spectra (Table 3.4(b)) shows reasonable agreement, although the values derived from the medium resolution data should be less uncertain, because of better resolution of the Hα, [N II] blend, and should therefore be adopted.

For most cases a comparison of the derived nitrogen abundances (Table 3.4(c)) shows reasonable agreement, except where the [O II]3727 Å line is either 'very uncertain' (designated ::) or an upper limit, which then leads to a very uncertain value, or lower limit, for the nitrogen ICF. For LMC N184, however, the two O^+ ionic abundances are in good agreement and it is the poor N^+ abundance derived from the low resolution data that has caused the discrepancy between the elemental abundances. Where both

low-resolution and medium-resolution spectra exist, the nitrogen ICF calculated using the low resolution [O II]3727 Å line intensity, together with the N^+ ionic abundance derived from the medium resolution data, yield the most accurate value for the nitrogen abundance.

The third line in the comparison of elemental abundances for each PN, Table 3.4(c), gives the adopted abundance of each element, derived from the mean of the low and medium resolution values where appropriate or, in the cases where there was a definite difference in quality between the two data sets, from the least uncertain data as outlined above.

3.4 Discussion

In Table 3.7(a) the derived mean abundances of helium, nitrogen, oxygen, neon, and argon for the LMC and SMC PN derived in this survey are presented . The mean abundances were calculated by excluding the 'Type I' objects, the 'low oxygen' objects, and the VLE objects, as well as N101 which has an indeterminate status, and all abundances shown as uncertain (::) or as an upper or lower limit. The number of objects used to determine each mean abundance is given in brackets after the abundance value, and the mean values themselves are presented in the form log X/H +12. The approximate standard deviation is ±0.2 dex for each logarithmic abundance, ±0.04 for the LMC He abundance, and ±0.08 for the SMC He abundance.

For comparison, the mean abundances of Aller (1983) and Aller *et al.* (1981) are given in the same table (again excluding Type I, 'low oxygen', or VLE objects), as are the mean abundances for Galactic, LMC, and SMC H II regions (Dufour, 1984), and Galactic PN (Aller and Czyzak, 1983a). Table 3.7(b) gives the differences between the mean elemental abundances of H II regions and PN (using the data of Aller and Czyzak, 1983a, Dufour, 1984, and the present study) for the LMC, SMC, and our own galaxy.

From a comparison of the mean abundances of the present study with those of Aller (1983), and Aller *et al.* (1981), for the LMC and SMC it is seen that there is good general agreement, allowing for an error of the order of 0.2 dex between the data

Table 3.7(a) Mean abundances for LMC, SMC and Galactic PN and H II regions.

		Mean Abundance (Log X/H + 12)					
		He	N	O	Ne	Ar	log N/O
LMC PN	a	11.02 (34)	7.66 (30)	8.49 (36)	7.63 (36)	5.91 (13)	-0.83
SMC PN	a	11.00 (16)	7.19 (7)	8.25 (15)	7.37 (13)	5.70 (11)	-1.06
LMC PN	b	11.07	7.38	8.31	7.60	6.08	-0.93
SMC PN	c	11.02	7.31	8.14	7.55	>5.72	-0.83
GAL PN	d	11.04	8.26	8.64	8.03	6.43	-0.38
LMC H II	e	10.93	6.97	8.43	7.64	6.20	-1.46
SMC H II	e	10.90	6.46	8.02	7.22	5.78	-1.56
GAL H II	e	11.00	7.57	8.70	7.90	6.42	-1.13

Notes:
a - This work
b - Aller (1983)
c - Aller *et al.* (1981)
d - Aller and Czyzak (1983a)
e - Dufour (1984)
Figures in brackets are the number of PN in each sample.

sets, although the helium abundance for the LMC from Aller (1983) appears to be a little high. It should also be noted that the mean nitrogen abundance for the SMC (this work) is likely to be an upper limit due to the selection of PN with moderate or high nitrogen abundance, since objects with lower nitrogen abundance are less likely to have their nitrogen emission lines detected at a measurable level.

In a comparison between the LMC PN and the LMC H II regions it is seen that there has been significant enrichment of helium and nitrogen, by 0.09 and 0.69 dex respectively, whilst abundances of oxygen, neon, and argon have remained reasonably unchanged. A similar comparison for the SMC shows increases of 0.10 and 0.73 dex for the helium and nitrogen abundances respectively, while again the oxygen, neon, and argon abundances remain approximately the same, although the 0.23 dex increase in oxygen would appear a little large. The similarity between the helium and nitrogen enhancements for the LMC and SMC is possibly significant, and is made more so when compared to our own galaxy, which shows helium and nitrogen enhancements (PN compared to H II regions) of 0.04 and 0.69 dex respectively. These comparisons show a

Table 3.7(b) Difference in the elemental abundances of PN and H II regions.

	Difference in Abundance (PN − HII)				
	He	N	O	Ne	Ar
LMC	0.09	0.69	0.06	−0.01	−0.29
SMC	0.10	0.73	0.23	0.11	−0.08
GAL	0.04	0.69	−0.06	0.13	0.01

remarkably uniform enhancement of nitrogen (relative to hydrogen), 0.7±0.2 dex, and the possible enhancement of helium through the stars lifetime. Although the scatter on the MC PN helium abundances is quite large, there is some indication that the enhancement of helium in MC PN, compared to MC H II regions, is greater than that for PN in the Galaxy (again compared to H II regions). The consequence of this possible effect is a narrowing of the differences between the helium abundances of PN in all three galaxies, compared to the helium abundance difference for H II regions. It is possible, then, that low and intermediate mass stars mix a small but significant amount of He into their envelopes, and that the amount mixed out may well be a function of stellar metallicity.

A comparison between the mean abundances of PN within the three galaxies shows a clear difference between the two Magellanic Cloud systems and our own galaxy, with deficiencies in nitrogen, oxygen, neon, and argon abundances of 0.6, 0.15, 0.4, and 0.52 dex respectively for the LMC, and of 1.07, 0.39, 0.66, and 0.73 dex respectively for the SMC, relative to our own galaxy. The SMC is also deficient when compared to the LMC with differences in the nitrogen, oxygen, neon, and argon abundances of 0.47, 0.24, 0.26, and 0.21 dex respectively.

The relative enrichment of nitrogen to oxygen (log N/O) is also given in the final column of Table 3.7(a) for PN and H II regions in the LMC, SMC, and our own galaxy. It is noticable that the mean value of log N/O for the H II regions is appreciably different for the two Magellanic Cloud galaxies compared to our own, with the LMC and SMC H II regions having smaller mean log N/O ratios, by 0.33 and 0.43 dex respectively, and that the SMC mean log N/O ratio is slightly smaller than that of the LMC. These trends are also reflected in the mean log N/O ratios of PN in the three galaxies, with differences

Table 3.8 Abundances of 'Type I' PN. (log X/H + 12)

Object or Class	He	N	O	Ne	log N/O
Type I ‡	>11.20	9.0	8.8	8.2	>0.2
Type I ‡‡	>11.10	9.0	8.8	8.2	> −0.3
SMC L536	11.36	7.70	7.30	<6.88	0.40
SMC L305	11.13	7.76	7.93	7.26	−0.17
LMC N97	11.18	8.38	8.28	7.55	0.10
LMC N102	11.25	8.27	8.15	7.37	0.12
LMC N122	11.20	8.52	8.27	7.61	0.25
LMC N181	11.09	8.71	8.74	8.32	−0.03
LMC N28	11.03	8.13	8.61	7.68	−0.48
LMC N66	11.03	8.15	8.51	7.74	−0.36
LMC N77F	11.06	8.39	8.69	7.75	−0.30
LMC N221	11.01	8.38	8.64	7.54	−0.26

Notes: ‡ - Peimbert (1978) ‡‡ - Peimbert and Torres-Peimbert (1982)

of 0.45 and 0.68 dex between our own galaxy and the LMC and SMC respectively, and a difference of 0.23 dex between the LMC and SMC.

Table 3.8 presents the abundances (log X/H + 12) of the helium- and nitrogen-rich PN of this survey as well as the classification for Galactic Type I PN (Peimbert, 1978, and Peimbert and Torres-Peimbert, 1983). On comparison with Peimbert's classification the first five PN in Table 3.8, SMC L536, LMC N97, N102, N122, and N181, seem to fall clearly into the Type I class of objects, where helium and nitrogen are enhanced by the three dredge up processes which are thought to be operating in the final stages of Red Giant evolution and throughout the AGB phase (Iben and Renzini, 1983, and references therein). LMC N97 and N102 have previously been reported as possible Type I PN by Aller (1983).

The enhancement of nitrogen, and helium, relative to hydrogen, and the enrichment of nitrogen relative to oxygen, (log N/O), for these objects compared to other LMC and SMC PN, are clearly seen in the plots of log N/H *vs.* He/H, log N/O *vs.* He/H, and log N/H *vs.* log O/H (Fig. 3.3 (a), (c), and (d), and Fig. 3.4 (a), (c), and (d), for the

Table 3.9 Abundances of 'low oxygen' PN (log X/H + 12)

Object	He	N	O	Ne	log
K648 (in M15)	11.00	6.07	7.67	6.53	−1.60
H 4-1	10.99	7.75	8.36	6.70	−0.61
BB-1	10.98	8.34	7.90	8.00	0.44
DDDM 1	11.02	7.4	8.1	7.3	−0.7
SMC N1	10.85	6.80::	7.67::	<6.52	−0.87
SMC N42	10.96	6.07::	7.41::	<6.98	−1.40
LMC N1	11.04	>6.42	7.64::	<6.74	> −1.22
LMC N25†	10.72	6.89::	7.62::	<5.85	−0.73
LMC N199	10.73	7.18::	7.74::	<6.73	−0.56
LMC S1	11.08	6.31::	7.53::	<6.91	−1.22

Notes to Table 3.9. † -Abundances for N25 from IPCS spectra, see §5.1.

LMC and SMC respectively). Figs. 3.3 (b) and 3.4 (b), log O/H *vs.* He/H, also show that SMC L536, L305, LMC N97, N102, and N122 exhibit signs of oxygen depletion.

A second group of objects also stands out as possible Type I PN, namely LMC N28, N66, N77F, and N221. These objects have enhanced nitrogen relative to hydrogen, N/H > 10^{-4}, compared to the mean LMC N/H value of 4.57 $\times 10^{-5}$, (see Fig. 3.3 (a)), and enhanced nitrogen relative to oxygen, log N/O > -0.3, compared to the mean LMC log N/O value of -0.83 (see Fig. 3.3 (c)). The helium abundance is only marginally increased, if at all, in these PN, but as these objects have a lower ZAMS helium abundance than PN of our own galaxy it is possible that the He/H abundance of the Peimbert and Torres-Peimbert (1983) Type I classification provides too severe a constraint for the Magellanic Cloud objects.

The group of PN with very low oxygen abundances, LMC N1, LMC N25, LMC N199, LMC S1, SMC N1, and SMC N42, stand out clearly on the plots of log O/H *vs.* He/H, Figs 3.3 (b) and 3.4 (b). The abundances of these objects are compared to the abundances of the known low-Z 'Halo' PN of our own galaxy (Torres-Peimbert *et al.* , 1981; Barker, 1980,1983), Table 3.9, and are remarkably similar although the nitrogen abundances of the Magellanic Cloud low oxygen PN are distinctly lower than those of the 'Halo' PN, presumably a reflection of the different initial compositions of the two groups of objects.

The elemental abundances of LMC N25, Table 3.9, are derived from recent wide and narrow slit IPCS spectra, with resolutions of 9.8 Å FWHM and 4.4 Å FWHM respectively (a full discussion of these observations is given in Chapter 5). Webster (1976) reported that this object is a possible member of the LMC red globular cluster NGC 1852, and was able to estimate a nitrogen abundance of 0.1 to 0.05 of the Solar value and an ionic abundance He^+/H^+ of 0.07, which give approximate agreement with the the results reported here.

The helium abundances of LMC N25 and LMC N199 are both remarkably low compared to the mean value for the LMC PN, which is possibly a consequence of LMC N25 and LMC N199 having a substantial amount of neutral helium. However, the the central star contribution to both the IDS spectra of LMC and SMC PN (Chapter 4), and the separate IPCS spectra for N25 (Chapter 5), show that these two nebulae have central star temperatures of the order of 40000-45000 K. This moderately high central star temperature coupled with the moderate excitation of each nebula ([O III] 5007 Å+4959 Å/[O II] 3727 Å $\geq$1) suggests that only a small amount of neutral helium may exist. It is therefore possible that LMC N25 and LMC N199 have substantially lower helium abundances than the other LMC PN.

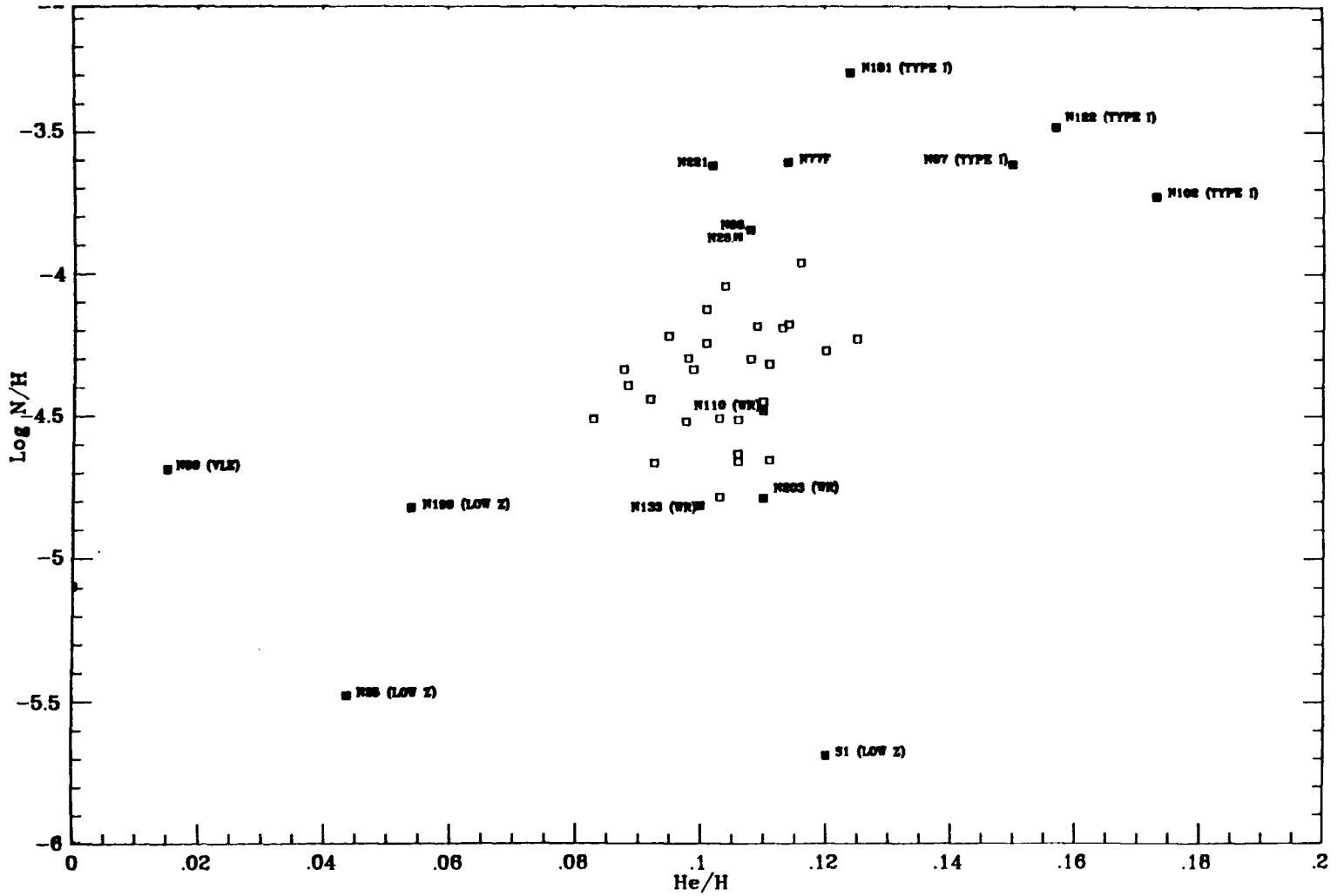

Figure 3.3(a). *Elemental abundance variations for LMC PN: log N/H vs. He/H.*

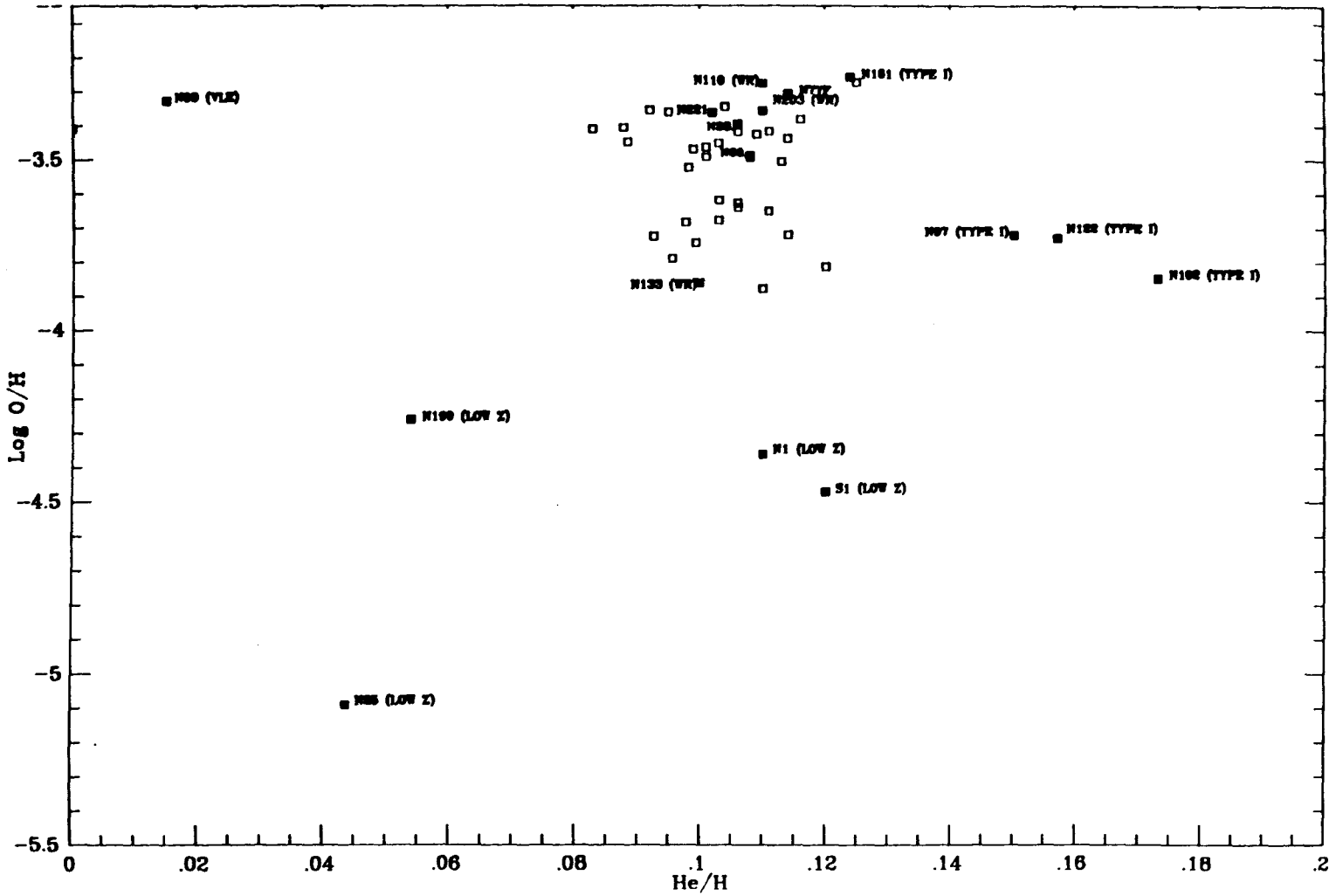

Figure 3.3(b). *Elemental abundance variations for LMC PN: log O/H vs. He/H.*

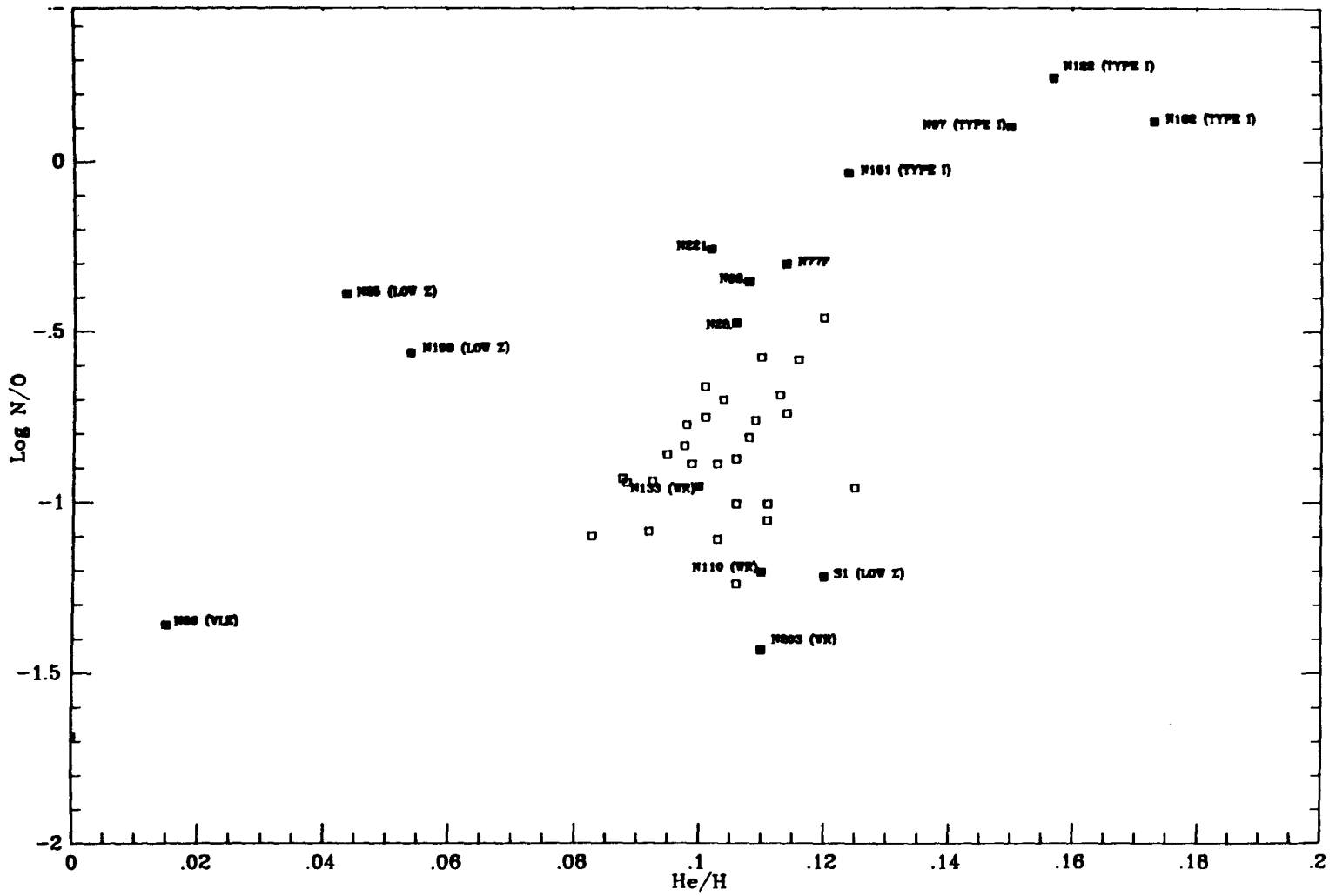

Figure 3.3(c). *Elemental abundance variations for LMC PN: log N/O vs. He/H.*

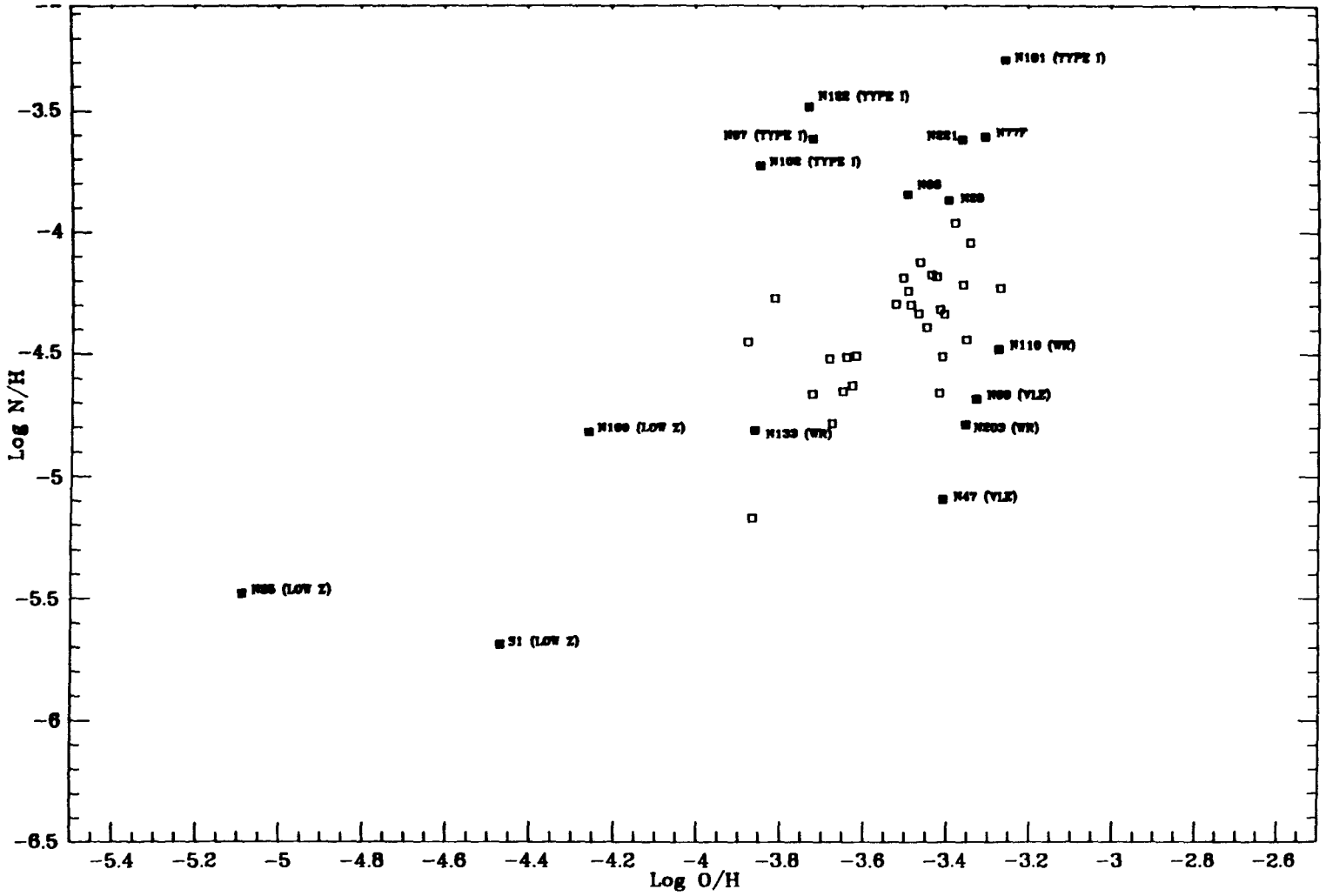

Figure 3.3(d). *Elemental abundance variations for LMC PN: log N/H vs. log O/H.*

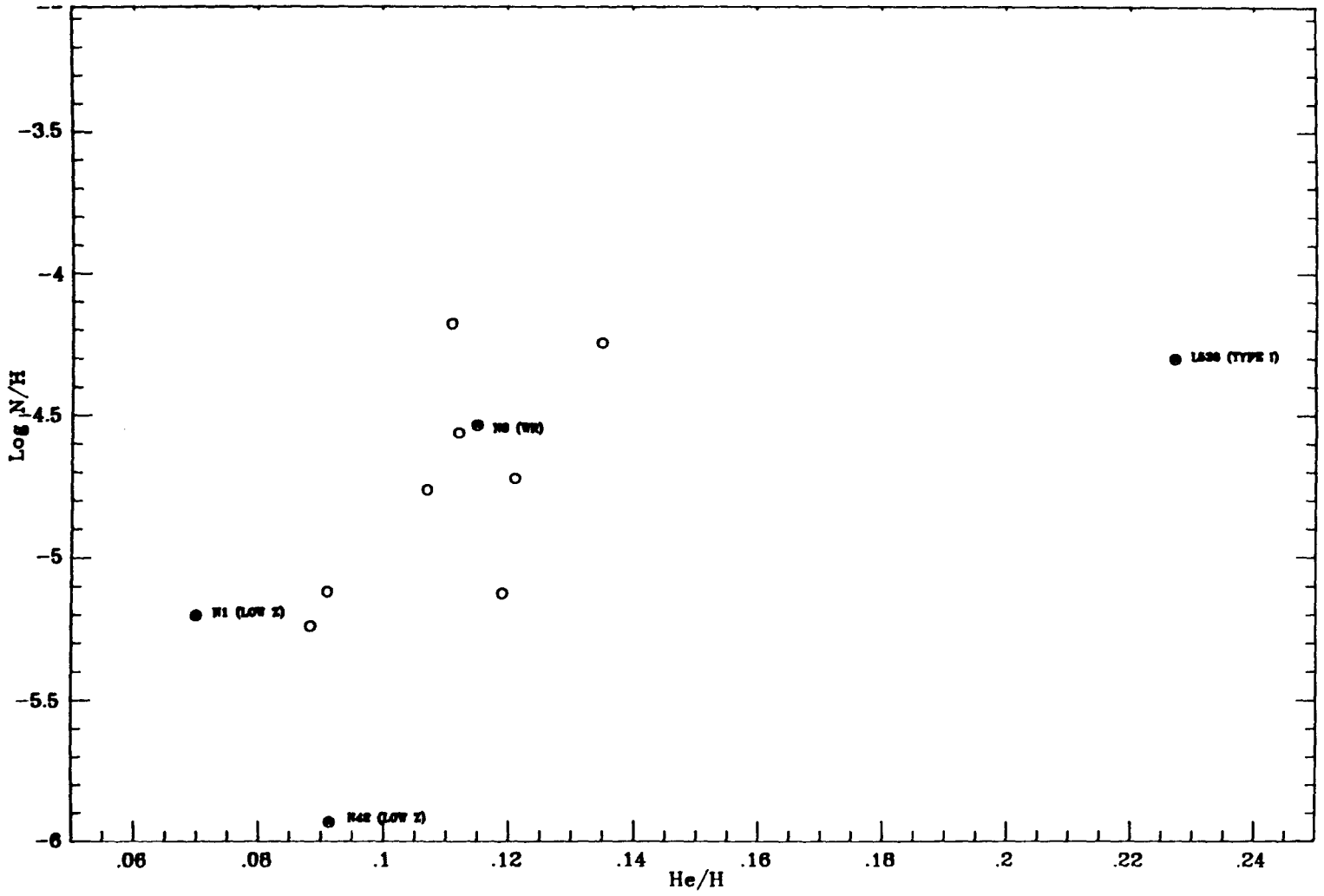

Figure 3.4(a). *Elemental abundance variations for SMC PN: log N/H vs. He/H.*

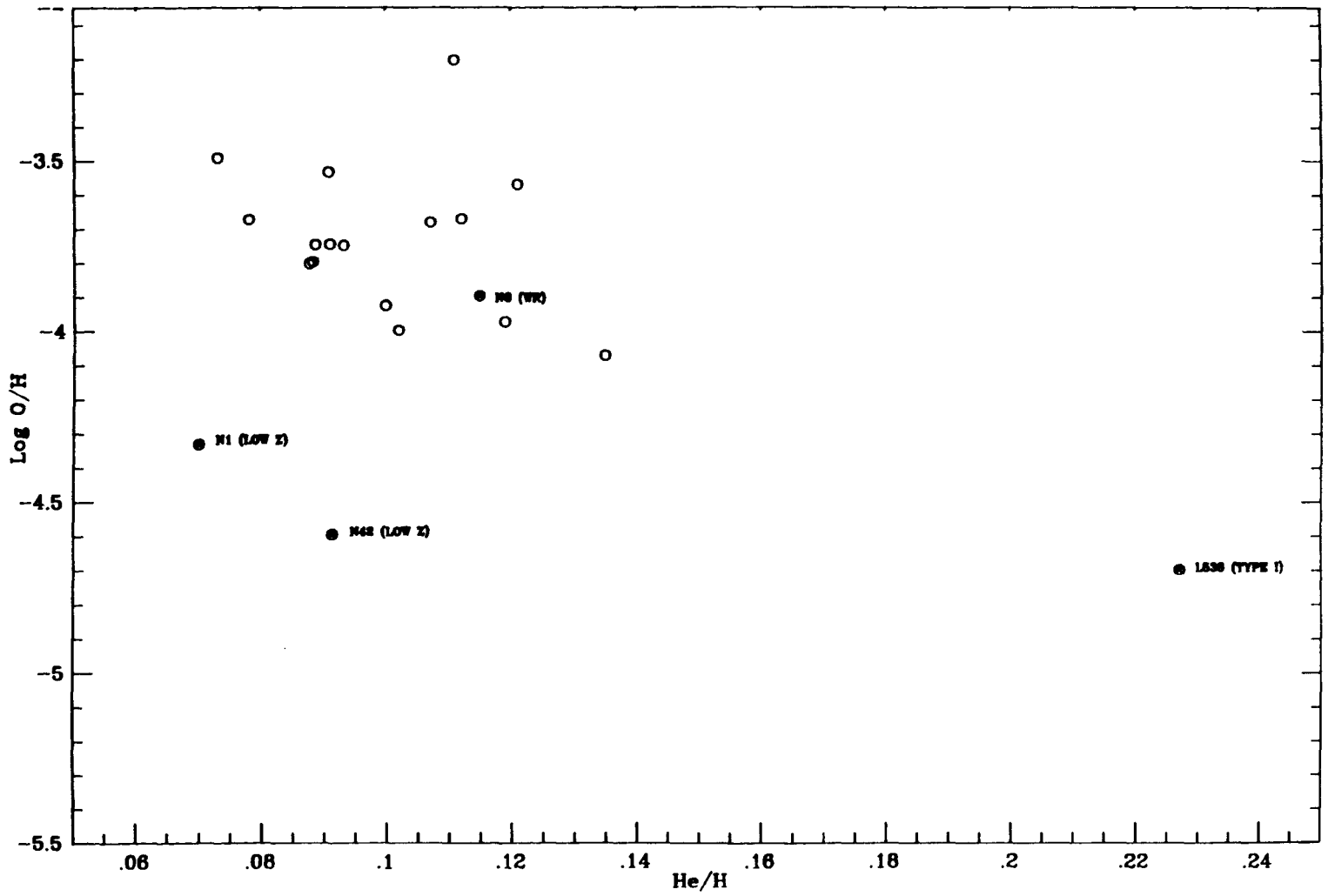

Figure 3.4(b). *Elemental abundance variations for SMC PN: log O/H vs. He/H.*

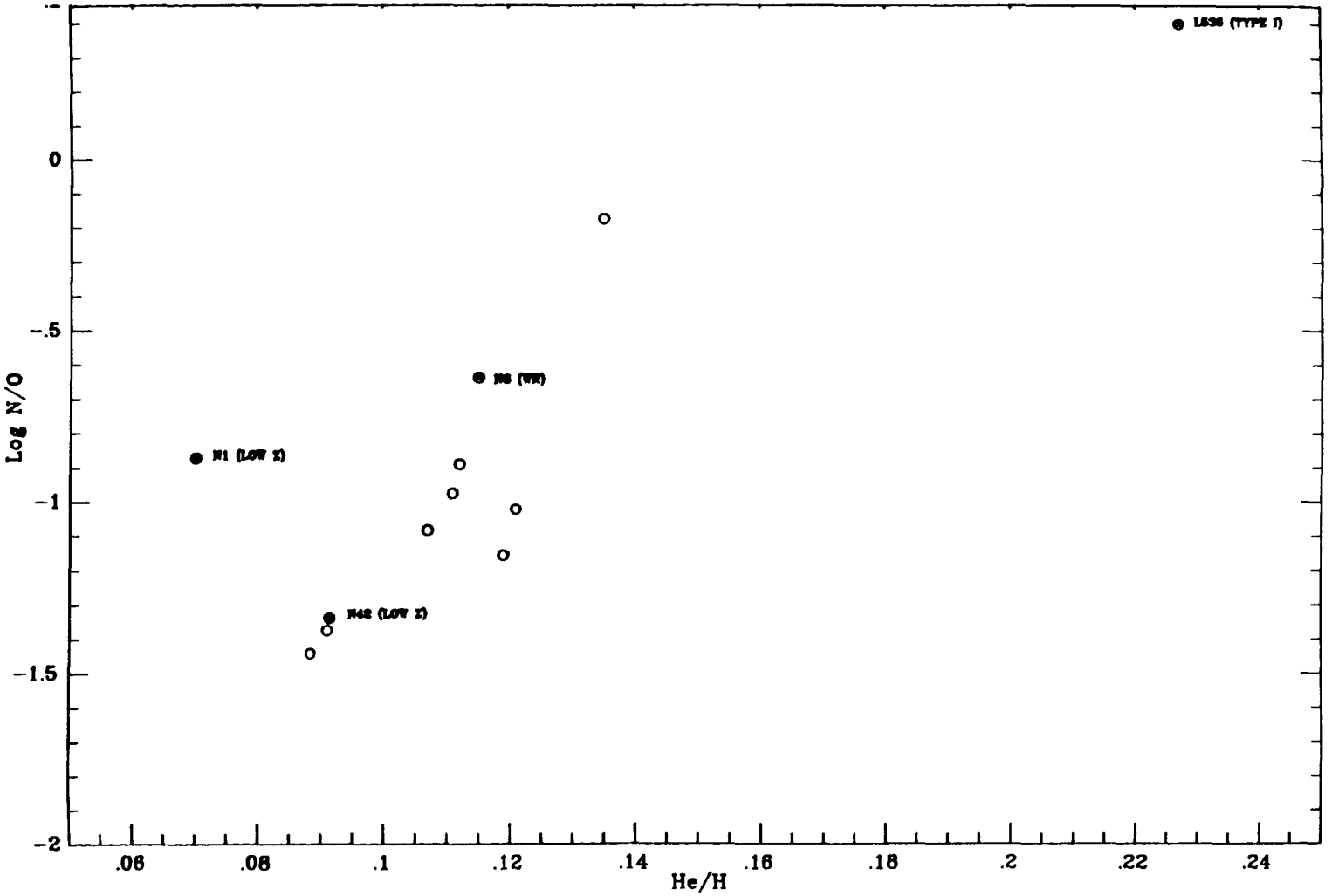

Figure 3.4(c). *Elemental abundance variations for SMC PN: log N/O vs. He/H.*

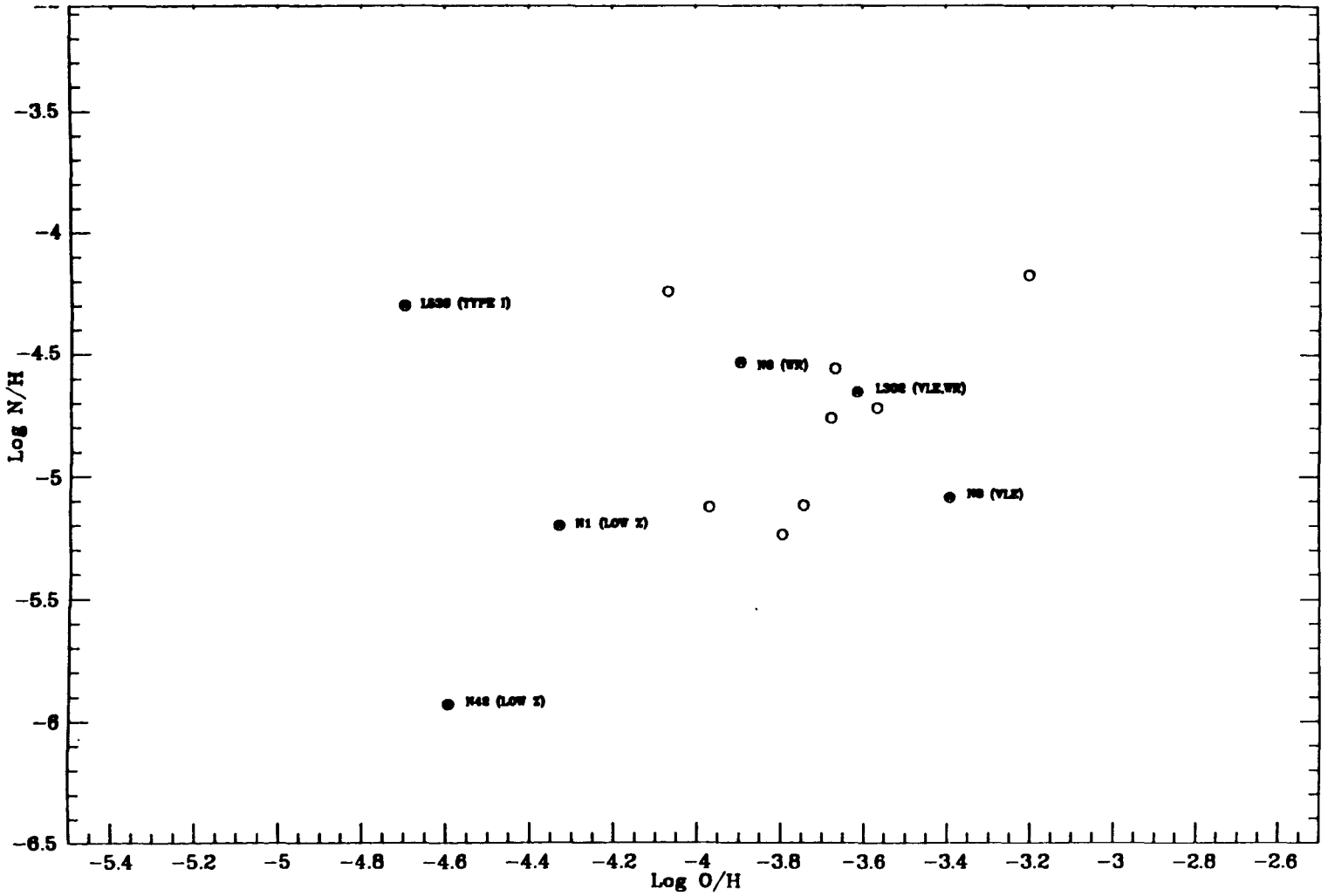

Figure 3.4(d). *Elemental abundance variations for SMC PN: log N/H vs. log O/H.*

Table 3.3 Comparison of electron temperatures.

Object	Ion	Electron Temperature			
		Medium	Low	Aller (1983) or Aller *et al.*(1981)	Adopted
LMC N24	[OIII]		12250	11370	12250
	[NII]				
LMC N42	[OIII]	15750	16000		15750
	[NII]				
LMC N66	[OIII]	15000	17750		15000
	[NII]	11000	11750		11000
LMC N97	[OIII]		20500	19500	20500
	[NII]		11000	11800	11000
LMC N102	[OIII]	22250	19250	19000	22250
	[NII]	12000	13250	14400	12000
LMC N104	[OIII]	13750	12750		13750
	[NII]				
LMC N153	[OIII]	13000		13600	13000
	[NII]				
LMC N178	[OIII]	12000		13000	12000
	[NII]				
LMC N184	[OIII]	12750	13500	14300	12750
	[NII]			11000	11000
LMC LM1-27	[OIII]	11250	15000		11250
	[NII]				
LMC LM1-61	[OIII]	14500		15000	14500
	[NII]				
SMC N1	[OIII]	(12750)	(15250)		(12750)
	[NII]				
SMC N2	[OIII]		13250	12800	13250
	[NII]				
SMC N5	[OIII]		14250	13000	14250
	[NII]				
SMC N6	[OIII]	14250	15250		14250
	[NII]	10000			10000

Table 3.4(a) Comparison of Helium abundances derived from medium and low resolution spectra.

OBJECT		He^+ (6678)	He^+ (4471)	He^+ (5876)	He^+ (Adopted)	He^{2+} (4686)
LMC						
N42	M	0.126		0.127	0.127	
N42	L	0.106	0.074	0.094	0.092	
N66	M			0.061	0.061	0.053
N66	L			0.043	0.043	0.058
N102	M		0.120	0.107	0.107	0.072
N102	L	0.113	0.111	0.100	0.105	0.064
N104A*	M			0.077	0.077	0.034
N104A	L	0.084		0.068	0.072	0.033
N184	M	0.111	0.076	0.080	0.080	0.039
N184	L	0.063	0.078	0.067	0.069	0.035
LM1-27	M			0.079	0.079	0.010
LM1-27	L	0.095		0.087	0.089	0.012
SMC						
N1	M	0.098	0.118	0.067	0.067	
N1	L	0.086	0.065	0.072	0.073	
N6	M	0.136	0.139	0.122	0.122	
N6	L	0.138	0.093	0.101	0.107	

Notes on Tables 3.4 (a),(b),(c):

a - Abundance calculated using Barlow (1986) flux.

b - ICF calculated using Barlow (1986) flux.

c - Abundance calculated using the N^+ abundance from the medium resolution spectra, and the N(ICF) calculated from the low resolution spectra.

:: - Abundance calculated using an uncertain flux, or T_e.

: - Abundance calculated using an assumed temperature of 10000 K.

* - Very low signal-to-noise spectrum

Table 3.4(b) Comparison of ionic abundances derived from medium and low resolution spectra.

OBJECT		N^+ (6585)	O^+ (3727)	O^{2+} (5007)	Ne^{2+} (3868)	S^+ (6717,31)	Ar^{2+} (7135)	Ar^{3+} (4740)
LMC								
N42	M	4.7(-6)	< 2.0(-5)	1.4(-4)	< 2.1(-5)	1.2(-7)		
N42	L	2.4(-6)	1.8(-5)	1.2(-4)	2.0(-5)	1.6(-7)	2.8(-7)	
N66	M	1.8(-5)	3.5(-5)a	1.1(-4)	2.1(-5)	3.7(-7)		1.0(-6)
N66	L	1.9(-5)	4.3(-5)	9.4(-5)	1.7(-5)	5.3(-7)	4.4(-7)	2.1(-6)
N102	M	4.6(-5)	3.2(-5)	5.4(-5)	7.9(-6)	1.1(-6)		9.0(-7)
N102	L	4.7(-5)	3.9(-5)	4.7(-5)	8.6(-6)	1.0(-6)	3.8(-7)	8.0(-7)
N104A*	M	8.0(-6)	< 6.1(-5)	2.2(-4)	2.7(-5)	4.1(-7)		
N104A	L	6.4(-6)	5.2(-5)	1.7(-4)	2.4(-5)	3.8(-7)	4.5(-7)	
N184	M	4.1(-6)	3.4(-5)	2.3(-4)	3.7(-5)	2.2(-7)		
N184	L	2.3(-6)	4.3(-5)	2.0(-4)	2.8(-5)	1.9(-7)	4.1(-7)	5.4(-7)
LM1-27	M	9.4(-6)	6.5(-5)	3.0(-4)	4.5(-5)	8.2(-7)		
LM1-27	L	1.0(-5)	1.1(-4)	2.9(-4)	5.4(-5)	8.1(-7)	1.0(-6)	4.1(-6)
SMC								
N1	M	1.8(-6)::	1.4(-5)::	3.4(-5)::	< 5.4(-6)			
N1	L	1.8(-6)::	1.3(-5)::	3.2(-5)::	< 2.4(-6)		2.3(-7)	
N6	M	5.4(-6)	2.5(-5)a	9.9(-5)	1.6(-5)a			
N6	L	6.2(-6)	2.5(-5)a	1.0(-4)	9.1(-6)	2.1(-7)	3.0(-7)	

Table 3.4(c) Comparison of elemental abundances derived from medium and low resolution spectra.

OBJECT		He	N	O	Ne	Ar
LMC						
N42	M	0.127	> 3.8(-5)	< 1.6(-4)	< 2.4(-5)	
N42	L	0.092	1.8(-5)	1.3(-4)	2.3(-5)	4.2(-7)
	Adopted	0.110	3.5(-5)a	1.3(-4)	2.3(-5)	4.2(-7)
N66	M	0.114	1.4(-4)b	2.7(-4)	5.2(-5)	
N66	L	0.101	1.4(-4)	3.2(-4)	5.7(-5)	6.6(-7)
	Adopted	0.108	1.4(-4)	3.2(-4)	5.5(-5)	6.6(-7)
N102	M	0.178	2.1(-4)	1.4(-4)	2.1(-5)	
N102	L	0.168	1.7(-4)	1.4(-4)	2.5(-5)	5.8(-7)
	Adopted	0.173	1.9(-4)	1.4(-4)	2.3(-5)	5.8(-7)
N104A*	M	0.110	> 5.2(-5)	< 4.0(-4)	5.0(-5)	
N104A	L	0.105	4.0(-5)	3.3(-4)	4.6(-5)	6.7(-7)
	Adopted	0.108	5.0(-5)c	3.3(-4)	4.8(-5)	6.7(-7)
N184	M	0.119	4.8(-5)	4.0(-4)	6.4(-5)	
N184	L	0.103	1.9(-5)	3.7(-4)	5.1(-5)	6.2(-7)
	Adopted	0.111	4.8(-5)	3.8(-4)	5.8(-5)	6.2(-7)
LM1-27	M	0.089	6.0(-5)	4.2(-4)	6.1(-5)	
LM1-27	L	0.101	4.3(-5)	4.5(-4)	8.4(-5)	1.5(-6)
	Adopted	0.095	6.0(-5)	4.4(-4)	7.3(-5)	1.5(-6)
SMC						
N1	M	0.067	6.3(-6)::	4.8(-5)::	< 7.5(-6)	
N1	L	0.073	6.2(-6)::	4.5(-5)::	< 3.3(-6)	3.4(-7)::
	Adopted	0.070	6.3(-6)::	4.7(-5)::	< 3.3(-6)	3.4(-7)::
N6	M	0.122	2.7(-5)b	1.2(-4)	2.1(-5)a	
N6	L	0.107	3.2(-5)b	1.3(-4)	1.1(-5)	4.5(-7)
	Adopted	0.115	2.9(-5)b	1.3(-4)	1.6(-5)	4.5(-7)

Table 3.5(a) Ionic Helium abundances for LMC PN.

OBJECT		He^+ (6678)	He^+ (4471)	He^+ (5876)	He^+ (Adopted)	He^{2+} (4686)
N1	M	0.108		0.110	0.110	
N24	L		0.106	0.092	0.096	
N25	M			0.044	0.044	
N28	L	0.058	0.060	0.070	0.066	0.040
N39	L	0.069	0.038	0.093	0.077	0.016
N52	M	0.112	0.100	0.083	0.083	0.020
N60	M	0.088	0.093	0.099	0.099	
N77F	M			0.054	0.054	0.060
N78	M	0.114:	0.145:	0.106:	0.106:	
N97	L		0.076	0.100	0.094	0.055
N101	M			0.009	0.009	
N107*	L			0.115::	0.115::	0.033
N110	M	0.137	0.094	0.110	0.110	
N122	M		0.108	0.120	0.120	0.036
N123	M	0.081	0.095	0.098	0.098	
N124	M	0.096	0.076	0.081	0.081	0.020
N125	M	0.136	0.090	0.111	0.111	
N133	M	0.075	0.092	0.100	0.100	
N141	M	0.092	0.090	0.098	0.098	
N151	M	0.126	0.100	0.103	0.103	
N153	M	0.075	0.084	0.075	0.075	0.026
N170	M	0.126	0.087	0.077	0.077	0.027
N178	M	0.062	0.059	0.091	0.091	0.008
N181	M		0.121	0.076	0.076	0.048
N182	M	0.086	0.083	0.106	0.106	

Table 3.5(a) . *-continued*

OBJECT		He^+ (6678)	He^+ (4471)	He^+ (5876)	He^+ (Adopted)	He^{2+} (4686)
N186A	L	0.042	0.054	0.083	0.069	0.023
N188	L	0.058		0.058	0.058	0.030
N192	L	0.069		0.048	0.053	0.053
N199	M	0.071	0.093	0.054	0.054	
N201	M	0.097	0.063	0.097	0.097	0.022
N203	M	0.086		0.110	0.110	
N207	M	0.089	0.107	0.079	0.079	0.037
N208	M	0.081	0.084	0.092	0.092	0.021
N209	M	0.111		0.089	0.089	0.020
N211	M	0.102	0.092	0.114	0.114	
N212	M			0.135::	0.135::	
N221	M	0.053	0.075	0.085	0.085	0.017
LM1-9	L	0.091		0.072	0.077	0.026
LM1-61	M		0.047	0.031	0.031	0.057
LM1-62	M	0.072	0.082	0.100	0.100	0.013
S1	M			0.120	0.120	
WS12	L		0.066	0.067	0.067	0.016
WS16	L			0.079	0.079	0.046
(VLE)						
N99	M			0.015	0.015	

Table 3.5(b) Ionic abundances for LMC PN.

OBJECT		N^+ (6585)	O^+ (3727)	O^{2+} (5007)	Ne^{2+} (3868)	S^+ (6717,31)	Ar^{2+} (7135)	Ar^{3+} (4740)
N1	M	3.3(-7)::	< 5.4(-6)	3.8(-5)::	< 4.9(-6)			
N24	L		1.3(-5)	1.5(-4)	1.7(-5)		5.3(-7)	
N25	M	2.3(-6)::	5.6(-6)::	2.6(-6)::	< 1.7(-6)			
N28	L	3.1(-5)	9.1(-5)	1.6(-4)	1.9(-5)	6.1(-7)	5.5(-7)	1.1(-6)
N39	L	7.2(-7)	6.3(-6)	1.5(-4)	2.1(-5)	6.8(-8)	2.3(-7)	
N52	M	2.2(-7)	< 1.6(-5)	2.7(-4)	3.0(-5)			1.2(-6)
N60	M	1.9(-6)	< 1.9(-5)	1.6(-4)	2.4(-5)	6.1(-8)		
N77F	M	5.0(-5)	1.0(-4)	1.3(-4)	1.5(-5)	3.5(-7)		
N78	M	3.8(-6):	2.8(-5):	2.0(-4):	3.2(-5):	1.2(-7):		
N97	L	8.0(-5)	6.3(-5)	5.7(-5)	1.1(-5)	1.2(-6)	3.6(-7)	5.0(-7)
N101	M	8.7(-6)	1.7(-5)	3.3(-7)	8.2(-6)			
N107*	L	2.5(-6)	< 9.2(-6)	1.8(-4)	3.2(-5)		5.6(-7)	
N110	M	9.1(-6)	1.5(-4)	3.8(-4)	5.7(-5)	5.1(-7)		
N122	M	2.3(-5)	1.3(-5)	1.3(-4)	2.9(-5)	2.2(-7)		1.2(-6)
N123	M	3.6(-6)	2.5(-5)	1.8(-4)	2.2(-5)	1.1(-7)		
N124	M	2.2(-6)	1.2(-5)	2.5(-4)	2.1(-5)	1.3(-7)		4.9(-7)
N125	M	1.8(-6)	1.8(-5)::	2.1(-4)	1.7(-5)::	1.1(-7)		
N133	M	7.5(-7)	6.7(-6)a	1.3(-4)	1.4(-5)a			
N141	M	3.1(-6)	1.8(-5)	2.8(-4)	2.6(-5)	1.4(-7)		
N151	M	2.7(-6)	< 2.1(-5)	2.2(-4)	3.5(-5)			
N153	M	4.1(-6)	1.9(-5)	2.3(-4)	3.1(-5)	1.3(-7)		7.4(-7)
N170	M	6.4(-6)	3.2(-5)	3.0(-4)	3.9(-5)	3.3(-7)		1.2(-6)
N178	M	3.7(-6)	2.7(-5)	2.9(-4)	3.6(-5)	1.3(-7)		6.3(-7)
N181	M	2.5(-4)	2.7(-4)	6.9(-5)	2.6(-5)	4.2(-6)		
N182	M	2.2(-6)	2.3(-5)	2.1(-4)	2.9(-5)			

Table 3.5(b) . *-continued*

OBJECT		N^+ (6585)	O^+ (3727)	O^{2+} (5007)	Ne^{2+} (3868)	S^+ (6717,31)	Ar^{2+} (7135)	Ar^{3+} (4740)
N186A	L	4.4(-6)	5.4(-5)	2.8(-4)	5.7(-5)	2.7(-7)	6.6(-7)	
N188	L	6.6(-6)	5.6(-5)	2.0(-4)	2.2(-5)	5.1(-7)	5.5(-7)	8.9(-7)
N192	L	1.5(-6)	2.5(-5)	1.6(-4)	2.1(-5)	2.4(-7)	3.9(-7)	1.1(-6)
N199	M	1.1(-5)::	4.0(-5)::	1.5(-5)::	< 1.4(-6)	8.3(-8)::		
N201	M	2.5(-6)	7.3(-6)	1.2(-4)	1.3(-5)	1.3(-7)		8.0(-7)
N203	M	5.3(-6)	1.4(-4)a	3.0(-4)	3.9(-5)	5.4(-7)		
N207	M	8.8(-6)	3.4(-5)	2.5(-4)	3.8(-5)	4.1(-7)		
N208	M	5.3(-6)	2.9(-5)	2.7(-4)	4.3(-5)	2.0(-7)		6.2(-7)
N209	M	4.0(-6)	2.3(-5)	2.8(-4)	3.9(-5)	2.2(-7)		9.4(-7)
N211	M	1.1(-6)	< 1.3(-5)	1.8(-4)	1.9(-5)::	8.7(-8)		6.2(-7)
N212	M	8.6(-7)	1.7(-5)	1.2(-4)	1.1(-5)::	6.2(-8)		
N221	M	1.8(-5)	3.2(-5)	3.3(-4)	2.6(-5)	3.5(-7)		4.3(-7)
LM1-9	L	1.1(-6)	1.4(-5)::	1.4(-4)	1.6(-5)	9.8(-8)	2.4(-7)	8.0(-7)
LM1-61	M	5.2(-7)	4.6(-6)a	1.2(-4)	1.3(-5)			7.9(-7)
LM1-62	M	3.3(-6)	1.6(-5)	2.6(-4)	4.1(-5)	1.4(-7)		5.1(-7)
S1	M	1.2(-6)::	1.9(-5)::	1.5(-5)::	< 3.5(-6)			
WS12	L	4.2(-6)	5.3(-5)	2.6(-4)	4.0(-5)	1.4(-7)	5.9(-7)	
WS16	L	1.4(-5)	1.3(-4)	2.1(-4)	3.8(-5)	9.0(-7)	1.1(-6)	
(VLE)								
N16	M	7.5(-6):	7.4(-4):	3.7(-6)::		1.8(-6)		
N47	M	8.0(-6):	3.9(-4):			2.7(-6):		
N99	M	2.0(-5)	4.7(-4)	1.7(-6)	7.5(-6)::			

Table 3.5(c) Elemental abundances for LMC PN.

OBJECT		He	N	O	Ne	Ar	X	Y
N1	M	0.110	> 2.6(-6)	4.4(-5)::	< 5.5(-6)		0.69	0.30
N24	L	0.096		1.6(-4)	1.9(-5)	7.9(-7)	0.72	0.28
N25	M	0.044	3.3(-6)::	8.2(-6)::	< 5.5(-6)		0.85	0.15
N28	L	0.106	1.3(-4)	4.0(-4)	4.8(-5)	8.3(-7)	0.70	0.30
N39	L	0.093	2.2(-5)	1.9(-4)	2.6(-5)	3.5(-7)	0.73	0.27
N42		0.110	3.5(-5)b	1.3(-4)	2.3(-5)	4.2(-7)	0.70	0.30
N52	M	0.103	> 4.9(-6)	3.5(-4)	3.9(-5)		0.71	0.29
N60	M	0.099	> 1.8(-5)	1.8(-4)	2.7(-5)		0.71	0.28
N66		0.108	1.4(-4)	3.2(-4)	5.5(-5)	6.6(-7)	0.70	0.30
N77F	M	0.114	2.5(-4)	4.9(-4)	5.6(-5)		0.68	0.31
N78	M	0.106:	3.1(-5):	2.3(-4):	3.6(-5):		0.70	0.30
N97	L	0.150	2.4(-4)	1.9(-4)	3.6(-5)	5.3(-7)	0.62	0.37
N101	M	0.009	8.8(-6)	1.7(-5)	4.3(-4)		0.96	0.04
N102		0.173	1.9(-4)	1.4(-4)	2.3(-5)	5.8(-7)	0.59	0.41
N104A*		0.108	5.0(-5)b	3.3(-4)	4.8(-5)	6.7(-7)	0.70	0.30
N107*	L	0.148::	> 6.7(-5)	2.4(-4)	4.3(-5)	8.4(-7)	0.63	0.37
N110	M	0.110	3.3(-5)	5.3(-4)	7.8(-5)		0.69	0.30
N122	M	0.157	3.3(-4)	1.9(-4)	4.2(-5)		0.61	0.38
N123	M	0.098	3.0(-5)	2.1(-4)	2.5(-5)		0.72	0.28
N124	M	0.101	5.7(-5)	3.2(-4)	2.8(-5)		0.71	0.29
N125	M	0.111	2.2(-5)	2.2(-4)	1.8(-5)::		0.69	0.31
N133	M	0.100	1.5(-5)b	1.4(-4)	1.4(-5)a		0.71	0.29
N141	M	0.098	5.0(-5)	3.0(-4)	2.7(-5)		0.72	0.28
N151	M	0.103	3.1(-5)	2.4(-4)	3.9(-5)		0.71	0.29
N153	M	0.101	7.5(-5)	3.4(-4)	4.5(-5)		0.71	0.29
N170	M	0.104	9.0(-5)	4.5(-4)	5.8(-5)		0.70	0.29
N178	M	0.099	4.7(-5)	3.5(-4)	4.3(-5)		0.71	0.28
N181	M	0.124	5.1(-4)	5.5(-4)	2.1(-4)		0.66	0.33
N182	M	0.106	2.3(-5)	2.4(-4)	3.2(-5)		0.70	0.30
N184		0.111	4.8(-5)	3.8(-4)	5.8(-5)	6.2(-7)	0.69	0.31

Table 3.5(c) . *-continued*

OBJECT		He	N	O	Ne	Ar	X	Y
N186A	L	0.092	3.6(-5)	4.4(-4)	9.0(-5)	9.9(-7)	0.73	0.27
N188	L	0.088	4.6(-5)	3.9(-4)	4.3(-5)	8.2(-7)	0.74	0.26
N192	L	0.106	2.2(-5)	3.8(-4)	4.9(-5)	5.8(-7)	0.70	0.30
N199	M	0.054	1.5(-5)::	5.5(-5)::	< 5.4(-6)		0.82	0.18
N201	M	0.120	5.4(-5)	1.5(-4)	1.7(-5)		0.67	0.32
N203	M	0.110	1.6(-5)b	4.4(-4)	5.7(-5)		0.69	0.30
N207	M	0.116	1.1(-4)	4.2(-4)	6.3(-5)		0.68	0.31
N208	M	0.114	6.6(-5)	3.7(-4)	5.9(-5)		0.68	0.31
N209	M	0.109	6.5(-5)	3.8(-4)	5.1(-5)		0.69	0.30
N211	M	0.114	> 1.7(-5)	1.9(-4)	2.1(-5)::		0.68	0.31
N212	M	0.135::	6.7(-6)	1.4(-4)	1.3(-5)::		0.65	0.35
N221	M	0.102	2.4(-4)	4.4(-4)	3.5(-5)		0.70	0.29
LM1-9	L	0.103	1.6(-5)	2.1(-4)	2.3(-5)	3.6(-7)	0.71	0.29
LM1-27		0.095	6.0(-5)	4.4(-4)	7.3(-5)	1.5(-6)	0.72	0.28
LM1-61	M	0.089	4.1(-5)b	3.6(-4)	3.9(-5)		0.73	0.26
LM1-62	M	0.113	6.5(-5)	3.1(-4)	4.9(-5)		0.69	0.31
S1	M	0.120	2.0(-6)::	3.4(-5)::	< 8.1(-6)		0.68	0.32
WS12	L	0.083	3.1(-5)	3.9(-4)	6.0(-5)	8.8(-7)	0.75	0.25
WS16	L	0.125	5.9(-5)	5.3(-4)	9.5(-5)	1.6(-6)	0.66	0.33
(VLE)								
N16	M		7.5(-6):	7.4(-4)::				
N47	M		8.0(-6):	3.9(-4):				
N99	M	0.015	2.1(-5)	4.7(-4)	2.0(-3)::			

Notes on Tables 3.5 (a),(b),(c):

a - Abundance calculated using Barlow (1986) flux.

b - ICF calculated using Barlow (1986) flux.

c - Abundance calculated using the N^+ abundance from the medium resolution spectra, and the N(ICF) calculated from the low resolution spectra.

:: - Abundance calculated using an uncertain flux, or T_e.

: - Abundance calculated using an assumed temperature of 10000 K.

* - Very low signal-to-noise spectrum

Table 3.6(a) Ionic Helium abundances for SMC PN.

OBJECT		He^+ (6678)	He^+ (4471)	He^+ (5876)	He^+ (Adopted)	He^{2+} (4686)
N2	L		0.041	0.076	0.067	0.022
N4	M		0.099a		0.099	0.007
N5	L	0.094	0.089	0.068	0.077	0.035
N7	L	0.123	0.086	0.097	0.100	
N18	L			0.078	0.078	
N29	L			0.073	0.073	
N38	L	0.091	0.074	0.091	0.088	
N40	L			0.061	0.061	0.029
N42	L			0.091	0.091	
N43	L	0.061	0.121	0.110	0.102	
N44	L	0.059	0.125	0.094	0.093	
N47	L	0.072	0.094	0.092	0.088	
N70	M	0.067	0.167	0.091	0.091	
N87	M	0.104	0.066	0.119	0.119	
L66*	M		0.051a		0.051a	0.059
L239	M	0.086	0.077	0.078	0.078	0.042
L305*	M			0.098	0.098	0.037
L536	M	0.182		0.176	0.176	0.051

Table 3.6(b) Ionic abundances for SMC PN.

OBJECT		N^+ (6585)	O^+ (3727)	O^{2+} (5007)	Ne^{2+} (3868)	S^+ (6717,31)	Ar^{2+} (7135)	Ar^{3+} (4740)
N2	L		2.3(-6)	1.3(-4)	1.5(-5)	5.5(-8)	2.1(-7)	
N4	M	4.5(-7)	5.5(-6)a	1.9(-4)	1.6(-5)a			
N5	L	2.1(-6)	1.6(-5)	1.3(-4)	1.7(-5)	1.5(-7)	2.4(-7)	
N7	L		4.4(-6)	1.1(-4)	9.3(-6)		1.3(-7)	
N18	L		8.0(-6)::	2.0(-4)	2.0(-5)	1.9(-7)	4.5(-7)	
N29	L		2.1(-4)	1.1(-4)	< 4.4(-5)	3.4(-7)	8.4(-7)	
N38	L		1.6(-5)	1.4(-4)	2.2(-5)		2.0(-7)	
N40	L		2.3(-5)	1.8(-4)	3.2(-5)		2.7(-7)	
N42	L	7.3(-7)::	1.6(-5)::	9.6(-6)::	< 3.6(-6)			
N43	L		5.2(-6)	9.6(-5)	1.5(-5)	2.7(-8)	2.0(-7)	
N44	L		9.6(-6)	1.7(-4)	3.2(-5)		2.3(-7)	
N47	L	2.5(-6)	6.9(-5)	9.1(-5)	1.7(-5)		5.6(-7)	
N70	M	2.3(-6)	5.6(-5)a	1.3(-4)	1.5(-5)a	5.8(-8)		
N87	M	4.6(-7)	6.7(-6)a	1.0(-4)	9.9(-6)a			
L66*	M	4.4(-6)	4.1(-5)a	2.5(-4)	2.6(-5)a			
L239	M	8.2(-7)	1.2(-5)a	1.7(-4)	2.1(-5)			
L305*	M	9.0(-6)	1.3(-5)a	4.8(-5)	1.0(-5)a			
L536	M	9.4(-6)	3.8(-6)a	1.2(-5)	4.4(-6)a	1.2(-7)		3.0(-7)
(VLE)								
N8	L	8.2(-6):	4.0(-4):			7.9(-7):		
L302	M	2.0(-5):	2.2(-4):	2.3(-5):				

Table 3.6(c) Elemental abundances for SMC PN.

OBJECT		He	N	O	Ne	Ar	X	Y
N1		0.070	6.3(-6)::	4.7(-5)::	< 3.3(-6)	3.4(-7)::	0.78	0.22
N2	L	0.089		1.8(-4)	2.0(-5)	3.2(-7)	0.74	0.26
N4	M	0.107a	1.7(-5)b	2.1(-4)	1.7(-5)a		0.70	0.30
N5	L	0.112	2.8(-5)	2.1(-4)	2.8(-5)	3.6(-7)	0.69	0.31
N6		0.115	2.9(-5)b	1.3(-4)	1.6(-5)a	4.5(-7)	0.69	0.31
N7	L	0.100		1.2(-4)	9.6(-6)	1.9(-7)	0.71	0.29
N18	L	0.078		2.1(-4)	2.0(-5)	6.7(-7)	0.76	0.24
N29	L	0.073		3.2(-4)	< 1.3(-4)	1.3(-6)	0.77	0.22
N38	L	0.088		1.6(-4)	2.5(-5)	3.0(-7)	0.74	0.26
N40	L	0.091		2.9(-4)	5.4(-5)	4.1(-7)	0.73	0.27
N42	L	0.091	1.2(-6)::	2.5(-5)::	< 9.6(-6)		0.73	0.27
N43	L	0.102		1.0(-4)	1.5(-5)	3.0(-7)	0.71	0.29
N44	L	0.093		1.8(-4)	3.3(-5)	3.5(-7)	0.73	0.27
N47	L	0.088	5.8(-6)	1.6(-4)	2.9(-5)	8.4(-7)	0.74	0.26
N70	M	0.091	7.6(-6)b	1.8(-4)a	2.2(-5)a		0.73	0.27
N87	M	0.119	7.5(-6)b	1.1(-4)	1.1(-5)a		0.68	0.32
L66*	M	0.111	6.7(-5)b	6.3(-4)a	6.5(-5)a		0.69	0.30
L239	M	0.121	1.9(-5)b	2.7(-4)	3.5(-5)		0.67	0.32
L305*	M	0.135	5.7(-5)b	8.5(-5)	1.8(-5)a		0.65	0.35
L536	M	0.227	5.0(-5)b	2.0(-5)	7.5(-6)a		0.52	0.48
(VLE)								
N8	L		8.2(-6):	4.0(-4):				
L302	M		2.2(-5):	2.4(-4):				

Notes on Tables 3.6 (a),(b),(c):

a - Abundance calculated using Barlow (1986) flux.

b - ICF calculated using Barlow (1986) flux.

c - Abundance calculated using the N^+ abundance from the medium resolution spectra, and the N(ICF) calculated from the low resolution spectra.

:: - Abundance calculated using an uncertain flux, or T_e.

: - Abundance calculated using an assumed temperature of 10000 K.

* - Very low signal-to-noise spectrum

CHAPTER 4

Central Star Parameters

In this chapter the central star temperature, luminosity, mass, radius, and surface gravity are derived for each of 19 objects within the main survey. In section 4.1 the theoretical basis for the temperature calculation is outlined, followed in sections 4.2 and 4.3 respectively, by a discussion of the procedure for the adoption of Hβ fluxes used in the analysis, and the reddening of individual objects. Section 4.4 presents the derived stellar temperatures and luminosities (along with a discussion of the errors involved), which are used to place the objects on a Hertzsprung-Russell diagram for comparison with the theoretical PN evolutionary tracks of Schönberner (1979,1981), Fig. 4.3. From this comparison stellar masses are derived, and, by calculating the stellar radius, the surface gravity can be estimated. This derived value of surface gravity is then compared to the surface gravity of the adopted model stellar energy distribution, used in determining the stellar temperature, and is used as a guide to the choice of model in a, broadly, self-consistent analysis. Section 4.6 presents the He II Zanstra analysis of LMC N201 using both optical and ultraviolet (UV) spectra.

4.1 The Zanstra method for the determination of the central star temperature of PN.

The basis of the Zanstra (1927) method is that in an optically thick nebula all ionising photons emitted by the central star are absorbed in the nebula, and, for a

nebula in equilibrium, the total number of ionisations will equal the total number of recombinations. So, from a knowledge of the total number of recombinations, the total number of ionising photons can be calculated. By choosing a spectral distribution for the ionising photons, and normalizing it to an observed continuum point, the central star temperature can be estimated.

4.1.1 Formulation

The determination is generally carried out for the recombination lines of H^+, He^+, and He^{++}, and the details of the method are easily outlined by choosing a recombination line of any one of these ions, e.g. Hβ. For a star of luminosity per unit wavelength interval L_λ, the total number of ionising photons will equal the number of recombinations in the entire nebula

$$\int_0^{\lambda_0} \frac{\lambda L_\lambda}{hc}\, d\lambda = \int \alpha_B^{eff} N_p N_e\, dV, \tag{4.1}$$

where N_p is the number of protons, N_e is the electron density, and α_B^{eff} is the total effective recombination coefficient (Case B). The luminosity of a particular emission line, *i.e.* Hβ, will also depend on the number of recombinations,

$$L(H\beta) = \frac{hc}{\lambda_{H\beta}} \int \alpha_{H\beta}^{eff} N_p N_e\, dV. \tag{4.2}$$

Dividing equation 4.2 by equation 4.1 gives

$$\begin{aligned} \frac{\frac{\lambda_{H\beta} L(H\beta)}{hc}}{\int_0^{\lambda_0} \frac{\lambda L_\lambda}{hc}\, d\lambda} &= \frac{\int \alpha_{H\beta}^{eff} N_p N_e\, dV}{\int \alpha_B^{eff} N_p N_e\, dV} \\ &\approx \frac{\alpha_{H\beta}^{eff}}{\alpha_B^{eff}}. \end{aligned} \tag{4.3}$$

The total number of ionising photons can be compared to the luminosity of the star at any particular wavelength point, L_{λ_x}, and can be introduced into equation 4.3 from the simple relationship

$$\frac{L_{\lambda_x}}{\int_0^{\lambda_0} \frac{\lambda L_\lambda}{hc}\, d\lambda} = \frac{L_{\lambda_x}}{\frac{\lambda_{H\beta} L(H\beta))}{hc}} \frac{\frac{\lambda_{H\beta} L(H\beta))}{hc}}{\int_0^{\lambda_0} \frac{\lambda L_\lambda}{hc}\, d\lambda}, \tag{4.4}$$

giving

$$\frac{L_{\lambda_x}}{\int_0^{\lambda_0} \frac{\lambda L_\lambda}{hc}\, d\lambda} = \frac{L_{\lambda_x}}{\frac{\lambda_{H\beta} L(H\beta))}{hc}} \frac{\alpha_{H\beta}^{eff}}{\alpha_B^{eff}}. \tag{4.5}$$

By replacing the ratio of luminosities for Hβ and λ_x with a ratio of observed fluxes, this becomes

$$\frac{L_{\lambda_x}}{\int_0^{\lambda_0} \frac{\lambda L_\lambda}{hc}\, d\lambda} = \frac{hc}{\lambda_{H\beta}} \frac{\alpha_{H\beta}^{eff}}{\alpha_B^{eff}} \frac{F_{\lambda_x}}{F_{H\beta}}. \tag{4.6}$$

Finally, the stellar energy distribution is approximated to a chosen, temperature dependent model, $\mathcal{F}_\lambda$, and substituting this in the LHS of equation 4.6 gives

$$\frac{\mathcal{F}_{\lambda_x}}{\int_0^{\lambda_0} \lambda \mathcal{F}_\lambda\, d\lambda} = \frac{1}{\lambda_{H\beta}} \frac{\alpha_{H\beta}^{eff}}{\alpha_B^{eff}} \frac{F_{\lambda_x}}{F_{H\beta}}, \tag{4.7}$$

multiplying through by λ_x^2 and inverting, gives

$$\int_0^{\lambda_0} \frac{\lambda \mathcal{F}_\lambda}{\lambda_x^2 \mathcal{F}_{\lambda_x}}\, d\lambda = G(T_*) = \frac{\lambda_{H\beta}}{\lambda_x^2} \frac{\alpha_B^{eff}}{\alpha_{H\beta}^{eff}} \frac{F_{H\beta}}{F_{\lambda_x}}, \tag{4.8}$$

where $G(T_*)$ is a dimensionless quantity.

4.1.2 Model stellar energy distribution.

The simplest choice of model stellar energy distribution is a Black Body, where flux, $\mathcal{F}_\lambda$, and temperature, T, are related by

$$\int \mathcal{F}_\lambda\, d\lambda = \int \frac{2\pi hc^2}{\lambda^5} \frac{1}{(exp\frac{hc}{\lambda kT} - 1)}\, d\lambda. \tag{4.9}$$

In this case, to solve equation 4.8, a value of $G(T_*)$ is derived for the RHS of the equation from observed parameters, and the LHS is then solved numerically for this value of $G(T_*)$ using

$$\int \frac{\lambda \mathcal{F}_\lambda}{\lambda_x^2 \mathcal{F}_{\lambda_x}\, d\lambda} = \frac{(e^{u_x} - 1)}{u_x^3} \int \frac{u^2}{(e^u - 1)}\, du, \tag{4.10}$$

where

$$u = \frac{hc}{\lambda kT}, \tag{4.11}$$

and

$$\int_x^\infty \frac{u^2}{(e^u - 1)}\, du = \sum_n \frac{y(nx)}{n^3}, \tag{4.12}$$

with

$$y(nx) = exp(-nx)\,(nx(nx + 2) + 2). \tag{4.13}$$

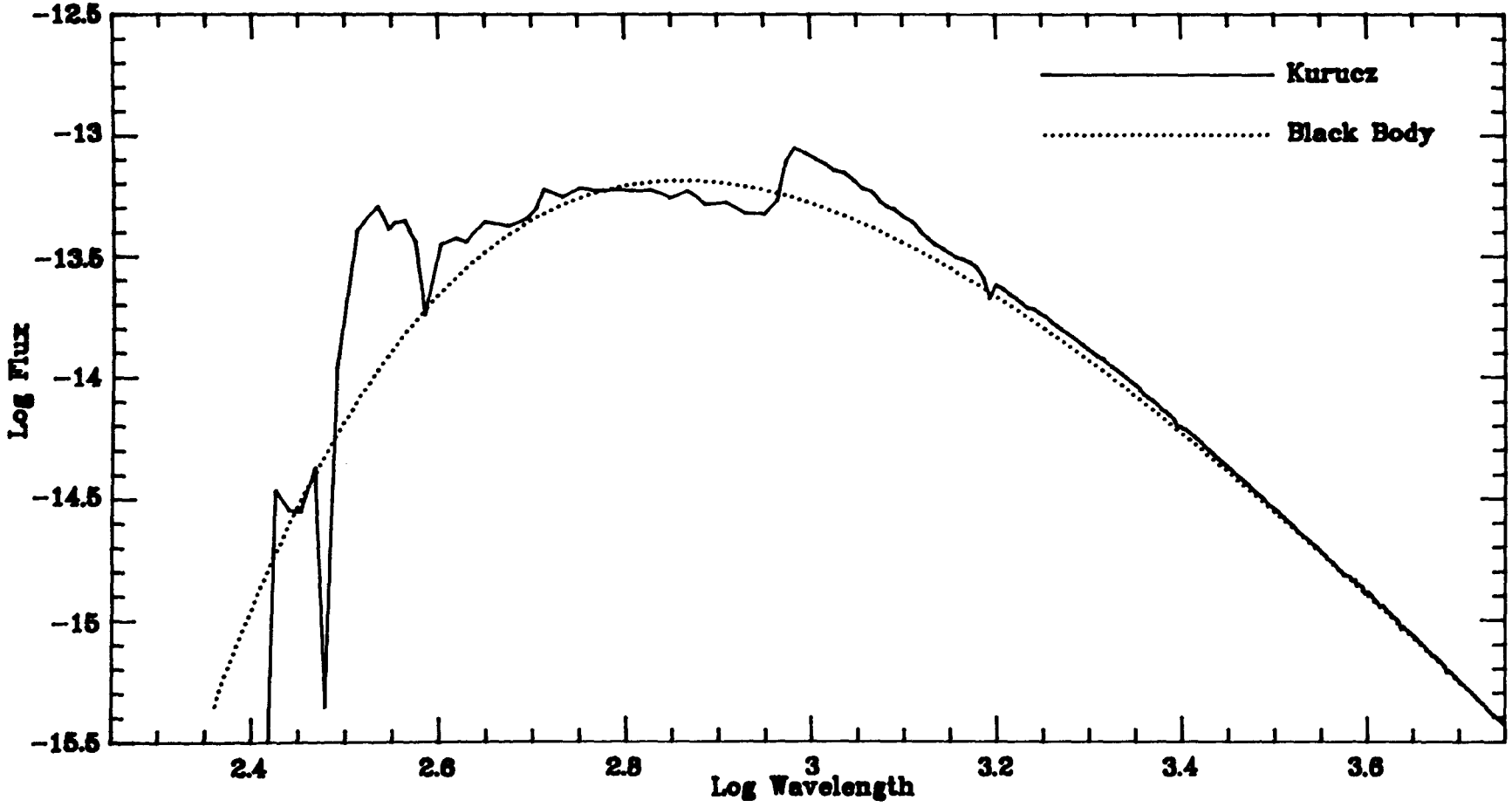

Figure 4.1(a). *Comparison of the energy spectrum of model atmospheres and Black Bodies: A Kurucz 40000 K, log g 4.0 model, and a 40000 K Black Body model.*

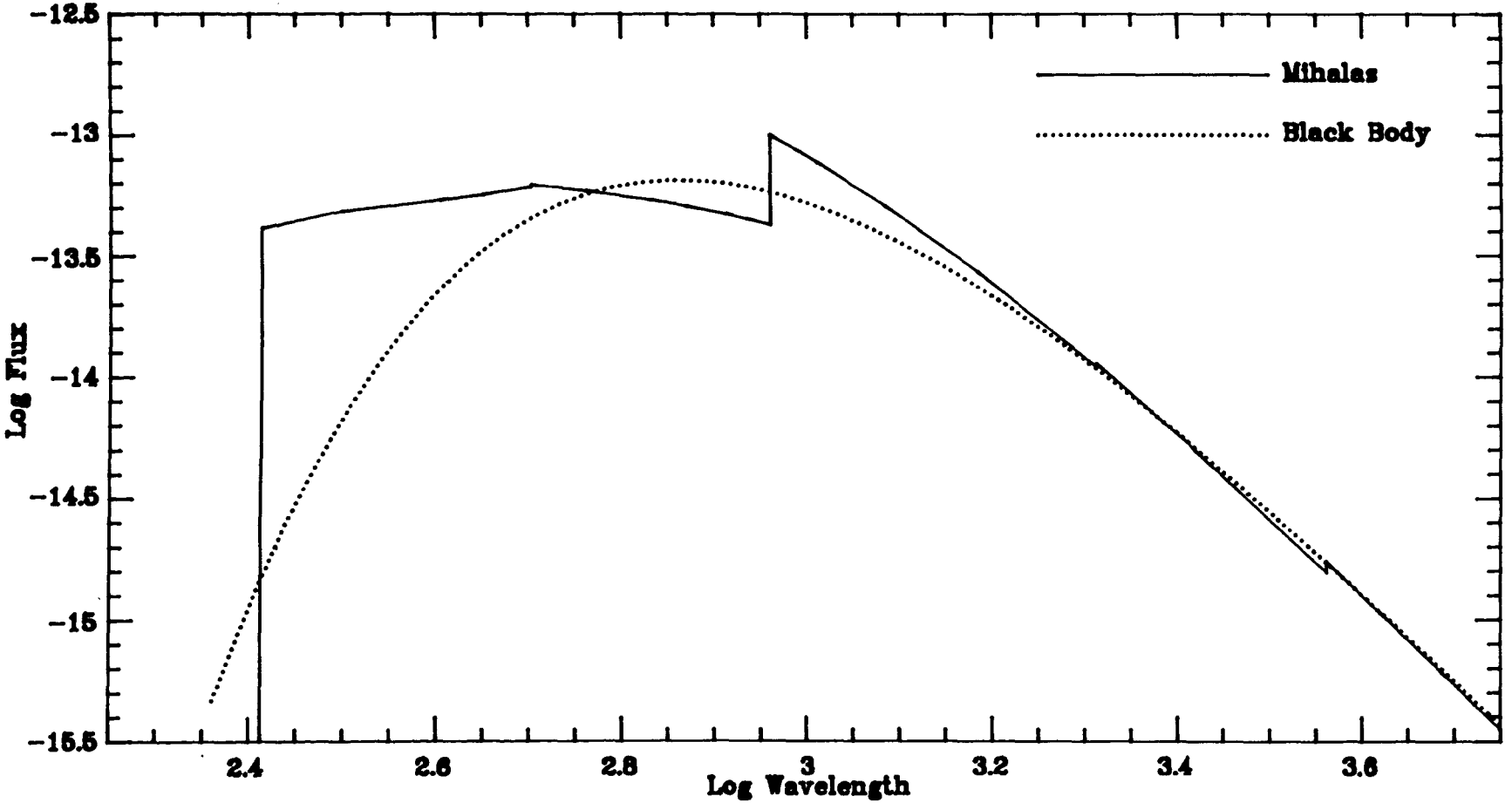

Figure 4.1(b). *Comparison of the energy spectrum of model atmospheres and Black Bodies: A Mihalas 40000 K, log g 4.0 model, and a 40000 K Black Body model.*

However, theoretically calculated models (Kurucz, 1979; Auer and Mihalas, 1972) display marked differences to Black Body models, particularly in the UV region (see Figs. 4.1 (a) and (b)), and a more realistic solution to equation 4.8 can be derived using these models. The stellar energy distribution of the theoretical models is, however, a function of both stellar temperature, and surface gravity, g (or customarily log g). The solution of equation 4.8 for T will therefore vary with the selected value of log g, as $G(T_*)$ increases with T, and decreases with log g (see Figs. 4.2 (a) and (b)). Generally, then, a secondary condition is needed to select log g, and in this study the predicted stellar parameters were used to derive a value for log g which was required to match the initial log g of the model selected. The integral on the LHS of equation 4.8 is solved by trapezoidal summation, and the 'best fit' model temperature is found by simple iteration between the various models available, to obtain agreement with the $G(T_*)$ derived from the observed fluxes (RHS of equation 4.8), an 'exact' solution being possible by interpolation between the models.

4.1.3 H I , He I , and He II ionising photons.

A further possible complication to the H I Zanstra temperature analysis is that, by simple reckoning, the photons with high enough energy to ionise and doubly-ionise helium are absorbed by this element and cannot ionise the hydrogen in these regions. It will now be shown, however, that hydrogen is ionised by photons emitted following the recombination of the helium ions with free electrons.

In a simple analysis of the recombination of singly ionised helium, using the most probable routes of decay (see Hummer and Seaton (1963,1964) for a full analysis), three-quarters of the recaptures are to triplet states, and one quarter are to singlet states. All captures to triplets lead ultimately to 2^3S (by downward transition) which is metastable and can decay by a forbidden transition to 1^1S emitting a photon of 19.8 eV. In nebulae with high enough electron densities ($N_e > 3000$ cm^{-3} at $T_e \sim 15000$ K) the 2^3S level can be depopulated by collisional excitations to the singlet levels 2^1S and 2^1P. This collisionally-excited population of the singlet levels is obviously important in PN where N_e is often greater than 3000 cm^{-3}, and must be included along with the recaptures to these levels, where two thirds of recaptures populate 2^1P, and one third populate 2^1S.

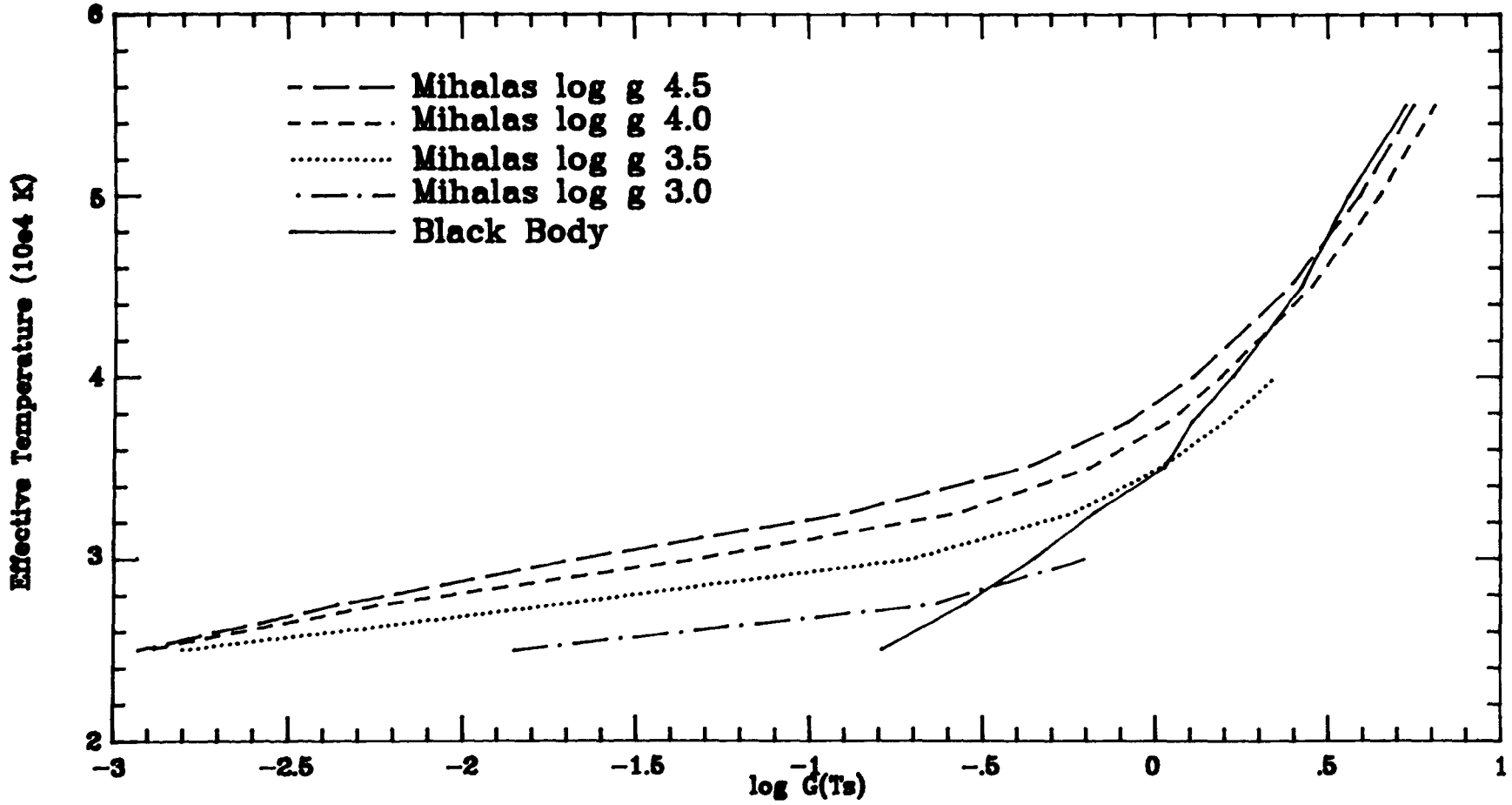

Figure 4.2(a). *Log $G(T_*)$ variations with effective temperature for Mihalas model atmospheres.*

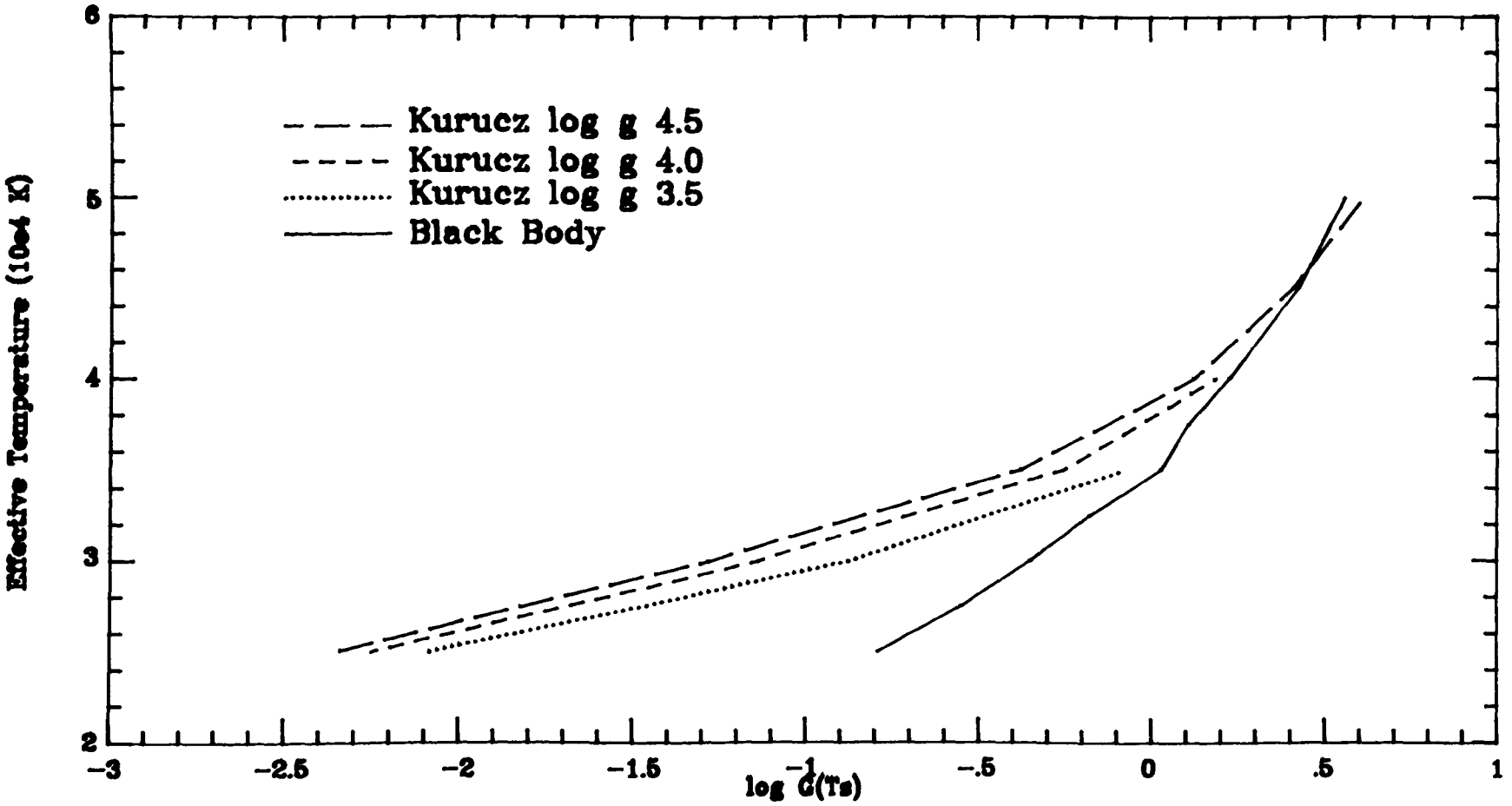

Figure 4.2(b). *Log $G(T_*)$ variations with effective temperature for Kurucz model atmospheres.*

Atoms in 2^1P decay mostly to 1^1S with the emission of a resonance photon of 21.3 eV, and atoms in 2^1S decay by two photon emission to 1^1S with a total energy of 20.7 eV. The fraction of photons per two photon decay that can ionise hydrogen is 0.56.

The fraction, p, of recombinations of singly ionised helium that can lead to photons capable of ionising hydrogen, p, is, therefore, given by,

$$p \approx \frac{3}{4} + \frac{1}{4}\left(\frac{2}{3} + \frac{1}{3}(0.56)\right) \approx 0.96$$

for the low density limit, and

$$p \approx \left(\frac{3}{4}(0.90) + \frac{1}{4}\cdot\frac{1}{3}\right)(0.56) + \left(\frac{3}{4}(0.10) + \frac{1}{4}\cdot\frac{2}{3}\right) \approx 0.67$$

in the high density limit, where 90% of the collisional excitations from 2^3S populate 2^1S, and 10% populate 2^1P.

Similarly, recombinations of He^{++} to He^+ populate 2^2P and 2^2S. Following decay to 1^2S the former ($2^2P \rightarrow 1^2S$) gives rise to an emission of a He II Lα photon, $h\nu = 40.7$ eV, and the latter ($2^2S \rightarrow 1^2S$) to two photon emission with the same total energy but with, on average, 1.42 photons capable of ionising hydrogen per decay. Also, recombinations directly to 2^2P and 2^2S give rise to He II Balmer continuum emission with the photon energies concentrated just above 13.6 eV.

In each case, although there is direct competition between helium and hydrogen for the ionising photons below the He I Lyman limit, there is generally one photon emitted by each recombination of helium ions that can ionise hydrogen. This approximation is good for He^{++} to He^+ recombinations, and is reasonably accurate for He^+ to He^0 recombinations where, at worst, 67% of recombinations result in the emission of a photon below the H I Lyman limit.

4.2 Absolute Hβ fluxes

The small spectrograph entrance aperture used in the observations made the absolute intensity calibration of the IDS unreliable and did not allow direct measurement of

Table 4.1(a) Absolute and IDS log F(Hβ). (LMC PN, Feb 5/6, medium resolution)

Object (LMC)	log F(Hβ) (IDS)	log F(Hβ) (Adopted)	Difference (Adopted−IDS)	Correction Term	log F(Hβ) ('corrected')
N182	−12.15	−12.50 a	−0.35	-	-
N1	−12.68	-	-	−0.33	−13.01
N78	−12.63	-	-	−0.33	−12.96
N99	−12.88	-	-	−0.33	−13.21
N101	−12.82	-	-	−0.33	−13.15
N25	−12.72	−12.90 i	−0.18	-	-
N110	−12.30	−12.63 f	−0.33	-	-
N122	−12.31	−12.54 a	−0.23	-	-
N123	−12.10	−12.50 a	−0.40	-	-
N199	−12.47	-	-	−0.30	−12.77
N201	−12.27	−12.32 a,b	−0.05	-	-
N133	−12.62	−12.53 f	+0.09	-	-
N125	−12.84	-	-	−0.30	−13.14
N207	−12.76	-	-	−0.30	−13.06
N208	−12.28	−12.55 a	−0.27	-	-
N209	−12.50	-	-	−0.28	−12.78
N141	−12.21	−12.48 a	−0.27	-	-
N212	−12.89	-	-	−0.28	−13.17
N124	−12.32	-	-	−0.28	−12.60
N153	−12.36	−12.63 a,b,e	−0.27	-	-
N178	−12.30	−12.68 a,b	−0.38	-	-
N181	−13.26	-	-	−0.28	−13.54
LM1-61	−12.62	−12.84 e	−0.22	-	-
LM1-62	−12.34	-	-	−0.22	−12.56
N221	−12.51	−12.57 a	−0.06	-	-

Notes to Tables 4.1 (a), (b), (c), and (d).

a - Webster, 1969 a, b, c.
b - Webster, 1976.
c - Webster, 1983.
d - Osmer, 1976.
e - Aller, 1983.
f - Barlow and Adams, 1986.
g - Low resolution, this work.
h - Medium resolution, Feb 5/6,this work.
i - This study.
k - Barlow, 1986.

the absolute Hβ flux. For 40 out of the 74 PN and VLE's, however, absolute Hβ fluxes were available from previous studies (Webster, 1969 a, b, c; Webster, 1976, Webster, 1983; Osmer, 1976; Aller, 1983; Barlow, 1986; Barlow and Adams, 1986), and for the other cases it was possible to make an empirical correction to the Hβ flux based on a night-by-night comparison of our observations with those of the other authors (as above).

Tables 4.1 (a), (b), (c), and (d) present this comparison along with the derived empirical corrections for each night. Successive columns of these tables give the object

Table 4.1(b) Absolute and IDS log F(Hβ). (LMC PN, Feb 6/7 and 7/8, medium resolution)

Object (LMC)	log F(Hβ) (IDS)	log F(Hβ) (Adopted)	Difference (Adopted−IDS)	Correction Term	log F(Hβ) ('corrected')
(6/7 Feb)					
N16	−12.74	-	-	-	-
N77F	−13.12	-	-	-	-
N78	−12.63	(−12.96) h	(−0.33)	-	-
S1	−13.01	-	-	-	-
N104A	−13.64	(−12.85) g	(+0.79)	-	-
N101	−12.90	(−13.15) h	(−0.25)	-	-
N47	−13.31	-	-	-	-
N52	−12.93	-	-	-	-
N151	−12.84	-	-	-	-
(7/8 Feb)					
N184	−13.36	−12.67 e	+0.69	-	-
N102	−13.38	−12.73 a,b	+0.65	-	-
LM1-27	−13.30	−13.07 a	+0.23	-	-
N42	−13.26	(−12.67) g	(+0.59)	-	-
N203	−13.05	−12.44 a,b	+0.61	-	-
N60	−12.80	−12.56 a	+0.24	-	-
N211	−13.06	-	-	-	-
N66	−13.19	−12.68 a	+0.51	-	-
N170	−13.02	−12.58 a	+0.46	-	-
LM1-61	−13.28	−12.84 e	+0.44	-	-
LM1-62	−13.06	(−12.56) h	(+0.50)	-	-
N221	−12.80	−12.57 a	+0.23	-	-

name (listed in order of observation), the logarithm of the Hβ flux (log F(Hβ)) measured by the IDS spectrograph, the adopted value for log F(Hβ) as measured by other studies, the difference between the values of columns 2 and 3, the correction term estimated from these differences, and finally the adopted log F(Hβ) for those objects with no correctly calibrated Hβ flux.

The adopted values of log F(Hβ) taken from previous studies are normalised to the Tüg *et al.* (1977) calibration of Vega which required the log F(Hβ) taken from Webster (1969 a, b, c and Webster, 1976) to be made fainter by 0.03 dex.

For the medium resolution observations it can be seen from Tables 4.1 (a) and (b) that the magnitude of the correction term varied from night to night, and sometimes

Table 4.1(c) Absolute and IDS log F(Hβ). (LMC PN, low resolution)

Object (LMC)	log F(Hβ) (IDS)	log F(Hβ) (Adopted)	Difference (Adopted−IDS)	Correction Term	log F(Hβ) ('corrected')
N184	−12.20	−12.67 e	−0.46	-	-
N192	−12.41	-	-	−0.51	−12.92
N188	−12.38	-	-	−0.51	−12.89
N186A	−12.28	-	-	−0.51	−12.79
LM1-9	−12.47	-	-	−0.51	−12.98
N97	−12.20	−12.72 d,e	−0.52	-	-
N102	−12.22	−12.73 a,b	−0.51	-	-
N107	−12.78	-	-	−0.51	−13.29
N104A	−12.33	-	-	−0.51	−12.84
N28	−12.29	−12.84 f	−0.55	-	-
N24	−12.16	−12.70 a,b	−0.55	-	-
LM1-22	−12.35	-	-	−0.51	−12.86
WS16	−12.80	-	-	−0.51	−13.31
LM1-27	−12.59	−13.07 a	−0.48	-	-
N39	−12.21	−12.72	−0.52	-	-
N42	−12.15	-	-	−0.51	−12.66
N66	−12.17	−12.68 a	−0.51	-	-

throughout the night, and therefore required that each night to be corrected separately. For the observations of 5/6 February, Table 4.1 (a), a mean correction term (for all objects) of −0.23±0.15 was derived, but it was felt that the variations of the differences throughout the night were sufficiently steady for separate corrections terms to be adopted for the beginning and the end of the night. Thus for objects observed between N182 and N110 (Table 4.1 (a)) a correction term to log F(Hβ) of −0.33±0.07 was adopted, and for objects observed between N208 and LM1-61 a correction term to log F(Hβ) of −0.28±0.06 was adopted. For N199, N125, and N207, which lie between these two groups a mean of the two correction terms was adopted, *i.e.* −0.30. For LM1-62 the correction term of the previous observation was adopted. The mean correction term for the whole night (−0.23) does not lie between the two separate correction terms (−0.33 and −0.28), as the procedure used to determine these two terms excludes the low differences of N201, N133, and N221. The mean correction for the whole night, excluding these three objects is −0.30±0.07, although the exclusion of these objects does throw some doubt on the accuracy of the procedure adopted.

For the night of 6/7 February no absolute log F(Hβ) values were available from previous studies for the LMC objects observed, although N78, N104A and N101 were each observed on other nights where corrections could be applied, Table 4.1(b). Six of the eight SMC objects observed on this night, however, did have absolute log F(Hβ) available from earlier studies, Table 4.1(c), and the log F(Hβ) of the remaining two objects were adopted from the low resolution spectra of N1, (see below), and the medium resolution, February 5/6, spectra of L239. The absolute Hβ fluxes of the PN N4 and L66 were taken from Barlow (1986), and are parenthesised as the spectra were taken through a narrow slit.

Of the LMC and SMC PN observed on 7/8 February, Tables 4.1 (b) and (d), 12 out of 17 had an absolute Hβ flux measured in previous studies. However, the scatter in the difference between these values and the Hβ flux measured by the IDS, was too large to make any reasonable estimate for the log F(Hβ) of the other 5 objects.

The aperture used for the low resolution observations was larger than that used for the medium resolution (see § 2.1) and led to the differences between the IDS Hβ fluxes and those adopted from other studies being more consistent, with far less scatter (Tables 4.1 (c) and (d)). For the LMC PN a mean difference of 0.51$\pm$0.03 was derived and used for the correction term for all other LMC objects observed at low resolution. For the SMC two correction terms were adopted, -0.66 for N1, N7, and N18, and -0.44 for N29, which follow the general trend of the differences for the night.

To summarise, $\sim$54% of the MC PN observed with the IDS had absolute log F(Hβ) available from previous studies, and were normalised to the Tüg *et al.* (1977) calibration of Vega before adoption. Of the remaining 34 objects, 12 were observed at low resolution with an uncertainty on the corrected log F(Hβ) of $\pm$0.03 dex. Another 14 LMC PN, and 2 SMC PN were observed at medium resolution on February 5/6 with uncertainties on the corrected log F(Hβ) of the order of $\pm$0.08 dex for both groups. Finally, for 6 LMC objects observed on the night of 6/7 February, N16, N77F, S1, N47, N52, and N151, no correction could be applied and in these cases the IDS Hβ flux is adopted but is flagged as doubtful when used.

Table 4.1(d) Absolute and IDS log F(Hβ). (SMC PN, Feb 6/7 and 7/8, medium resolution, and low resolution)

Object (SMC)	log F(Hβ) (IDS)	log F(Hβ) (Adopted)	Difference (Adopted−IDS)	Correction Term	log F(Hβ) ('corrected')
Feb 6/7					
N1	−12.62	(−12.89) h	(−0.27)	-	-
N4	−13.05	(−13.21) k	−0.16	-	-
N8	−13.80	−13.23 f	+0.57	-	-
L66	−13.38	(−13.85) k	−0.47	-	-
L239	−12.86	(−12.93) k	(−0.07)	-	-
N70	−12.53	−12.72 c	−0.19	-	-
N87	−12.32	−12.48 c	−0.17		
L536	−13.05	-	-	−0.18	−13.23
Feb 7/8					
N6	(−12.94)	(−12.82) a	(+0.12)	-	-
L239	−13.10	(−12.93) k	(+0.17)	-	-
L302	−13.91	−13.35 f	+0.56	-	-
L305	−13.93	−13.04 c	+0.89	-	-
Low Resolution					
N1	−12.89	-	-	−0.66	−12.23
N2	−12.13	−12.78 d	−0.65	-	-
N5	−12.17	−12.86 c	−0.69	-	-
N6	−12.17	−12.82 a	−0.65	-	-
N7	−12.19	-	-	−0.66	−12.85
N18	−12.40	-	-	−0.66	−13.06
N29	−12.50	-	-	−0.44	−12.94
N40	−12.46	−12.89 a	−0.43	-	-
N38	−12.05	−12.49 c	−0.44	-	-
N43	−12.03	−12.44 c	−0.41	-	-
N42	−12.38	−12.77 a	−0.39	-	-
N44	−12.17	−12.65 c	−0.48	-	-

4.3 The logarithmic extinction coefficient

Owing to the narrow apertures used in the the observations, the effects of atmospheric dispersion could not be distinguished from those of interstellar extinction (by our own galaxy and by the Magellanic Clouds).

To determine the reddening within both galactic systems the maps of the neutral hydrogen column density, N(H I), of each system were used. For the extinction due to our own galaxy the colour excess, $E(B-V)$, in any particular line of sight, was taken directly from the maps of Burstein and Heiles (1982), and converted into a logarithmic extinction using $c(H\beta) = 1.452\ E(B-V)$. The SMC region has been mapped in N(H I) by Hindman (1967), and using $N(H\,I)/E(B-V) = 8.7 \times 10^{22} cm^{-2} mag^{-1}$ (Fitzpatrick, 1985) for the SMC, with $c(H\beta) = 1.427\ E(B-V)/2$, (*i.e.* assuming the object is halfway into the SMC), the logarithmic extinction could be calculated from the N(H I) value. The N(H I) tables of Rohlfs *et al.* (1984) together with $N(H\,I)/E(B-V) = 2 \times 10^{22} cm^{-2} mag^{-1}$ (Koornneef, 1982) for the LMC, and $c(H\beta) = 1.427\ E(B-V)/2$, allowed the $c(H\beta)$ in the LMC to be calculated.

Tables 4.2(a) and 4.2(b) present the adopted values of log $F(H\beta)$ (see § 4.1), the extinction due to each galactic system, and finally log $I(H\beta)$, the adopted dereddened absolute $H\beta$ intensity.

4.4 The H I Zanstra temperatures and central star luminosities.

After subtraction of the nebula continuum (calculated theoretically from the values of log $F(H\beta)$, T_e, N_e, and the elemental abundances given in Chapter 3, using the *NEBCONT* routine (written by P.J.Storey, J.P.Harrington and S.Adams, UCL.) 11 LMC and 8 SMC objects displayed evidence of a stellar continuum with good enough signal to noise to allow a determination of the central star temperature from the Zanstra method, §4.1.

Table 4.2(a) Adopted values of log F(Hβ), c(Hβ), log I(Hβ) for LMC objects.

Object (LMC)	log F(Hβ)	c(Hβ) Galactic	LMC	log I(Hβ)
N1	−13.01	0.03	0.02	−13.01
N24	−12.71	0.09	0.04	−12.58
N25	−12.90	0.09	0.90	−11.91
N28	−12.84	0.09	0.16	−12.59
N39	−12.72	0.09	0.04	−12.59
N42	−12.66	0.09	0.04	−12.53
N60	−12.56	0.09	0.05	−12.42
N66	−12.68	0.09	0.05	−12.54
N78	−12.96	0.14	0.04	−12.78
N97	−12.72	0.11	0.07	−12.54
N99	−13.21	0.14	0.01	−13.06
N101	−13.15	0.12	0.04	−12.99
N102	−12.73	0.11	0.05	−12.57
N104A	−12.84	0.09	0.06	−12.69
N107	−13.29	0.09	0.06	−13.14
N110	−12.63	0.15	0.02	−12.46
N122	−12.54	0.13	0.04	−12.37
N123	−12.50	0.13	0.04	−12.33
N125	−13.14	0.13	0.03	−12.98
N133	−12.53	0.13	0.03	−12.37
N141	−12.48	0.11	0.03	−12.34
N153	−12.63	0.11	0.06	−12.46
N170	−12.58	0.11	0.12	−12.35
N178	−12.68	0.11	0.10	−12.47
N181	−13.54	0.11	0.07	−13.36
N182	−12.50	0.16	0.02	−12.32
N184	−12.67	0.16	0.01	−12.50
N186A	−12.79	0.15	0.01	−12.63
N188	−12.89	0.14	0.01	−12.74
N192	−12.92	0.13	0.02	−12.77
N199	−12.77	0.11	0.03	−12.63
N201	−12.32	0.11	0.09	−12.12
N203	−12.44	0.15	0.02	−12.27
N207	−13.06	0.12	0.02	−12.92
N208	−12.55	0.12	0.03	−12.40
N209	−12.78	0.12	0.04	−12.62
N212	−13.17	0.12	0.05	−13.00
N221	−12.57	0.15	0.01	−12.41
LM1-9	−12.98	0.15	0.01	−12.82
LM1-27	−13.07	0.08	0.03	−12.96
LM1-61	−12.84	0.11	0.01	−12.72
LM1-62	−12.56	0.17	0.00	−12.39
WS12	−12.86	0.04	0.02	−12.80
WS16	−13.31	0.06	0.02	−13.23

Table 4.2(b) Adopted values of log F(Hβ), c(Hβ), log I(Hβ) for SMC objects.

Object (SMC)	log F(Hβ)	c(Hβ) Galactic	c(Hβ) SMC	log I(Hβ)
N1	−12.89	0.03	0.01	−12.85
N2	−12.78	0.07	0.01	−12.70
N4	−13.23	0.03	0.02	−13.18
N5	−12.86	0.06	0.02	−12.78
N6	−12.82	0.03	0.43	−12.38
N7	−12.85	0.09	0.01	−12.75
N18	−13.06	0.06	0.04	−13.06
N29	−12.94	0.05	0.09	−12.80
N38	−12.49	0.03	0.04	−12.42
N40	−12.89	0.03	0.04	−12.82
N42	−12.77	0.09	0.03	−12.65
N43	−12.44	0.03	0.02	−12.39
N44	−12.54	0.09	0.00	−12.45
N47	−12.65	0.09	0.03	−12.53
N70	−12.72	0.09	0.03	−12.60
N87	−12.48	0.03	0.02	−12.43
L66	−13.56	0.03	0.06	−13.47
L239	−13.04	0.06	0.06	−12.92
L302	−13.35	0.09	0.02	−13.24
L305	−13.04	0.09	0.05	−12.90
L536	−13.23	0.04	0.01	−13.18
VLE N8	−13.23	0.05	0.58	−12.60

Despite the fact that the stellar continuum level is stronger at the blueward end of the spectra, the effects of atmospheric dispersion and decreasing signal to noise at wavelengths less than 4500 Å made continuum measurements in this part of the spectrum unreliable. However, there was sufficient signal to noise for all 19 objects to determine the continuum level in the 5500 Å region.

The continuum level was measured from the spectra after correction for both atmospheric dispersion and interstellar extinction (*i.e.* by correcting to the theoretical Balmer decrement, section 2.3), and after normalisation to the adopted dereddened absolute Hβ intensity.

Tables 4.3(a) and 4.3(b) present the results of the Zanstra analysis, where columns 1 and 2 give the object name and resolution of the spectra, 'Low' indicating a low resolution spectrum, and 'M5/6', 'M6/7', and 'M7/8' indicating medium resolution

Table 4.3(a) Central star parameters for LMC objects

Object	Spectrum	$\frac{N(He^+)}{N(H^+)}$	T_e (K)	log I(Hβ)	$log\frac{I(5876)}{I(Hbeta)}$	Model	T_{eff} (K)	log g	log I(Hβ)	$log\frac{I(5876)}{I(Hbeta)}$	F. $\left(\frac{10^{-11}ergs}{cm^{-2}s^{-1}}\right)$	L. ($L_\odot$)	M. ($M_\odot$)	R. ($R_\odot$)	log g
N24	Low	0.096	12250	−12.58	−0.91	BB	42000	-	−12.59	−0.81	3.684				
						K	40000	4.0	−12.71	−0.68	3.698‡				
						M	40000	4.0	−12.70	−0.52	3.992‡				
												2657	0.555	1.07	4.1
N25	M5/6	0.044	16000	−11.91	−1.31	BB	41000	-	−11.91	−0.87	18.41				
						K	40000	4.0	−11.98	−0.71	19.87‡				
						M	40000	4.0	−11.97	−0.56	21.45‡				
												(see Table 5.4)			
N78	M5/6	0.106:	10000	−12.78	−0.83	BB	48500	-	−12.77	−0.63	2.068				
						K	45000	4.5	−12.89	−0.48	1.974‡				
						M	45000	4.5	−12.90	−0.37	2.106‡				
												1393	0.538	0.61	4.6
	M7/8					BB	53500	-	−12.77	−0.54	1.904				
						K	50000	4.5	−12.83	−0.39	1.942‡				
						M	50000	4.5	−12.86	−0.30	2.044‡				
												1393	0.538	0.50	4.8

Table 4.3(a) *continued*

Object	Spectrum	$\frac{N(He^+)}{N(H^+)}$	T_e (K)	log I(Hβ)	$log\frac{I(5876)}{I(H\beta=1)}$	Model	T_{eff} (K)	log g	log I(Hβ)	$log\frac{I(5876)}{I(H\beta=1)}$	F. $\left(\frac{10^{-11}ergs}{cm^{-2}s^{-1}}\right)$	L. ($L_\odot$)	M. ($M_\odot$)	R. ($R_\odot$)	log g
N101	M5/6	0.009	13500	−12.99	−1.92	BB	26500	-	−12.99	−1.55	3.907				
						K	30000	3.5	−13.22	−2.24	6.107				
						M	30000	3.5	−13.06	−2.55	6.947‡				
												4800	0.580	2.56	3.4
N123	M5/6	0.098	11000	−12.33	−0.88	BB	47000	-	−12.33	−0.68	5.823				
						M	45000	4.0	−12.36	−0.41	6.602‡				
												4562	0.575	1.11	4.1
N199	M5/6	0.054	15750	−12.63	−1.17	BB	41000	-	−12.62	−0.97	3.593				
						K	40000	4.0	−12.69	−0.73	3.826‡				
						M	40000	4.0	−12.69	−0.55	4.131‡				
												2750	0.556	1.09	4.1
N201	M5/6	0.120	15500	−12.12	−0.92	BB	45000	-	−12.12	−0.77	9.995				
						M	45000	4.0	−12.08	−0.45	12.79				
												(see Table 4.4)			
S1	M6/7	0.120	21000	(−12.94)	(−0.80)	BB	34000	-	−12.95	−1.19	(2.362)				
						K	35000	4.0	−13.11	−1.60	2.836				
						M	35000	4.0	−13.05	−1.07	3.188‡				
												(2200)	(0.555)	(1.28)	(4.0)

Table 4.3(a) *continued*

Object	Spectrum	$\frac{N(He^+)}{N(H^+)}$	T_e (K)	log I(Hβ)	$log\frac{I(5876)}{I(Hb\text{-}ta)}$	Model	T_{eff} (K)	log g	log I(Hβ)	$log\frac{I(5876)}{I(Hb\text{-}ta)}$	F. $\left(\frac{10^{-11}ergs}{cm^{-2}s^{-1}}\right)$	L. ($L_\odot$)	M. ($M_\odot$)	R. ($R_\odot$)	log g
VLE															
N16	M6/7		10000†	(−12.60)	-	BB	23500	-	−12.60	−2.78	15.12				
						M	30000	3.0	−11.83	−1.17	36.15‡				
												(24980)	(0.869)	(5.85)	(2.8)
N47	M6/7		10000†	(−13.24)	-	BB	18250	-	−13.18	−2.46	13.35				
						K	25000	3.0	−13.22	−3.17	32.57‡				
						M	25000	3.0	−13.29	−3.89	37.38				
												(22506)	(0.830)	(8.00)	(2.6)
N99	M5/6	0.015	11250	−13.06	−1.7	BB	26750	-	−13.05	−1.51	3.312				
						K	30000	3.5	−13.29	−2.22	4.950				
						M	30000	3.5	−13.12	−2.54	5.631‡				
												3890	0.565	2.31	3.5

Table 4.3(b) Central star parameters for SMC objects

Object	Spectrum	$\frac{N(He^+)}{N(H^+)}$	T_e (K)	log I(Hβ)	$log\frac{I(5876)}{I(Hbeta)}$	Model	T_{eff} (K)	log g	log I(Hβ)	$log\frac{I(5876)}{I(Hbeta)}$	F. $\left(\frac{10^{-11}ergs}{cm^{-2}s^{-1}}\right)$	L. ($L_\odot$)	M. ($M_\odot$)	R. ($R_\odot$)	log g
N1	Low	0.070	12750	−12.85	−1.06	BB	39750	-	−12.85	−0.89	2.260				
						K	40000	4.0	−12.86	−0.68	2.632‡				
						M	40000	4.0	−12.85	−0.53	2.842‡				
												2830	0.560	1.11	4.1
N7	Low	0.100	12500	−12.75	−0.89	BB	45000	-	−12.75	−0.77	2.312				
						K	45000	4.5	−12.76	−0.52	2.700‡				
						M	45000	4.5	−12.76	−0.40	2.848‡				
												2869	0.558	0.88	4.3
N18	Low	0.078	11000	−12.96	−0.97	BB	38500	-	−12.96	−0.92	1.715				
						K	40000	4.0	−12.92	−0.66	2.200‡				
						M	40000	4.0	−12.92	−0.50	2.375‡				
												2366	0.551	1.01	4.2
N29	Low	0.073	10000†	−12.80	−1.00	BB	29250	-	−12.80	−1.41	4.545				
						K	30000	3.5	−13.25	−2.20	5.557				
						M	30000	3.5	−13.09	−2.51	6.320‡				
												6536	0.611	2.99	3.3

Table 4.3(b) *continued*

Object	Spectrum	$\frac{N(He^+)}{N(H^+)}$	T_e (K)	log I(Hβ)	$log \frac{I(5876)}{I(H\beta+He)}$	Model	T_{eff} (K)	log g	log I(Hβ)	$log \frac{I(5876)}{I(H\beta+He)}$	F. $\left(\frac{10^{-11}\,ergs}{cm^{-2}s^{-1}}\right)$	L. ($L_\odot$)	M. ($M_\odot$)	R. ($R_\odot$)	log g
N43	Low	0.102	13250	−12.39	−0.85	BB	54000	-	−12.39	−0.57	4.655				
						K	50000	4.5	−12.47	−0.42	4.587‡				
						M	50000	4.5	−12.50	−0.34	4.773‡				
												4839	0.585	0.93	4.3
N70	M6/7	0.094	12750	−12.60	−0.91	BB	50000	-	−12.60	−0.64	2.339				
						K	50000	4.5	−12.56	−0.41	3.761‡				
						M	50000	4.5	−12.57	−0.34	3.956‡				
												3990	0.573	0.84	4.4
VLE															
N8	Low		10000†	−12.60	-	BB	26250	-	−12.60	−1.55	9.997				
						M	25000	3.0	−13.78	−3.89	12.13‡				
						M	30000	3.0	−12.12	−1.11	18.32‡				
												15743	0.765	4.64	3.0
L302	M6/7		10000†	−13.24	-	BB	30250	-	−13.24	−1.3	1.484‡				
												2241*	0.549	1.72	3.7

Notes to Tables 4.3 (a) and (b)

* L302 luminosity increased by a factor of 1.46, see § 5.3.

( ) IDS Hβ flux used to derive value

† Assumed value for T_e

‡ Values of F. used for the calculation of the stellar luminosity

spectra taken on the nights of 5/6, 6/7, and 7/8 February, respectively. Columns 3 to 6 present the nebular parameters, $n(He^+)/n(H^+)$, the electron temperature T_e (derived in this study), the dereddened absolute log Hβ intensity, and the log ratio of I(He I 5876 Å) to I(Hβ). Predicted, model-dependent, parameters are given in columns 7 to 12 (for the best fit Mihalas, Kurucz, and Black Body models), where T_{eff} is the model effective temperature, and F_* is the total flux of the model. The final four columns give the derived stellar luminosity, mass, radius, and surface gravity.

The 'best fit' model, used to derive T_{eff} and F_*, was determined by the closeness of agreement between the observed and predicted dereddened Hβ intensity, and by a self consistent agreement between the predicted log g and that of the chosen model. The He I flux was not used to determine the stellar temperature but to indicate the extent of the ionisation of helium, by comparison between the predicted and observed ratios of the He I 5876 Å and Hβ fluxes. If a particular model predicts a larger value for this ratio than is observed, then it can be assumed that the helium is completely ionised to the edge of the H^+ Stromgren sphere, where the remaining photons are absorbed by hydrogen. This is the case for most PN in Tables 4.3 (a) and (b) with the exception of those nebulae with $T_{eff} \leq 35000$ K (*i.e.* LMC N99, LMC N101, LMC N16, LMC N47, SMC N29, SMC N8, and SMC L302) where we can assume that a substantial fraction of neutral helium is still present in the nebula.

The T_{eff} presented for the Mihalas and Kurucz models in Table 4.3 are not the H I Zanstra temperatures, but are the nearest models to that temperature. The actual H I Zanstra temperature can be calculated by interpolation between models, but for the grid of models used the predicted T_{eff} will be within ±2500 K of the actual H I Zanstra temperature, which is within the uncertainty in T_{eff} due to the uncertainty in the continuum level. The T_{eff} presented for the Black Body models are the actual H I Zanstra temperatures.

The distances to both galaxies (used for the calculation of stellar luminosities) have been the subject of recent work, and consistent values are available which can be adopted for all objects with little error, a situation which is the reverse of that for Galactic PN. The recommended distance modulus for the LMC (Reid and Strugnell, 1986) is $18^m.35$ (47 kpc), which is adopted here for luminosity calculations. However, the situation for the SMC is less straight forward owing to the spread of distances, along the line of

sight, of the order of 32 kpc (Mathewson *et al.*, 1986). The distance modulus given by Reid and Strugnell (1986), $18^m.78$ (57.5 kpc), does give reasonable agreement with the 'maximum concentration' distance of Mathewson *et al.* (1986), 59 kpc, though, and the former value is adopted here.

Except for SMC L302, LMC N25, and LMC N201, the luminosities of the central stars (column 13, Tables 4.3 (a) and (b)) were calculated from the total flux of the Mihalas and Kurucz models, as it was felt that these would give a more representative stellar continuum in the UV. Where good agreement existed between these models the mean F_* of both were used, otherwise the model which more accurately predicts the observed $F(H\beta)$ was used. For objects with more than one spectrum, the average derived F_* of all of the Kurucz and Mihalas models presented is used to calculate the stellar luminosity. For SMC L302 a Black Body model was adopted for all derived parameters, as it gives closer agreement to the Wolf-Rayet spectral distribution. In all cases the values of F_* used to determine the stellar luminosity are indicated by a ‡ to the right of column 12. For LMC N25 the adopted stellar luminosity (Table 5.4) was derived from a recent IPCS spectrum described in Chapter 5; the full results of this analysis are presented in Tables 5.1 (line intensities) and 5.2 (stellar parameters). The adopted stellar luminosity for LMC N201 (Table 4.4) was derived from a He II Zanstra analysis of an ultraviolet spectrum and is discussed in § 4.6.

The error in the luminosity derived from the IDS spectra is determined by the following factors: (1) the uncertainty in the continuum level, (2) the uncertainty in the spectral distribution used, and (3) the error in the distance adopted. The first of these is a combination of the effects of the correction made for atmospheric dispersion and interstellar extinction, the calculation and subtraction of the nebula continuum, and the signal to noise ratio of the spectrum. The errors due atmospheric dispersion and the overall correction to the Balmer decrement should be small in the wavelength region used for continuum measurements (5500 Å), although the final, adopted value of the logarithmic extinction constant can be an important determinant of the continuum level through the adopted value of log $F(H\beta)$. Generally, however, the error in the extinction constant should only produce small errors in the continuum level, since the mean interstellar extinction to the LMC and SMC is low, and has only a small spatial variation. For a few cases in this survey there could be local variations on a scale smaller

than that of the H I maps used to derive $E(B-V)$, or large intrinsic reddening of the nebula itself, and this would lead to large errors on the continuum levels used here (see discussion of LMC N25, Chapter 5).

The adopted value of log I(Hβ) (itself dependent on the value of c(Hβ) adopted) would have a dual effect on the stellar continuum level. First the calculated nebula continuum is very sensitive to the Hβ flux and for a change in log I(Hβ) of $\pm$0.1 dex variations in the nebula continuum level of $\pm$23% can be expected. The second, generally smaller, contribution is due to the scaling of the stellar continuum level to the log I (Hβ) flux, which will be important in cases where either the logarithmic extinction constant, or the absolute Hβ flux are badly in error, a situation that cannot be judged by a single data set.

Of the 19 objects in question, 8 have absolute Hβ fluxes adopted from previous studies (estimated errors $\pm$0.02 dex), 4 have absolute Hβ fluxes adopted from corrected low resolution spectra (estimated errors $\pm$0.03 dex), 4 more have absolute Hβ fluxes adopted from corrected medium resolution spectra of the 5/6 February (estimated errors $\pm$0.08), and the final 3, LMC S1, LMC N16, and LMC N47, have uncorrected IDS Hβ fluxes only. The percentage error in the nebular continuum level due to the uncertainty in log F(Hβ) will be approximately $\pm$10% , $\pm$10% , and $\pm$20% , for the first three of these four groups, but these convert to a percentage error in the stellar continuum in the ratio of the magnitude of the total continuum compared to the nebular continuum. That is, for a nebular continuum level which is $\pm$30% of the total continuum, the error on the stellar continuum will be $\pm$5% , $\pm$5% , and $\pm$10% , in each of the three cases above. The nebular continuum level for the objects in the first two groups of log F(Hβ) is never more than 50% of the total continuum, and the expected errors on the stellar continuum due to nebula subtraction are therefore $<$10% . For the objects with absolute Hβ fluxes adopted from medium resolution spectra, the nebular contribution at 5500 Å is 10% for N99 and N101, 50% for N199, and 60% for N78, corresponding to errors in the stellar continuum of 2% , 20% , and 30% , repectively.

The final cause of error in the stellar continuum level will be due to the continuum signal to noise ratio of the spectra. This varied slightly from object to object depending on continuum strength, with a mean uncertainty of $\pm$ 25% , and is considered to be the major source of error in the total luminosities derived in this study. For objects

with a strong stellar continuum (T_{eff} < 35000 K) the signal to noise error will be significantly lower, whilst for the weaker continua (T_{eff} > 50000 K) even larger errors can be expected.

The uncertainty in the total luminosity due to the uncertainty of the spectral distribution (point 2), is mainly due to the error in the derived stellar temperature resulting from the uncertainty in the stellar continuum level in the Zanstra analysis, although the adoption of any particular theoretical spectral shape will also have an effect. The mean error in the continuum level corresponds to uncertainties of the order of ±15% in the T_{eff} derived (approximately ±5000 K), this will again be smaller for the lower temperature, strong continuum objects.

The final contribution to the error in the derived stellar luminostity (point 3), is the errors in the adopted distances for the LMC and SMC. These are estimated as ±0.15, and ±0.2 in the distance modulus for each galaxy respectively (Reid and Strugnall, 1986), corresponding to errors of ±9% in the distance, and ±18% in the luminosity. In addition, the spread in distance, along the line of sight, to the SMC (Mathewson *et al.*, 1986), implies an uncertainty on the adoption of a single distance of ±26% , although no direct account of of this uncertainty is included in this work.

In summary, the mean errors in the stellar continuum level due to signal to noise and the uncertainty in the Hβ flux, are ±25% , and ±15% (mean value), respectively, corresponding to a ±29% overall error in the final continuum level. This combined with the uncertainty in the adopted distance of ±9% , gives a total uncertainty in the derived stellar luminosities of Tables 4.3 (a) and (b) of ±34% .

4.5 Stellar mass, radius, and surface gravity.

From the stellar luminosity and effective temperature it is possible to estimate the stellar mass, and then go on to calculate a corresponding stellar radius and surface gravity. To calculate the the stellar mass the evolutionary tracks of Schönberner (1979,1981) were used. These depict the evolution of PN central stars (mass range 0.55 $M_{\odot}$ to 0.60 $M_{\odot}$) in the log L_* *vs.* log T_{eff} plane of an HR diagram (Fig. 4.3). By placing the

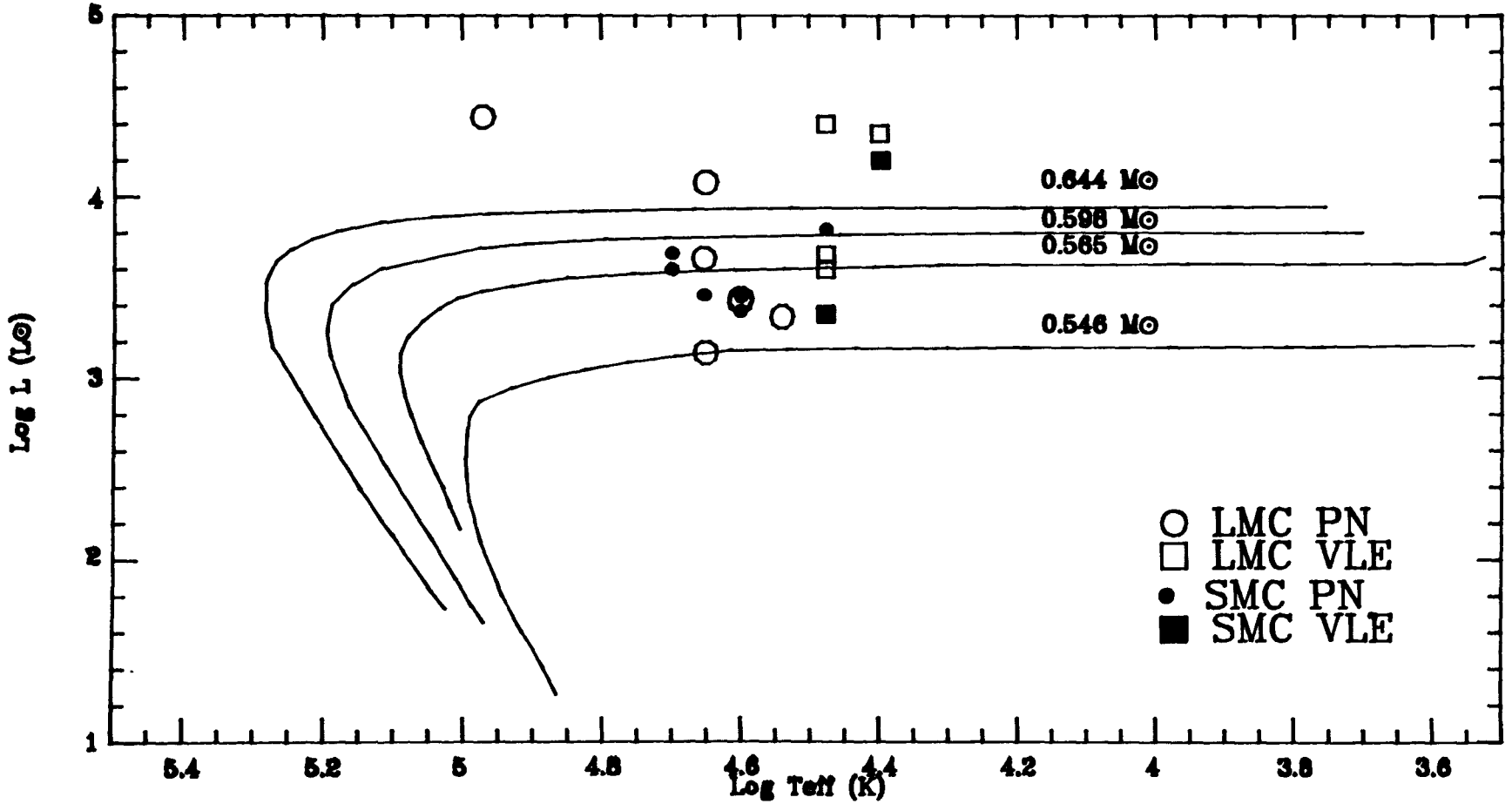

Figure 4.3. *Comparison of the central star parameters of MC PN with the theoretical evolutionary tracks of the central stars of PN (Schönberner, 1979,1983).*

central stars on this diagram and interpolating between the various model tracks an estimate of the stellar mass could be made. Any errors in the interpolation are small compared with the uncertainty in the luminosity, and a mean error of ± 0.015 $M_{\odot}$ is estimated. The position of LMC N25 and LMC N201 in the HR diagram (Fig. 4.3) is in accordance with the stellar luminosity and stellar temperature derived for these two objects in § 5.1 and § 4.6 respectively.

The position of the planetary nebulae nuclei (NPN) on the HR diagram (Fig. 4.3) show good general agreement with the Schönberner tracks, falling either within, or close to, them. The derived mass range of the NPN is from 0.54 $M_{\odot}$ to 0.72 $M_{\odot}$, with a mean mass of 0.56 ± 0.02 $M_{\odot}$, with only LMC N25 and LMC N201 being noticably above the mean value.

The general trend of the positions of the NPN on the HR diagram (Fig. 4.3) is one of a narrow band of stellar mass, around 0.6 $M_{\odot}$, with a small percentage of higher mass stars. This is in good agreement with the distribution for NPN given by Schönberner (1981), although the small number of objects involved does not allow confirmation of this distribution. The lowest luminosity PN of this sample is N78, which has a luminosity of 1317 $L_{\odot}$, and consequently a position below the 0.546 $M_{\odot}$ track (Fig. 4.3). This luminosity is below the lower limit of 2500 $L_{\odot}$ (Schönberner, 1981), and although this is within the error limits for this object ($\pm 34\%$) it probably reflects the fact that the stellar continuum of this object is near the limits of detection for this survey. The LMC PN S1 also has a low derived luminosity, 2082 $L_{\odot}$, and mass, 0.547 $M_{\odot}$, but these were derived from a stellar continuum based on an IDS, not an absolute, log $F(H\beta)$, and its position on the HR diagram is consequently uncertain.

It should be noted that the position of the 19 objects on the HR diagram presented in Fig.(4.3) are derived on the assumption that the nebulae are optically thick to the ionising photons of hydrogen. This assumption is by no means necessarily true for the objects studied, but as the analysis provides a lower limit to the derived stellar temperature and luminosity, and further UV analysis would be needed to obtain a Stoy 'energy balance' temperature to determine whether the nebulae are optically thick or thin, it is reasonable initial assumption to make. Barlow (1986) has shown SMC L302 to be optically thin by comparison of Stoy and Zanstra temperatures, and has indicated that SMC N43 and SMC N70 are optically thick. A comparison of the Stoy and Zanstra

temperatures for LMC N201 (Barlow *et al.*, 1986) shows this object to be optically thin in the H I Lyman continuum, and further analysis of its central star properties are given in § 4.6.

The VLE's SMC N8, LMC N16, and LMC N47, when placed on the HR diagram, Fig. 4.3, tend to cluster in the higher luminosity/lower temperature region, compared to the other NPN. The luminosities of LMC N16 and LMC N47 are, however, derived from stellar continua based on IDS, not absolute, log F(Hβ), their position on the HR diagram is therefore somewhat uncertain, although they, and SMC N8, are clearly separate from the main body of NPN. The two objects, LMC N99 and SMC L302, classified as VLE's by Sanduleak and Davis-Philip (1977), and a third object, LMC N101, have spectra similar to those of VLE's, but have luminosities around 5 times less than SMC N8, LMC N16, and LMC N47. Their consequent positions in the HR diagram, Fig. 4.3, indicate that they are PN and not Population I objects (a classification discussed in more detail in Chapter 5), whereas the higher luminosity objects, SMC N8, LMC N16, and LMC N47, would appear to be of Population I type.

The stellar radius can be derived from the luminosity and effective temperature using the relationship $L_* = 4\pi\ R_*^2\ \sigma\ T_{eff}^4$. From the errors in L_* and T_{eff} the corresponding error in R_* is $\pm$ 35% . The calculated value of R_* for each object is given in column 14 of Table 4.3.

Finally the surface gravity can be calculated from the stellar mass and radius, from the relationship $g = GM_* / R_*^2$. Using errors of $\pm$ 5% and $\pm$ 35% , for M_* and R_* respectively, the error in g is $\pm$ 70%, or approximately $\pm$0.3 dex in log g. The derived values of log g are given in the final column of Table 4.3, and were of sufficient accuracy to allow guidance on the choice of log g in the stellar model, giving the procedure for the adoption of temperature, luminosity, and mass a broadly self consistent nature.

4.6 He II Zanstra Temperature Analysis of LMC N201.

In an analogous treatment to H I Zanstra temperatures (§4.1), He II Zanstra temperatures can be derived using the recombination lines of doubly ionised helium, *i.e.*

He II 4686 Å , where equation 4.6 can be written as

$$\frac{L_{\lambda_z}}{\int_{228}^{\lambda_0} \frac{\lambda L_\lambda}{hc}\, d\lambda} = \frac{hc}{\lambda_{4686}} \frac{\alpha_{4686}^{eff}}{\alpha_B^{eff}} \frac{F_{\lambda_z}}{F_{4686}}. \tag{4.14}$$

again assuming that the nebula is optically thick to He II Lyman continuum photons.

Table 4.4 presents the results of this analysis, for which Black Body models were used (there being no suitable grid of high temperature Kurucz or Mihalas models available). The stellar luminosities, and other stellar parameters, must be treated with a certain amount of caution as they are derived from Black Body models, but do serve as a first approximation to the true values.

For comparison the results of the H I Zanstra analysis (§ 4.4) of LMC N201 are repeated in Table 4.4, and it is clear that there is a large discrepency between the central star temperature derived from the H I Zanstra analysis compared to the He II results. The difference in the two analyses is that the intensity of the He II 4686 Å emission line predicts a larger number of photons in the He II (and, therefore, H I) Lyman continuum than does the intensity of the Hβ emission line. This results in a lower predicted stellar temperature for the H I Zanstra analysis.

It is possible that there could be some stellar contribution to the He II 4686 Å line which would result in a derived He II Zanstra temperature higher than the H I Zanstra temperature (Natta and Panagia, 1980), but, in this case, it is more likely that the assumption that the nebula is optically thick to the H I Lyman continuum does not hold. For this object it is assumed that the nebula is optically thick to He II Lyman continuum photons, but optically thin to H I Lyman continuum photons. The total number of hydrogen recombinations would now be a measure of the number of hydrogen photo-ionisations and not of the total number of ionizing photons below 912 Å . This assumption that LMC N201 is optically thin to H I Lyman continuum photons is supported by the analysis of an ultraviolet spectrum (Barlow *et al.*, 1986) taken with the short wavelength prime focus camera (SWP) on board the International Ultraviolet Satellite (IUE). From this analysis, the Stoy 'energy balance' temperature is 80000 K, determined from a fit to a Mihalas 80000 K, log g 4.5, model (Barlow *et al.*, 1986). The 'energy balance' temperature is below the derived Black Body He II Zanstra temperature but is still in good agreement with it. The Stoy analysis is less affected by assumptions

Table 4.4 Central star parameters for LMC N201.

Object	Spectrum	$\frac{N(He^+)}{N(H^+)}$	T_e (K)	log I(Hβ)	log I(4686)	Ion	Model	T_{eff} (K)	F_* $\left(\frac{10^{-11}ergs}{cm^{-2}s^{-1}}\right)$	L_* ($L_\odot$)	M_* ($M_\odot$)	R_* ($R_\odot$)	log g
N201		0.120	15500	−12.12	−12.72								
	M5/6					HI	BB	45000	9.995				
	M5/6					HeII	BB	85750	58.88				
	IUE					HI	BB	48750	9.342				
	IUE					HeII	BB	93500	39.80‡				
										27502	0.90	0.63	4.8

Notes to Table 4.4

‡ Values of F_* used for the calculation of the stellar luminosity

M5/6 Medium resolution IDS optical spectrum, Febuary 5/6

IUE Ultraviolet IUE spectrum, SWP 14216

of the nebular opacity to ionizing photons than the Zanstra analysis, and generally sets a lower limit to the central star temperature.

Although the full analysis of the *IUE* spectrum of LMC N201 is reported elsewhere (Barlow *et al.*, 1986), it is useful, in terms of this study, to include the H I and He II Zanstra analysis based on the stellar continuum in the ultraviolet region. The spectrum was dereddened by c(Hβ)=0.11 for the foreground reddening of the Galaxy using the Galactic extinction curve of Seaton (1979), and by c(Hβ)=0.09 for the LMC reddening using the LMC extinction curve of Howarth (1983). The estimated values of Galactic and LMC reddening are taken from § 4.3. Despite the greater relative reddening for the ultraviolet spectrum there are advantages in using it for a Zanstra analysis as opposed to an optical spectra, the most obvious of which is that the hot central star will be brighter in the ultraviolet than in the optical. Additionally, the nebular continuum contribution will be a smaller fraction of the total continuum in this region, compared to the optical, and the uncertainty involved in its subtraction will be smaller. The results of the Zanstra analysis are presented in the second part of Table 4.4, and it is clear that the H I and He II Zanstra temperatures derived from the *IUE* spectrum (48750 K and 93500 K respectively) are in good agrement with the H I and He II Zanstra temperatures derived from the IDS spectrum (45250 K and 85750 K respectively), although the former are ~9% higher. The agreement between the two analyses is a useful (though by no means rigorous) check on the procedure adopted for correcting the IDS spectra; it also eliminates the possibility that the optical continuum is from a cooler star while the He II 4686 Å emission line is from the nebula of a hotter companion, which could have provided an explanation of the optical spectrum alone. The full decomposition of the nebula continuum and 93500 K Black Body stellar continuum is presented in Fig. 4.4 and compared to the ultraviolet (IUE wide slit) and optical (IDS) spectra. The total continuum fit (nebula plus Black Body) is good although it is slightly below the optical spectrum continuum, a reflection of the lower temperature predicted by the optical He II Zanstra analysis.

The stellar luminosity derived from the He II Zanstra temperature, based on the ultraviolet continuum of LMC N201 is presented in Table 4.4, and is a first approximation to the actual value as it is based on a Black Body stellar continuum. In adopting values for the stellar temperature and luminosity for LMC N201 it was felt that the

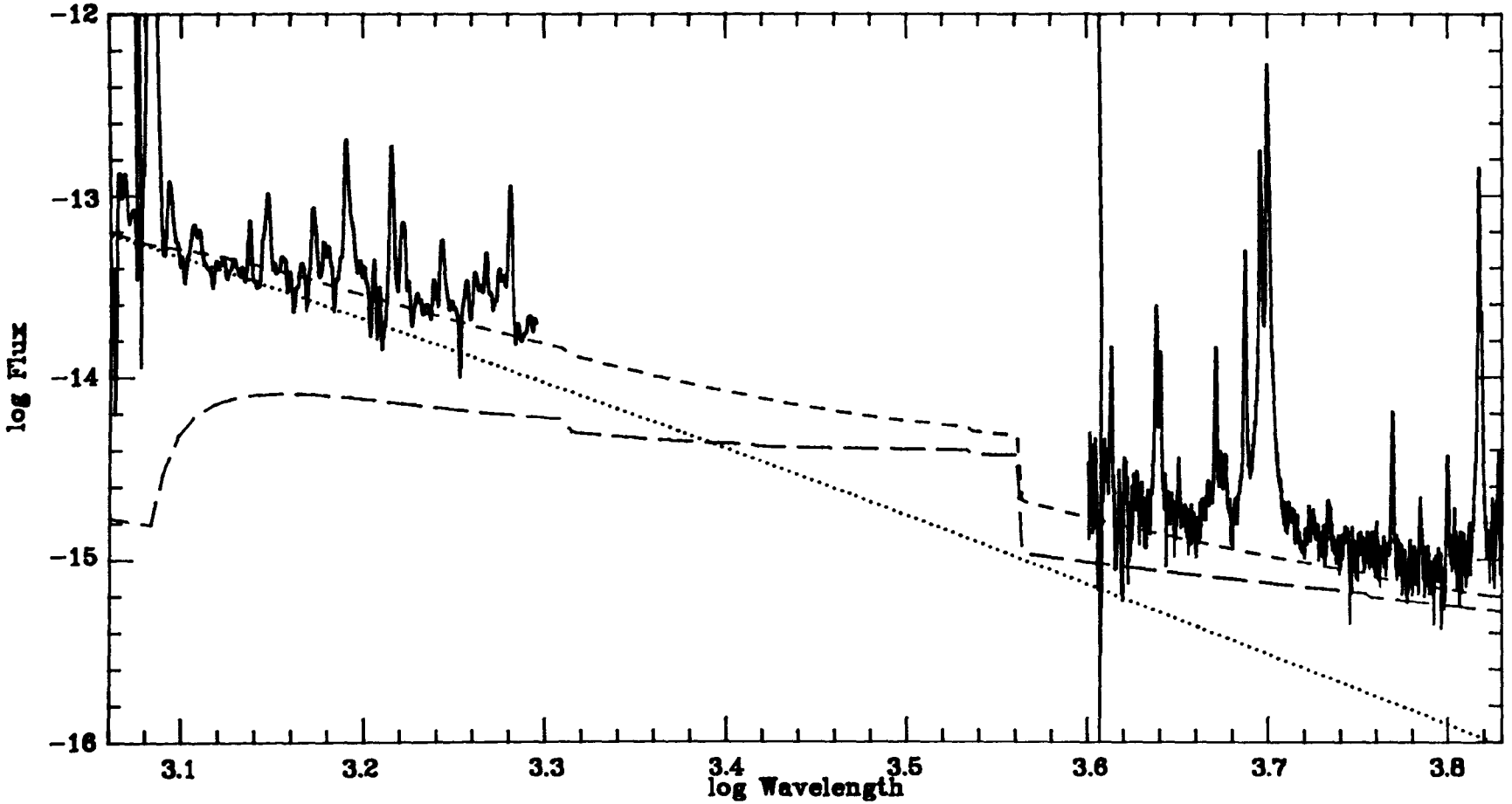

Figure 4.4. *Decomposition of the optical and ultraviolet spectra of LMC N201, showing the 93500 K Black Body (dotted line), the nebula continuum (long dashed line), and the sum of the two (short dashed line).*

He II Zanstra analysis of the ultraviolet spectrum gave the least uncertain analysis (for the reasons outlined above) and these adopted values are used to place the object in the $\log T_{eff}$, log g plane of the HR diagram (Fig. 4.3). The stellar mass, radius, and surface gravity are also derived from the adopted values of stellar temperature and luminosity (Table 4.4) by the method outlined in § 4.4.

The stellar luminosity of 27502 $L_{\odot}$ derived for LMC N201, and the interpolated stellar mass of 0.90 $M_{\odot}$, place the central star considerably above the theoretical tracks of Schönberner (Fig. 4.3). This high luminosity and high mass position for LMC N201 is not very significant, by itself, in terms of the theoretical studies of recent years, as a few high mass central stars are generally predicted (Schönberner, 1981). The marginally increased helium and nitrogen abundances of this object (log He/H +12 = 11.08, log N/H + 12 = 7.73, log N/O=−0.45), when compared to the mean LMC values (Table 3.7(a)) indicate that this object could almost be classed with the second group of 'Type I' objects (Table 3.8) and could therefore have had a high mass precursor. However, it is the only object in this study for which the adopted stellar temperature is above 60000 K, as the weak optical stellar continuum of high temperature central stars imposes a selection effect on the observations, and it would be of great interest to see if more of the higher temperature central stars had luminosities similar to LMC N201 and if they agree with the present theoretical distribution. Observations of Magellanic Cloud PN in the ultraviolet are therefore of prime importance in future studies of PN in the Magellanic Cloud galaxies.

CHAPTER 5

Further Observations of LMC N25.

In this chapter recent optical spectra of LMC N25 are analysed. The details of the observations are given in §5.1, and the reddening derived from the Balmer decrement method is discussed in §5.2. The measured emission line intensities, and derived electron temperature and density, are presented in §5.3. The derived elemental abundances are discussed in §5.4, and the stellar parameters derived from the spectra are presented in §5.5. In §5.6, the high reddening of this object is further discussed with reference to IRAS point source data. Finally, in §5.7, the helium abundance of LMC N25 is discussed with reference to the primordial value of helium, and the implications it could have for the hot big bang theory.

5.1 Optical IPCS observations of LMC N25.

Optical spectrophotometric data have recently been obtained for LMC N25. The spectra were taken on a service night, 18/19 January 1986, at the 3.9m Anglo-Australian Telescope, using the Royal Greenwich Observatory (RGO) spectrograph (Blades, 1980; Robinson, 1985) with the UCL Image Photon Counting System (IPCS; Boksenberg, 1972) as detector.

The spectra were obtained with the 250B grating and 25cm camera (blaze to collimator) giving a dispersion of 156 Å per mm at 5500 Å , and covering the wavelength range 3150-7350 Å . Both narrow slit (0.33 arc sec) and wide slit (6.7 arc sec.) spectra

were taken, providing resolutions of 4.4 Å FWHM and 9.8 Å FWHM respectively. The 'seeing' was typically 2 arc sec. throughout the night.

After flat fielding, the image data were extracted from the central cross-sections of the detector (cross-sections 25-27), and outer cross-sections, containing sky flux only, were summed and subtracted from these to yield net spectra of the central star and nebula of LMC N25. The net spectra were then corrected for the neutral density filters used, and for atmospheric extinction using the standard Siding Spring extinction coefficients. The spectra were finally calibrated spectrophotometrically using similarly processed observations of a standard star, L970-30 (Oke, 1974).

5.2 Interstellar extinction and absolute Hβ flux.

The spectra were corrected for interstellar extinction by assuming a foreground reddening of c(Hβ)=0.09 (§4.3) using the optical Galactic extinction curve of Howarth (1983), and were then corrected to the theoretical Balmer decrement (Brocklehurst, 1971) using the optical LMC reddening law (Howarth, 1983). The LMC extinction determined from the wide slit spectrum by this method is c(Hβ)=0.90, and for the narrow slit spectrum is c(Hβ)=1.06, giving total line of sight extinctions of c(Hβ)=0.99, and c(Hβ)=1.15 respectively. The total reddening of c(Hβ)=0.99, as determined from the wide slit spectrum, is adopted here.

The 6.7 arc sec slit used for the lower resolution observations provided absolute fluxes for LMC N25. The absolute Hβ flux as measured from this spectrum is log F(Hβ) = -12.90, which with a reddening of c(Hβ)=0.99 gives an absolute dereddened Hβ flux of log I(Hβ) = -11.91.

Both the logarithmic extinction coefficient and the absolute dereddened Hβ flux of this object are high compared to typical values of c(Hβ) and log I(Hβ) for LMC PN (0.16 ± 0.04 and -12.65 ± 0.30 respectively). The consequently high stellar luminosity and stellar mass derived from these spectra are discussed in §5.5, and the possibility of local or internal dust being responsible for this particularly high reddening is discussed in §5.6.

5.3 Emission line intensities and nebular diagnostics.

The IPCS narrow slit, IPCS wide slit, and IDS spectra are presented in Figs. 5.1, 5.2, and 5.3 respectively. The dereddened emission line intensities of each spectra, measured using the *DIPSO* package of routines (Howarth and Maslen, 1984), are presented (on a scale Hβ=100) in Table 5.1, with the adopted dereddened line intensities for LMC N25 given in the final column of this table. The IDS line intensities are reproduced from Table 2.1(a) for ease of comparison, and show good agreement with the IPCS data, particularly for the important He I 5876 Å , and [N II] 5755 Å ,6548 Å , and 6584 Å lines. The adopted intensities (final column of Table 5.1) are taken from the IPCS data only, with all weaker lines, or lines involved in blends, taken from the higher resolution narrow slit spectrum. One important aspect of the IPCS intensities, in view of the large extinction correction applied to them, is the consistent agreement between the adopted and theoretical Balmer line intensities throughout the spectral range from H9 to Hα, with a mean difference between observed and theoretical intensities of 6±5% .

The electron temperature of the N^+ zone of the nebula can be determined from the [N II] line intensity ratio of (6584 Å + 6548 Å)/ 5755 Å (in a similar way to the O^{++} electron temperature, §3.2, Fig. 3.1), and the electron density in the O^+ region can be determined from the [O II] line intensity ratio of 3727 Å /7325 Å . The derived values for these ratios from the adopted intensities of LMC N25 are 24.5 and 1.78 respectively, and the variation in the T_e,N_e plane for these two ions based on these ratios are presented in Fig. 5.4. The intersection point in this plane gives the adopted values of the two parameters for the whole nebula, T_e=14400 K, N_e=2.9×10^4 cm^{-3}. It is important to note that the electron density is more reliably determined than the electron temperature by these diagnostics. Measurement of the [O III]4363,4959,5007 Å line fluxes would provide a more reliable temperature diagnostic but the upper limit for the [O III]4363 Å emission line did not allow a reliable value for the [O III] electron temperature to be calculated. However, at the adopted T_e and N_e of 14400 K and 2.9×10^4 cm^{-3} the [O III] line intensity ratio, (5007 Å + 4959 Å) / 4363 Å , would theoretically be 68.0, which with [O III]5007 Å + 4959 Å = 89.6 gives [O III]4363 Å = 1.32, as compared to the observed upper limit of 0.94.

Table 5.1 Emission line intensities of LMC N25, from IPCS (wide and narrow slit) and IDS spectra.

λ (Å)	Ion	IDS	IPCS		Adopted
			Narrow	Wide	
3727	[OII]	58.9	65.1	65.4	65.3
3798	H10		5.91		5.91
3835	H9		7.00	7.75	7.00
3868	[NeIII]	<19.2	<2.3		<2.3
3889	H8,HeI	33.3 ::	10.2	9.1	9.7
3970	H7		17.1	18.0	17.6
4068,4076	[SII]		2.79		2.79
4101	Hδ	31.5	23.9	28.9	26.4
4267	CII		1.13::		1.13::
4340	Hγ	48.7	46.3	48.1	47.2
4363	[OIII]	<9.7	0.94::		0.94::
4471	HeI		2.40	2.17::	2.40
4861	Hβ	100.0	100.0	100.0	100.0
4959	[OIII]	17.4	21.8	20.1	21.0
5007	[OIII]	47.7	70.4	66.8	68.6
5755	[NII]	3.2	2.92	2.20:	2.92
5876	HeI	4.9	5.56	6.29	5.93
6300	[OI]		2.88		2.88
6312	[SIII]		0.83:		0.83:
6363	[OI]		1.02		1.02
6548	[NII]	17.1	17.2	16.0	17.2
6563	Hα	282.8	283.9	284.9	284.5
6584	[NII]	49.8	55.6	54.4	55.6
6678	HeI		2.15		2.15
7065	HeI		2.71	3.85:	3.28
7136	[ArIII]		2.12		2.12
7236	CII		0.87		0.87
7325	[OII]		34.2	39.5	36.9

Notes to Table 5.1. : - Uncertain flux
:: - Very uncertain flux

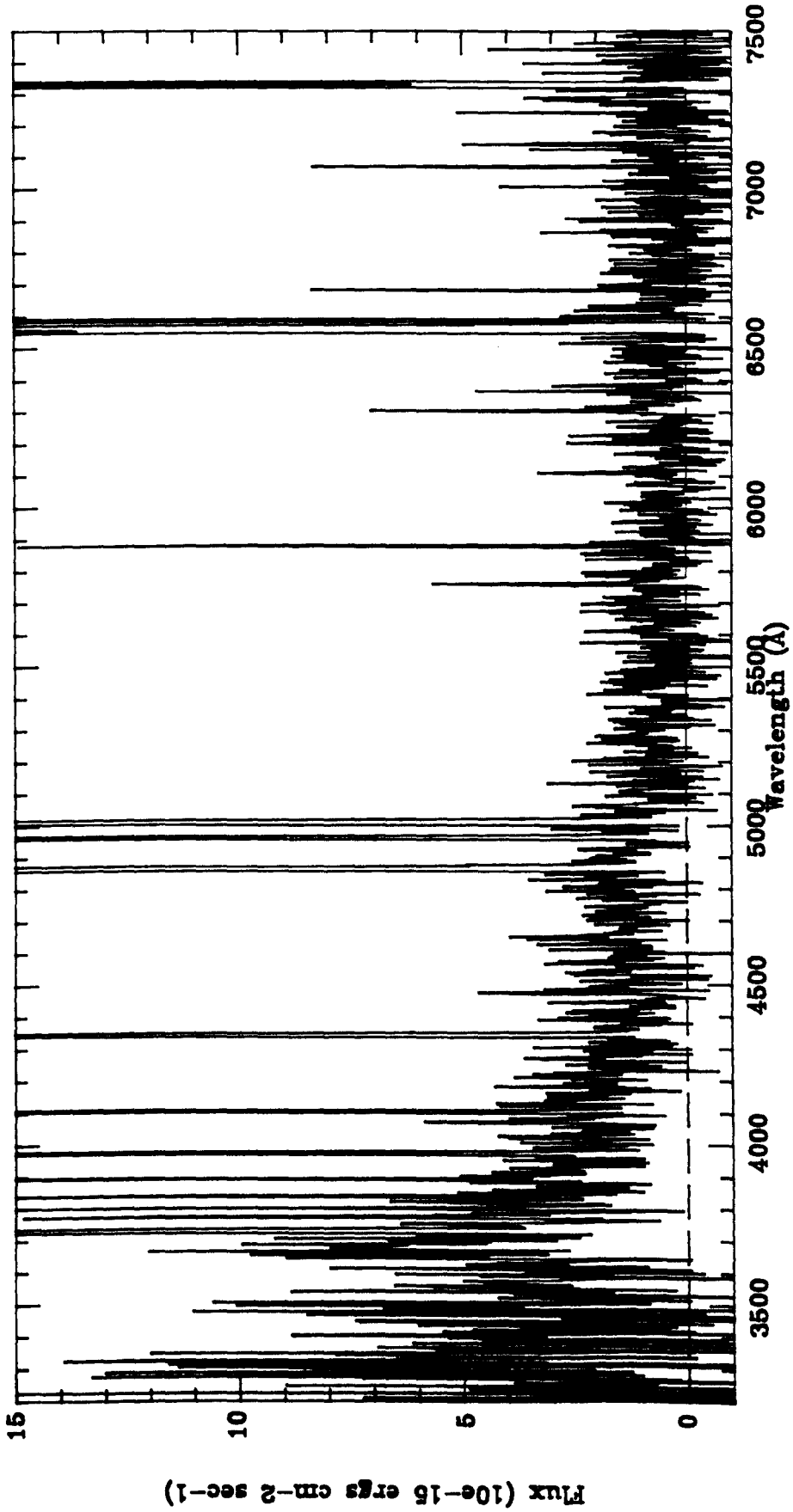

Figure 5.1. *IPCS narrow slit spectrum of LMC N25 (for continuum level comparison).*

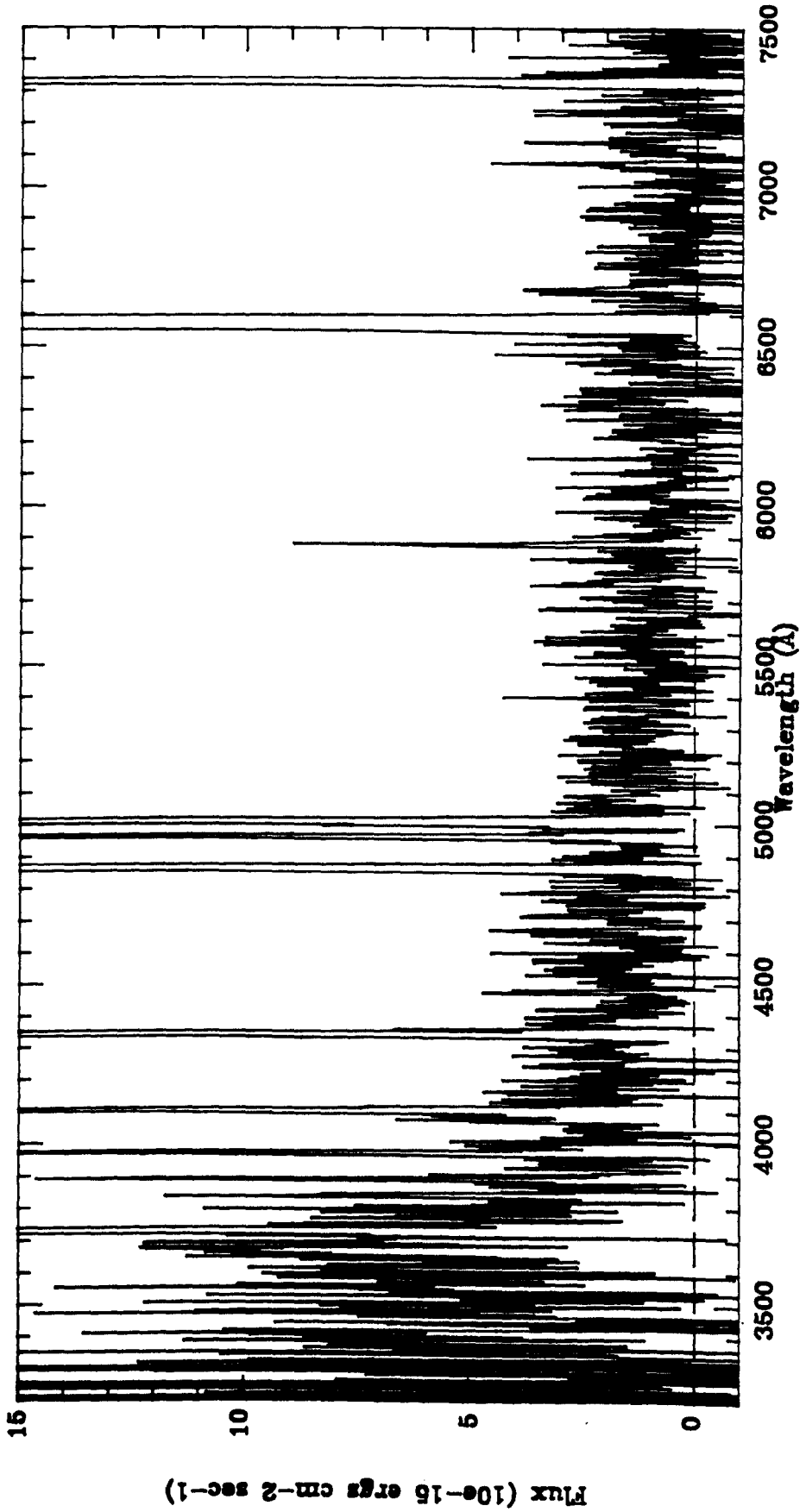

Figure 5.2. *IPCS wide slit spectrum of LMC N25 (for continuum level comparison).*

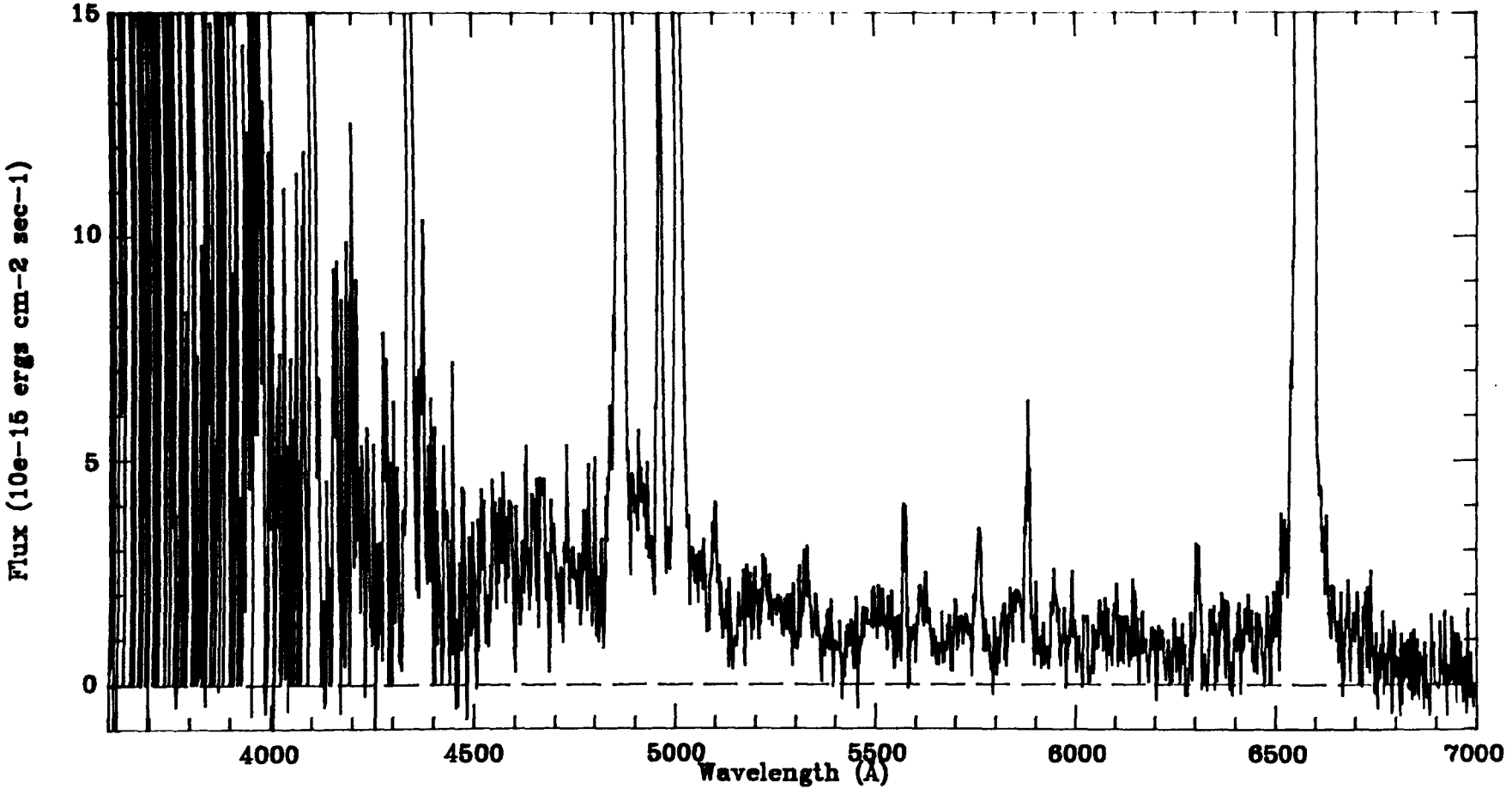

Figure 5.3. *IDS medium resolution spectrum of LMC N25 (for continuum level comparison).*

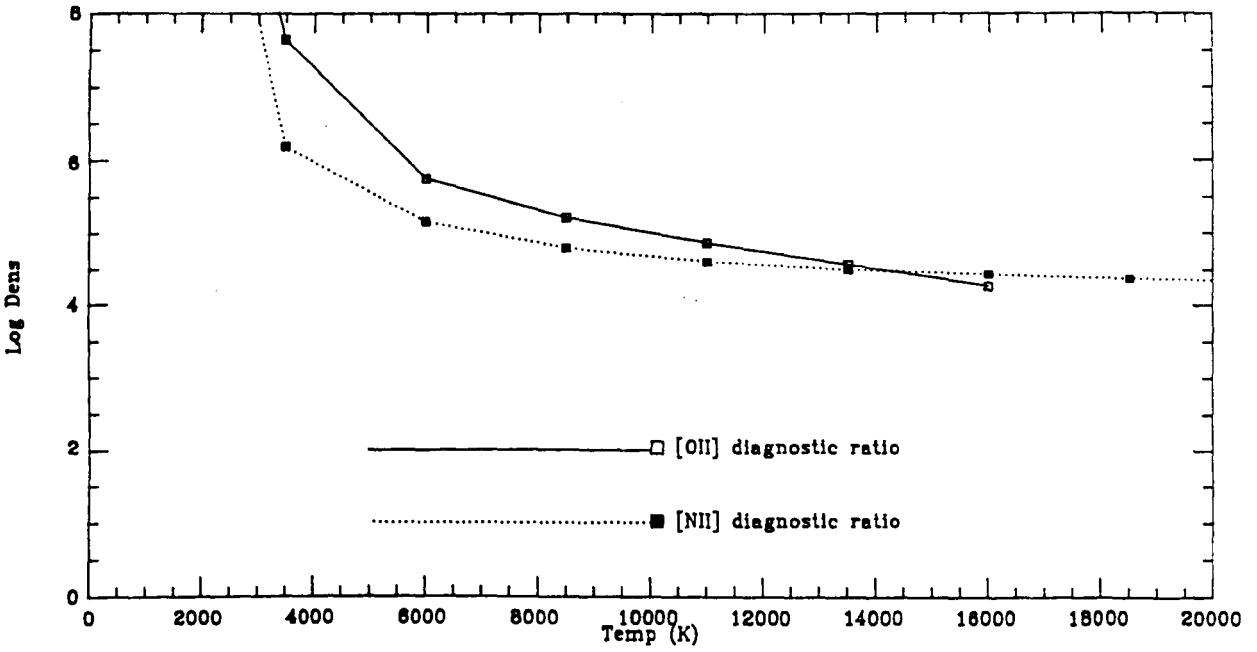

Figure 5.4

The variation of T_e with N_e for LMC N25.

The excitation class of the nebula, using the classification scheme of Morgan (1984), is 0.5 to 1.0, based on

$$\frac{[OIII]5007}{H\beta} = 0.67$$

$$\frac{H\beta}{HeII4686} > 4.00$$

and

$$\frac{H\beta}{[NeIII]3868} > 4.00.$$

This classification is reflected in the line intensities of the two major oxygen ions

$$\frac{[OII]3727}{H\beta} = 0.65$$

and

$$\frac{[OIII]5007}{[OII]3727} = 1.03.$$

Table 5.2 Ionic and elemental abundances for LMC N25.

Ion	λ(Å)	$\frac{n(ion)}{n(H^+)}$	Element	Elemental Abundance
N^+	6548+6584	5.81×10^{-6}	N	7.70×10^{-6}
O^0	6300	1.81×10^{-6}		
O^+	3727	3.17×10^{-5}		
O^+	7325	3.17×10^{-5}		
O^{++}	5007+4959	8.49×10^{-6}	O	4.20×10^{-5}
Ne^{++}	3868	$< 5.30 \times 10^{-7}$	Ne	$< 7.02 \times 10^{-7}$
S^+	4068+4076	1.71×10^{-7}		
S^{++}	6312	4.57×10^{-7}	S	8.32×10^{-7}
Ar^{++}	7135	9.23×10^{-8}	Ar	1.39×10^{-7}

The [O III]5007 Å line intensity is less than the Hβ intensity, indicating a low excitation nebula, but is still of a similar intensity to the [O II]3727 Å line, as is the case in very low excitation nebulae.

5.4 Elemental abundances of LMC N25.

Using the same procedures as outlined in chaper 3, with the adopted line intensities and the adopted T_e and N_e, the ionic and elemental abundances of N, O, Ne, Ar, and S for LMC N25 were calculated. The ionisation correction factors used are as given in §3.3 with the inclusion of the ICF of sulphur (Barker, 1983):

$$S/H = (S^+ + S^{++})/H^+ \quad \times \quad (O/O^+)$$

which was used to calculate the sulphur abundance from the [S II]4068+4076 Å and [S III]6312 Å line intensities. The ionic and elemental abundances are presented in Table 5.2.

To determine the elemental abundance of helium the ionic ratio of He^+/H^+ was derived from the He I 4471 Å , 5876 Å , and 6678 Å line intensities of the narrow slit

Table 5.3 Ionic and elemental helium abundances for LMC N25.

λ (Å)	Spectrum	$\frac{N(He^+)}{N(H^+)}$	Weight
4471	narrow	0.0514	1
5876	narrow	0.0446	4
6678	wide	0.0606	2
(4471)	wide	(0.0464)	0
5876	wide	0.0505	2.5
	Weighted Mean	0.050±0.007	

spectrum, and the He I 5876 Å line intensity of the wide slit spectrum. The final abundance of He^+ was calculated using a weighted mean of these line intensities in the ratio of 1 :4 :2 :2.5 for each line respectively. The ratio reflecting the approximate signal-to-noise ratios of the emmission lines in the two spectra. The uncertain He I 4471 Å line intensity from the wide slit spectrum was not used for deriving the He^+ abundance. Table 5.3 presents the He^+ abundances for LMC N25.

The absence of He II 4686 Å indicates that little or no doubly ionised helium exists in the nebula, whilst the central star temperature of 45000 ± 5000 K (§5.5) indicates that the amount of neutral helium in the nebula could also be negligible. The mean He^+/H^+ abundance is therefore adopted as the total elemental abundance of helium in the nebula, ie

$$He/H = 0.050 \pm 0.007.$$

In §3.4 the elemental abundances of LMC N25 derived from the IPCS line intensities, and the abundances of other low-oxygen MC PN, were compared to Galactic low-Z and Halo PN abundances, Table 3.9. The comparison showed a definite similarity between the two groups of objects, although the nitrogen abundances of the MC PN were distinctly lower.

Three of the four Galactic low-Z PN have approximately 1/100 of the Solar abundance of S and Ar (Barker, 1980,1983), and have N, O, Ne (Torres-Peimbert *et al.*, 1981) of approximately 1/4, 1/7, and 1/9 Solar abundance respectively. By comparison, LMC N25 is depleted, compared to Solar, by factors of 20 and 30 in S and Ar,

and by 10, 20, and >150 in N, O, and Ne respectively (all approximate). The very low neon abundance could be a result of substantial amounts of Ne^+ being present in the nebula and not being corrected for accurately by the ICF used. Apart from this the most striking features of the comparison are that the oxygen abundance of LMC N25 is 3 times lower than that of the Galactic low-Z PN, while the S and Ar abundances are 3-5 times higher.

The relative abundances of S, Ar, and O are the reverse of what might be expected both on the basis of simple nuclear processing arguments for low mass stars and by comparison with the S and Ar abundances derived for Galactic low-Z PN (Barker 1980,1983). First, it would be expected that the lighter elements, including to some extent oxygen, would undergo nuclear processing during the lifetime of a low mass star, whereas the heavier elements, S and Ar included, would only be processed in the higher mass stars in explosive nucleosynthesis. Second, the S and Ar abundances of Galactic low-Z PN would be (based on the first point) the abundances of the original star forming material, and, being old objects, would represent early Galactic abundances of these elements. Third, based on the present day underabundance of heavier elements in the Magellanic Clouds, the S and Ar abundances measured in old metal poor MC PN would be expected to be lower than those of their Galactic counterparts.

However, the higher S and Ar abundances of LMC N25 compared to Galactic low-Z PN seem to go against point 3, and the lower oxygen abundance of LMC N25 compared to the lower heavy element abundance Galactic low-Z PN is in conflict with the ideas of point 1. The oxygen, sulphur and argon abundances of both groups of objects taken together also give conflicting evidence to point 2 and 3. A similar situation also exists for a comparison between the Galactic low-Z PN DDDM 1 and the other three Galactic low-Z PN (Clegg *et al.*, 1986).

The conflicting evidence of the above comparison indicates the complexity of the real situation where different evolution paths for low mass stars of different initial heavy element abundance, and variations in the starting abundances, could be possible, not only from galaxy to galaxy, but also between different regions within the same galaxy.

An important extension to the above comparison would be the inclusion of carbon abundances for low-oxygen abundance MC PN, and abundances of further ionic species

of Ar, S, Ne, and O. The first of objective be achieved with *IUE* observations of Magellanic Cloud PN, and the second with the launch of the Infrared Space Observatory (ISO), which will provide flux measurements of many important infrared emission lines.

5.5 Central star parameters for LMC N25.

Using the same procedure as outlined in chapter 4 for the IDS spectra, the IPCS spectra of LMC N25 were used to determine both the temperature and luminosity of its central star. The wide slit dereddened spectrum yielded the absolute flux of the object and needed no further calibration. The dereddened, narrow slit spectrum, however, was normalised to the adopted Hβ intensity before analysis of its central star contribution. The continuum level of the normalised narrow slit spectrum was slightly below that of the wide slit spectrum, but still in good agreement with it.

The H I Zanstra temperature and stellar luminosity derived from these two spectra are given in Table 5.4, along with the stellar mass, radius, and surface gravity (determined as outlined in §4.5). The major advantages of determining these various quantities from the IPCS spectra as opposed to the IDS spectrum, are (1) the improved signal to noise ratio of the IPCS spectra, which can be seen in Figs. 5.1, 5.2, and 5.3; (2) the increased accuracy of the correction to the theoretical Balmer decrement; (3) the absolute nature of the fluxes in the wide slit spectrum; and (4) the sensitivity of the IPCS at the blue end of the spectral range. This latter point allowed the H I Zanstra analysis to be carried out at the short wavelength end of the spectrum where the stellar continuum is stronger. The wide slit spectrum also suffers little from the effects of atmospheric dispersion and should therefore be even more reliable at the blue end of the spectrum.

The adopted stellar parameters for LMC N25 (Table 5.4) are derived from the mean total stellar flux, F_*, of the Mihalas 45000 K, log g 4.0 models, normalised to the continuum levels of both the wide and narrow slit spectra. The derived stellar luminosity, 12085 $L_\odot$, and stellar mass, 0.685 $M_\odot$, of LMC N25 are both anomalous compared to the type of object generally associated with low elemental abundances.

Table 5.4 Central star parameters for LMC N25.

Object	Spectrum	$\frac{N(He^+)}{N(H^+)}$	T_e (K)	log I(Hβ)	$log\frac{I(5876)}{I(Hbeta)}$	Model	T_{eff} (K)	log g	log I(Hβ)	$log\frac{I(5876)}{I(Hbeta)}$	F. $\left(\frac{10^{-11}ergs}{cm^{-2}s^{-1}}\right)$	L. ($L_\odot$)	M. ($M_\odot$)	R. ($R_\odot$)	log g
N25	narrow	0.050	14400	−11.91	−1.23	BB	48250	-	−11.91	−0.69	15.29				
						M	45000	4.0	−11.98	−0.44	16.12‡				
	wide					BB	46250	-	−11.91	−0.73	15.95				
						M	45000	4.0	−11.92	−0.44	18.86‡				
												12085	0.685	1.81	3.76

Notes to Table 5.4

narrow - High resolution, narrow slit IPCS spectrum
wide - Low resolution, wide slit IPCS spectrum
‡ - Flux used for luminosity calculation

That is, the low oxygen, sulphur, and argon abundances of LMC N25 would indicate an old, low mass object which could evolve into a PN with a central star luminosity and mass at the lower end of the PN distribution. The high stellar luminosity and mass indicate, however, a PN precursor at the high mass end of the distribution. A possible scenario is for an old, $1M_{\odot}$ star which experiences low mass loss due to its low metallicity, and evolves into a PN with a high mass central star with a low mass nebula. The ionised nebula mass of LMC N25 can be estimated using

$$I(H\beta) = \frac{N_e^2}{(1 + y^+ + y^{++})} \epsilon \frac{V}{4\pi d^2} t_e^{-0.88} \alpha_{H\beta}^{eff} h\nu,$$

and

$$M = N_e \epsilon V M_H \frac{1 + 4y}{1 + y^+ + y^{++})},$$

giving

$$\frac{M}{M_{\odot}} = 8.07 \times 10^{11} I(H\beta) d^2 t_e^{0.88} \frac{1 + 4y}{N_e},$$

where M is the mass of the ionised gas, d is the distance to the nebula (in kpc), t_e is the electron temperature in unit of 10^4K, and y is the helium abundance, y^+ and y^{++} are the ionic abundances of singly and doubly ionised helium, V is the volume of the nebula, and ϵ is the filling factor. This gives the ionised nebula mass of LMC N25 as 0.14 $M_{\odot}$, which is considerably smaller than the 0.36 $M_{\odot}$ envelope mass of a star at the tip of the AGB, with a core mass of 0.64 $M_{\odot}$ (Wood *et al.*, 1983), and could possibly support the low mass loss rate scenario, although the estimate is for the ionised gas only and includes no neutral gas.

The anomaly could also arise through the use of an incorrect logarithmic extinction constant, which, in this case, was derived from the Balmer decrement and was found to be very much larger than typical LMC reddenings, c(Hβ)=0.99, §5.2. However, there is no evidence to suggest that this extinction coefficient is incorrect; moreover there is evidence of dust associated with the nebula or within its general location which could support the high reddening derived for this object.

5.6 IRAS observations of LMC N25.

A possible detection of infrared emission from LMC N25 was located in the Infrared Astronomical Satellite (IRAS) point source catalogue (see the IRAS explanatory Supplement, Beichman *et al.*, 1984) by association of the position of the object (α 05 09 26.4, δ -67 51 02) with that in the catalogue entry (α 05 09 25.7, δ -67 51 03). The entry gives photometric data for four infrared bands at effective wavelengths of 12μm, 25μm, 60μm, and 100μm, with inband flux measurements of $<$ 0.25 Jy, 0.46 Jy, $<$ 2.37 Jy, and $<$ 12.37 Jy respectively in each band. The entry also indicates the possibility that the band 2, 25μm, flux is confused with emission due to a local 'small scale structure' and not to a point source.

At the distance of the LMC, 47.5 kpc, and assuming similar infrared emission properties to Galactic PN (Pottasch *et al.*, 1983), the measurement of a flux in band 2 at reasonable signal-to-noise could indicate the presence of a substantial amount of dust in LMC N25, or in its vicinity, a factor that could explain the high reddening to LMC N25. The IRAS data alone, though, is of too low a quality to determine the extent, temperature, or mass of the dust, and only provides a possible, but unconfirmed, explanation for the reddening of LMC N25.

5.7 The helium abundance of LMC N25.

The helium abundance of LMC N25 was derived in §5.4 from the weighted mean of the He^+ emission lines of the IPCS wide and narrow slit spectra, and was found to be 0.050±0.007.

The absence of a He II 4686 Å emission line, and the H I Zanstra temperature of 45000±5000 K, derived in §5.5, indicate that little or no helium exists in either the neutral or doubly ionised state. The stellar temperature is somewhat below that where He^{++} would be present in the nebula in significant amounts (~60000 K, Harman and Seaton, 1966), but is high enough to ionise most of the neutral helium. According to Kaler (1978) neutral helium is only present in nebulae with central star temperatures

<44600 K, and is only present in substantial amounts for stellar temperatures <36000 K.

Torres-Peimbert and Peimbert (1977) compared the degree of ionisation of a nebula, log O^+/O, to the ionic helium abundance, $y^+ + y^{++}$, in an attempt to determine the extent of neutral helium withtin a nebula. They found that for nebulae with log O^+/O < -0.4 there is no systematic trend in the ionic helium abundance, and therefore no substantial neutral helium contribution. For objects with a larger fraction of oxygen in the O^+ state, however, there was a systematic trend to a higher neutral helium content. The exact extent of the neutral helium contribution cannot be gauged from the data presented in Torres-Peimbert and Peimbert (1977), although for the log O^+/O ratio derived for LMC N25, ~0.12, up to 25% neutral helium could be present. The small number of data points in their comparison below log $O^+/O = 0.25$, and the large scatter on the ionic helium abundance, however, makes any neutral helium estimate highly uncertain.

Based on the central star H I Zanstra temperature of 45000 K, the clear relationship between central star temperature and neutral helium content (Kaler, 1978), and the systematic but uncertain relationship between log O^+/O and neutral helium content (Torres-Peimbert and Peimbert, 1977), no correction was made for neutral helium content. The ionic abundance of He^+/H^+ is, therefore, adopted as the total helium abundance for this object, with the major uncertainty being that a small amount of neutral helium could be present. From Fig. 1 of Kaler (1978), a scatter of ± 0.015 in He/H at a temperature of 45000 K appears to be a reasonable estimate to make (in agreement with the +0.015 increase that would be due to a 25% neutral helium content). The adopted value for the total helium abundance of LMC N25, including this uncertainty is therefore,

$$\mathrm{He/H} = 0.05 \pm 0.015$$

The significance of this figure is more clearly seen when expressed as a mass fraction,

$$Y = 0.17 \pm 0.03,$$

compared to the generally accepted value or upper limit for the primordial helium abundance, Y_p, of

$$Y_p = 0.23 \pm 0.01, Y_p < 0.25$$

(Pagel, 1982; Yang *et al.*, 1984), and an estimated lower limit from Yang *et al.* (1984) who "find no convincing evidence that Y_p is less than 0.22".

The determination of Y_p is normally carried out by observing old, metal poor, objects, which are thought not to have experienced significant stellar processing, and therefore contain elemental abundances of an early epoch of the universe. Such objects would be H II regions (possibly Galactic but generally in metal poor galaxies), or blue compact galaxies (which resemble isolated extragalactic H II regions). Detailed discussion of both methods is given in Pagel (1982), Kunth and Sargent (1983), and Pagel *et al.* (1986), and is not repeated here. Planetary nebulae are rarely used for primordial helium determinations as they are generally strongly enhanced in helium by stellar nuclear processing, and correction for this enhancement must be included with any calculation of Y_p. Some empirical corrections have been obtained (Peimbert, 1983, and references therein) but are generally too uncertain to determine an accurate value for Y_p compared to other methods.

LMC N25, however, provides an interesting special case for the determination of Y_p from the helium abundance of a PN, as the derived Y_p is below that of the generally accepted value, 0.23, and would be an upper limit if due account is made of any stellar nuclear processing. That is, LMC N25 predicts a primodial helium abundance of

$$Y_p \leq 0.17 \pm 0.03.$$

It is possible that the helium abundance is not in fact this low, and that LMC N25 is a unique object which has its helium 'locked up' in some unobservable neutral helium 'pockets' in the nebula, or is helium poor through some other means. However, the presence of the object in the metal poor LMC galaxy, its association by position with the red globular cluster NGC 1852 (Webster, 1976), and the similarity of at least one other object, LMC N199 (§3.4), all give secondary supporting evidence to the above suggestion that LMC N25 is in fact a metal poor planetary nebula with a low, possibly primodial, abundance of helium.

The low oxygen abundance of the object, 4.2×10^{-5}, gives further support to this view, as a correlation between the helium abundance of an object, Y, and its heavy element abundance, Z (as measured by the oxygen abundance, O/H), is expected, although the nature of the correlation is a matter of contention (Peimbert *et al.*, 1978;

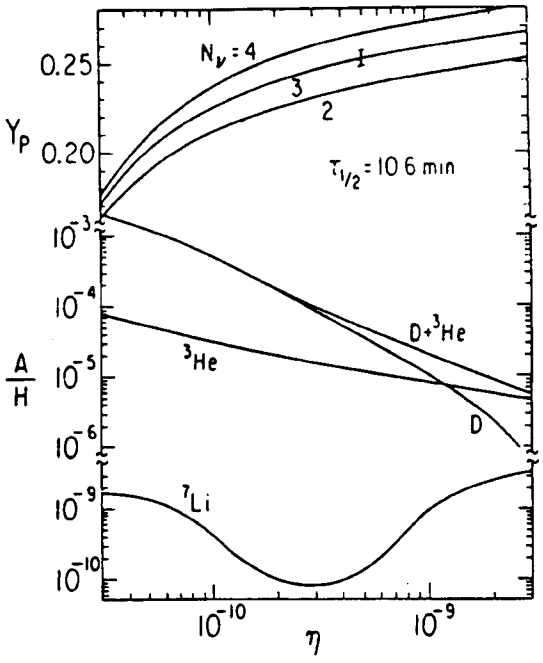

Figure 5.5

The abundance of ^4He (by mass and number) as a function of the nucleon-to-photon ratio (η) for $N\nu = 2,3,4$ species of light, two-component neutrinos, and for three choices for the neutron half-life $\tau_{\frac{1}{2}} = 10.4, 10.6, 10.8$ minutes), from Yang et al. (1984).

Shaver *et al.*, 1983; Kunth, 1982; and Pagel *et al.*, 1986). In the most recent paper on this topic Pagel and his co-workers find a maximum-likelihood linear fit to the observed values of Y and O/H for H II galaxies of

$$Y = 0.236\ (\pm 0.005)\ + 5.7Z\ (\pm 2.7).$$

Despite the fact that the Y and O/H values of LMC N25 are a long way outside of this particular correlation, this clear evidence of decreasing helium abundance with decreasing oxygen abundance lends support to the suggestion that the low oxygen abundance of LMC N25 implies that a low, possibly primordial, helium abundance would be found in the nebula. (It could be alternatively argued that the disagreement between the Y and O/H values for LMC N25 and the above correlation is evidence in favour of the LMC N25 helium abundance being anomalous.)

Taken as a true representation of the primordial helium abundance, and bearing in mind the uncertainties involved in such an assumption, the Y_p value predicted by the LMC N25 helium abundance represents a severe challenge to the present ideas on ^{4}He production in the early universe, based on the standard hot big bang model (an excellent review of which is given by Yang *et al.*, 1984, including a comparison between observation and theory). The upper limit to Y_p derived from the observations of LMC N25 provides some crucial constraints on the parameters that determine the ^{4}He abundance in the big bang model, namely the neutron to proton ratio, n/p, the number of species of light, two-component neutrinos, N_ν, and the neutron half-life, $\tau_{\frac{1}{2}}$. For a simple view, as warrented by this study, of the relationship between these parameters, the nucleon to photon ratio, η, and the primodial helium abundance, Fig. 1 of Yang *et al.* is reproduced here as Fig. 5.5, and relates Y_p and η over the normally observed range of values for various vales of N_ν and $\tau_{\frac{1}{2}}$.

With the upper-limit of $Y_p < 0.17$ derived from the helium abundance of LMC N25 (which is clearly outside of the normal range of derived values), the following assumptions can be drawn:

1) Assuming that η is well defined by observed abundances of D, ^{3}He, and ^{7}Li, to the range

$$3 - 4 \times 10^{-10} \leq \eta \leq 7 - 10 \times 10^{-10},$$

(Yang *et al.*, 1984), then $Y_p < 0.17$ would predict far too low a value of N_ν and $\tau_{\frac{1}{2}}$.

2) Assuming $N_\nu \geq 3$, $\tau_{\frac{1}{2}}$ to be well defined by the range given in Fig. 5.5, and that Y_p continues to decrease with η, then $Y_p < 0.17$ would predict a value for η far below that predicted from the observed values of D, ^{3}He, and ^{7}Li.

In either case the upper-limit of Y_p derived from the helium abundance of LMC N25 combined with the range of η values given by Yang *et al.* (1984) is seen to be in conflict with the predictions of the hot big bang model, and with most of the current estimates of Y_p. It is also of interest to note that if 1/3 of the helium content of LMC N25 were in the form of neutral helium, and that no account was taken of stellar nuclear enhancement of helium, then the derived primordial helium abundance from the LMC N25 helium abundance would be 0.23, although in this case the stellar temperature would need to be in the range 30000 - 35000 K, compared to its derived H I Zanstra temperature of 45000 ±5000 K.

CHAPTER 6

VLE's and Wolf-Rayet PN

In this chapter two classes of object that fall on the boundaries of the standard classification of planetary nebulae are briefly discussed. In §6.1 the spectra of the very low excitation (VLE) objects of this survey are presented, and their position on an HR diagram is dicussed with respect to earlier descriptions of this class of object. In the second part of the chapter, §6.2, the spectra of MC PN with Wolf-Rayet spectral features are presented, and classified according to the scheme of Torres (1985).

6.1 Very low excitation nebulae.

In this section, following a short review of earlier observations of MC VLE objects, §6.1.1, the IDS spectra of 4 LMC VLE's (including N101) and 2 SMC VLE's are presented, and discussed in §6.1.2. In the discussion a distinction is drawn between MC VLE's with stellar luminosities >15000 $L_{\odot}$, and those with stellar luminosities of the order of 4000 $L_{\odot}$. It is suggested that the first class of VLE's are Population I type objects, and the second class are PN type VLE's.

6.1.1 Earlier observations of VLE objects.

Sanduleak and Stephenson (1972) identified and discussed a group of 23 very low excitation (VLE) emission line nebulae in our own galaxy. As a group they exhibited

strong [O II]3727 Å emission lines (generally much greater than Hβ), and weak or absent [O III]4959,5007 Å emission lines (significantly weaker than Hβ). Other reported features of the VLE spectra were the lower lines of the Balmer series and a strong blue continuum, possibly arising from an underlying early-type star. They also list maximum diameters of <15 arc sec for 13 of these objects, and 6 others are denoted as stellar in appearance on the large scale direct plates of Westerlund and Henize (1967). For either case the objects seemed to be very compact nebulae.

It was suggested by Merrill (1932) that this type of unresolved, low excitation object could be a star with a greatly extended atmosphere. Sanduleak and Stephenson (1972) noted that the rarity of these objects (~5% of the PN type objects in the survey) could be accounted for if the VLE objetcs were PN in an initial, brief, stage of development. They went on to mention, however, that three other Galactic nebulae, NGC 40, HD 167362, and BD +30 3639 (which were not included in the survey), all had very low excitation spectra but had, additionally, spectral features that were indicative of Wolf-Rayet type stars. In the case of NGC 40, the nebula has a diameter of ~40 arc sec, and is therefore not a compact nebula, or a young PN.

Sanduleak and Davis-Philip (1977) carried out an objective prism survey of the Magellanic Clouds and identified 29 compact nebulae with low excitation spectra similar to those of the Galactic VLE's. They suggested that, due to the presence of a strong OB starlike continuum of generally greater strength than typical PN, the VLE spectra could be the result of a luminous blue star centrally located in a small Strömgren sphere. They further suggested that the star could either have recently formed from this associated gas cloud, or that the nebula is formed, by mass loss, around a rapidly evolving massive star. The range of absolute magnitudes (derived from apparent blue magnitudes) was $-5 > M_{BOL} > -3$, and the fact that very low excitation spectra are found to occur in H II regions with a B0, or later, exciting star (Chopinet and Lortet-Zuckerman, 1976), led them to the interpretation that the MC VLE's are extreme Population I objects.

However, two pieces of evidence were also present in their work that could possibly lead to a different interpretation for some of the VLE's identified by them. First, only 3 SMC VLE's were identified, compared to 26 LMC VLE's, the ratio of 1:4 being in conflict with the total mass ratio of the two galaxies, but in agreement with the approximate ratio of PN. Second, some of the objects in their list of VLE's were identified as having

a 'sharp' [O II]3727 Å line, implying an upper limit of 0.5 pc for the linear diameter of the nebula (Sanduleak and Davis-Philip, 1977). Both of which point to very compact PN type objects as the interpretation for some of these MC VLE's.

More recently *IUE* spectra of two LMC VLE's were reported by Nandy *et al.* (1986) who classified one of the stars, S24, as being a possible H II region excited by a small group of B2-B3 III-V stars, where the stars had recently formed from the nebula. The second object, S163, was proposed as a Bep star with an associated nebula formed by mass loss from the exciting star.

6.1.2 IDS spectra of MC VLE's.

The analysis of the IDS spectra of the 4 LMC VLE's (N16, N47, N99, and N101) and the 2 SMC VLE's (N8 and L302), is presented in chapter 2 (line intensities), chapter 3 (ionic and elemental abundances), and chapter 4 (stellar parameters). The IDS spectra of each of the 6 VLE objects are presented in Figs. 6.1 (a), (b), (c), and (d) (LMC objects), and Figs. 6.2 (a), and (b) (SMC objects). The spectra display the characteristic emission line structure and strong stellar continua characteristic of VLE's, and all have been previously classified as such (Sanduleak and Davis-Philip, 1977) except LMC N101 which has a remarkably 'VLE like' spectrum except that the [O II]3727 Å line is relatively weak. In some of these plots the [O II] line is not clearly seen, due to noise or the choice of the flux scale to emphasise the continuum level as opposed to the line structure (all spectra are plotted with an equal flux scale for direct comparison between objects). For these objects the [O II]3727 Å line intensity can be compared using Tables 2.1 (a), (b), (c), or (d).

For each object there is a strong, clear, continuum, except SMC L302 where the continuum is barely discernable at the flux scale used for the plot. A comparison between the strengths of the continua for the LMC objects shows a clear difference between N16 and N47 compared with N99 and N101, the former having by far the stronger, and therefore more luminous, continua. This is also the case for a comparison between the continuua of SMC N8 and SMC L302, although it is less clearly seen due to the decreased signal to noise on the spectra of the more distant SMC objects. The derived stellar luminosities for LMC N16, LMC N47, and SMC N8 are all >15000 $L_{\odot}$, whereas

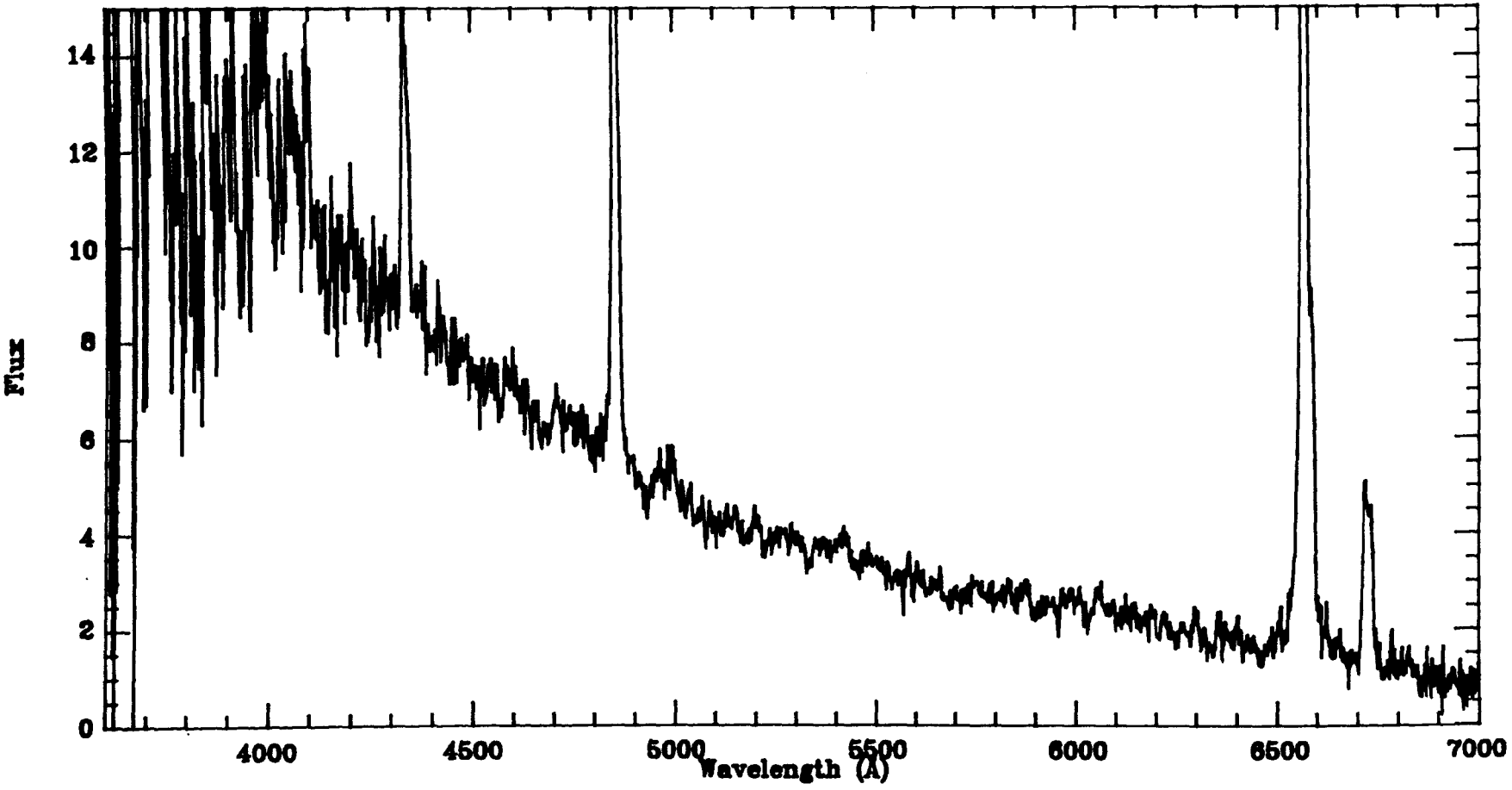

Figure 6.1(a). *IDS medium resolution spectra of LMC VLE's (for continuum level comparison): LMC N16. (Flux units of 10^{-14} ergs cm^{-2} sec^{-1}).*

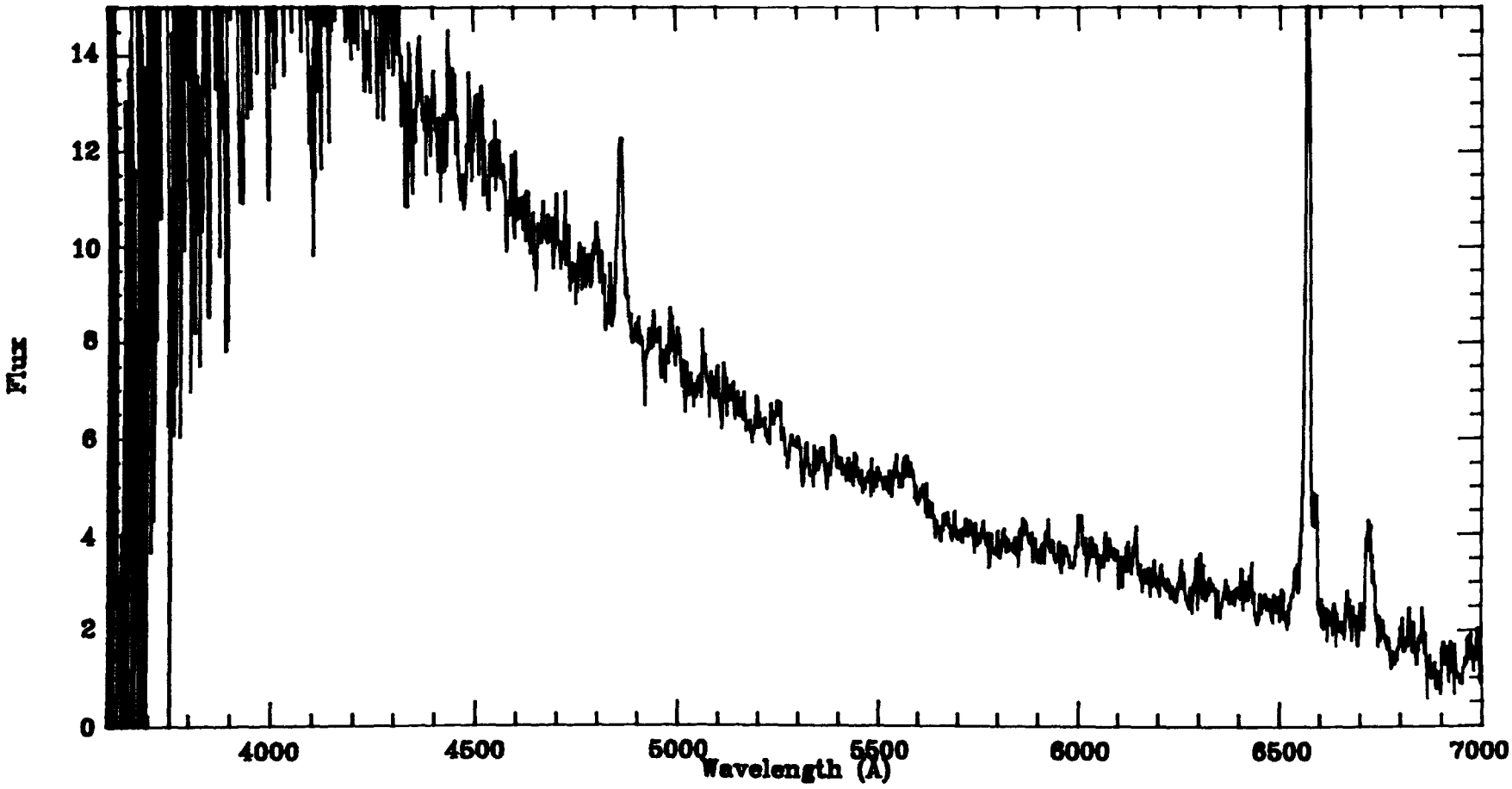

Figure 6.1(b). *IDS medium resolution spectra of LMC VLE's (for continuum level comparison): LMC N47. (Flux units of 10^{-14} ergs cm^{-2} sec^{-1}).*

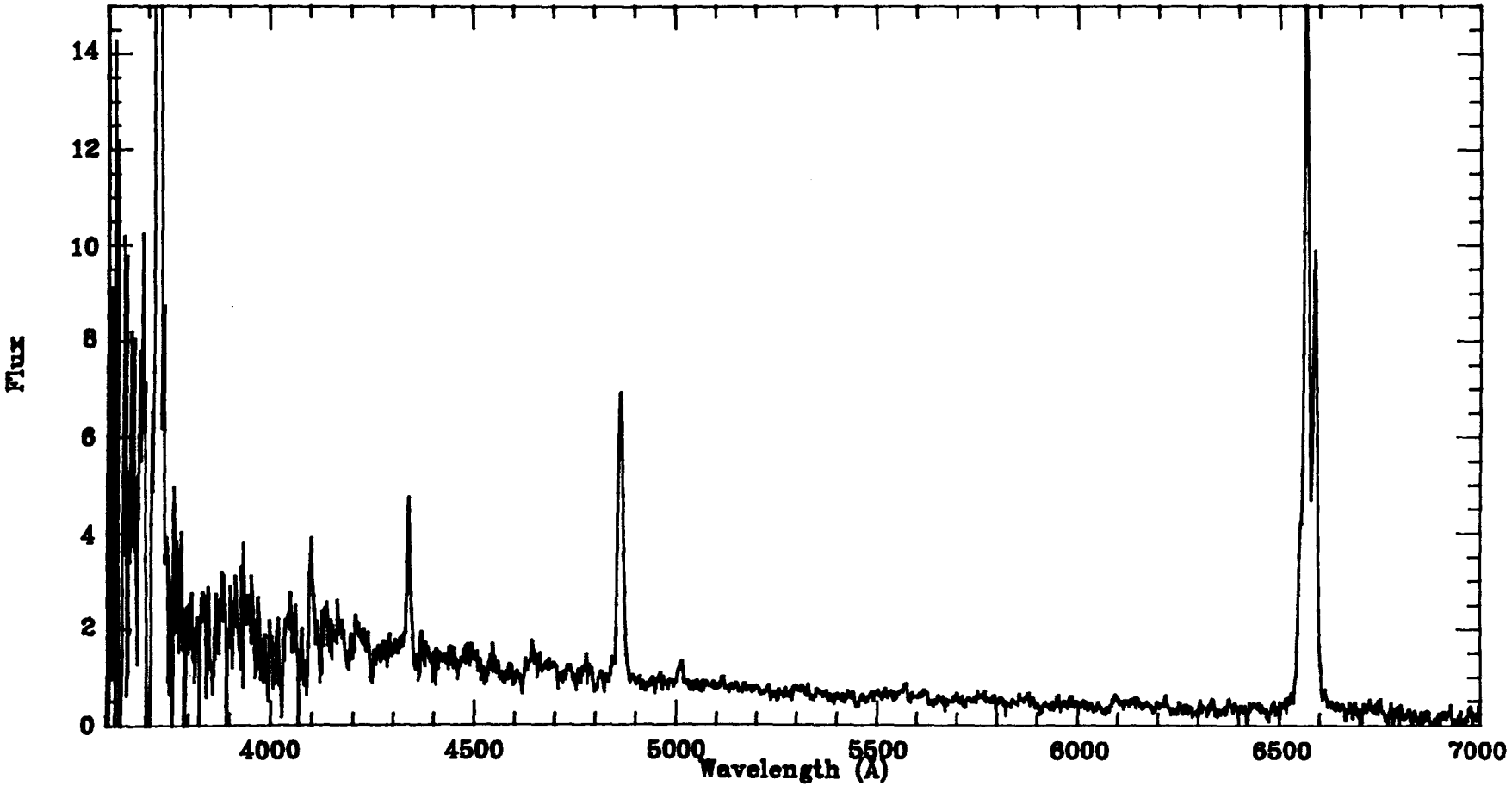

Figure 6.1(c). *IDS medium resolution spectra of LMC VLE's (for continuum level comparison): LMC N99. (Flux units of 10^{-14} ergs cm^{-2} sec^{-1}).*

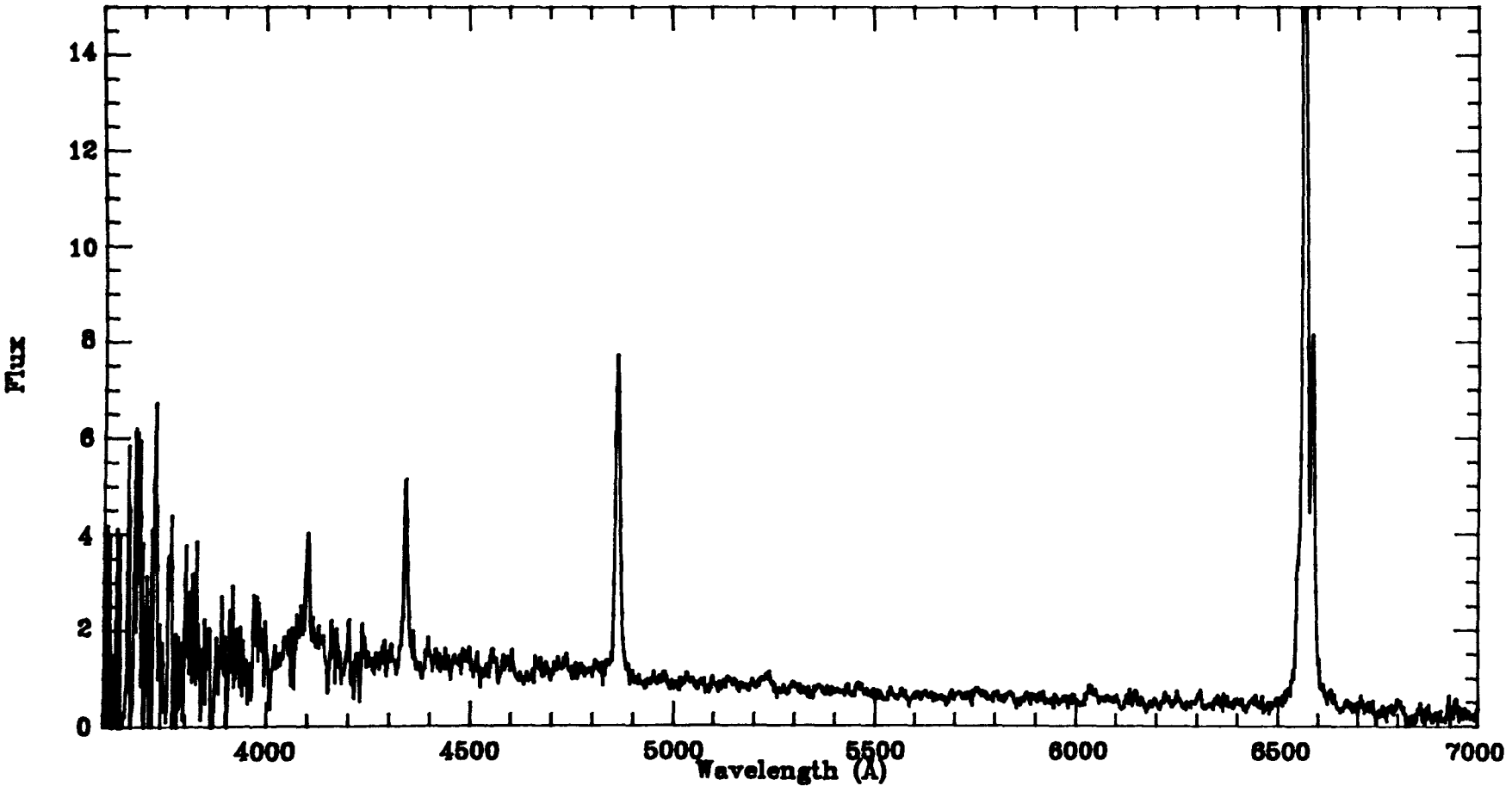

Figure 6.1(d). *IDS medium resolution spectra of LMC VLE's (for continuum level comparison): LMC N101. (Flux units of 10^{-14} ergs cm^{-2} sec^{-1}).*

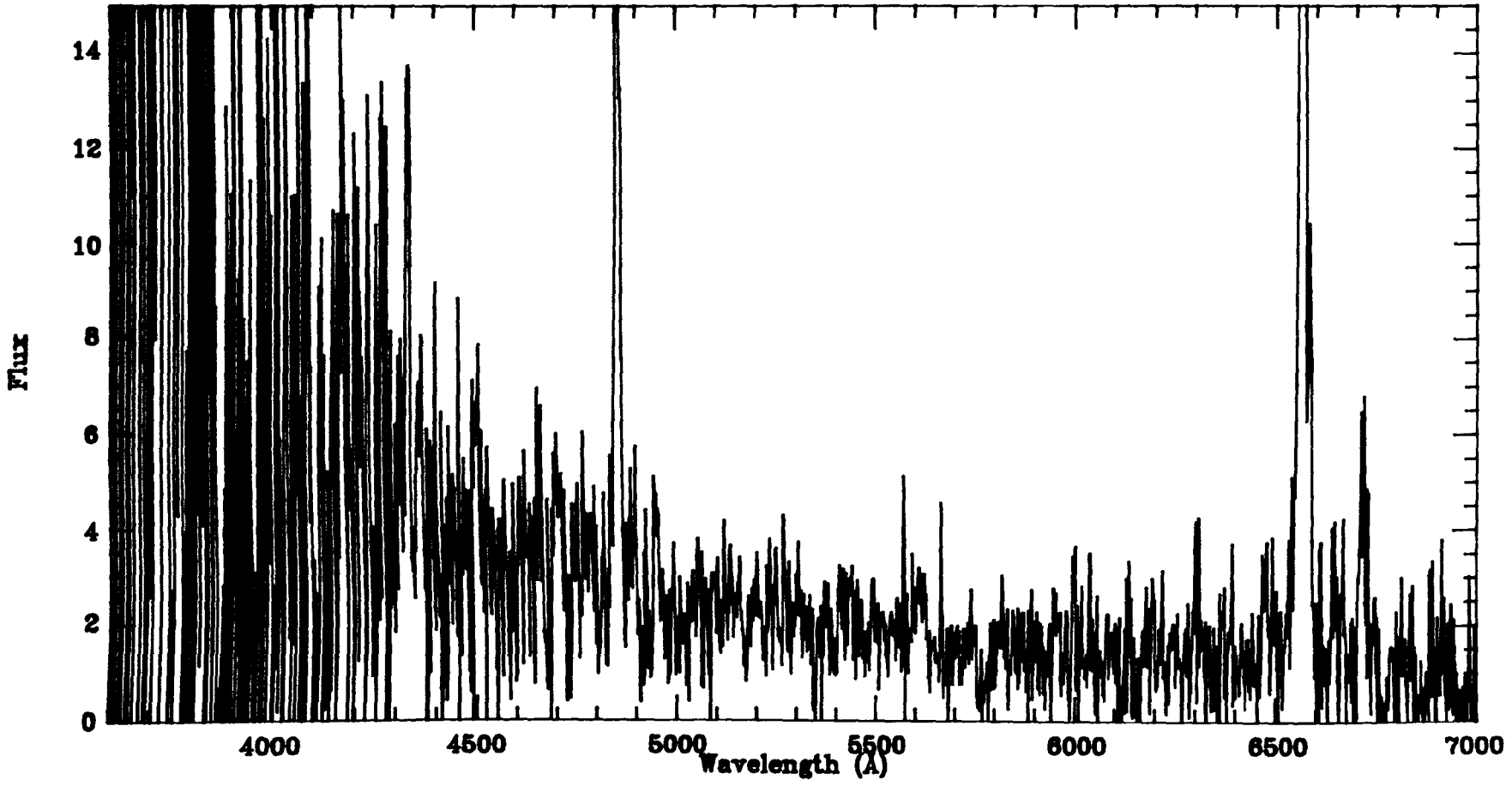

Figure 6.2(a). *IDS medium resolution spectra of SMC VLE's (for continuum level comparison): SMC N8. (Flux units of* 10^{-14} *ergs* cm^{-2} sec^{-1}*).*

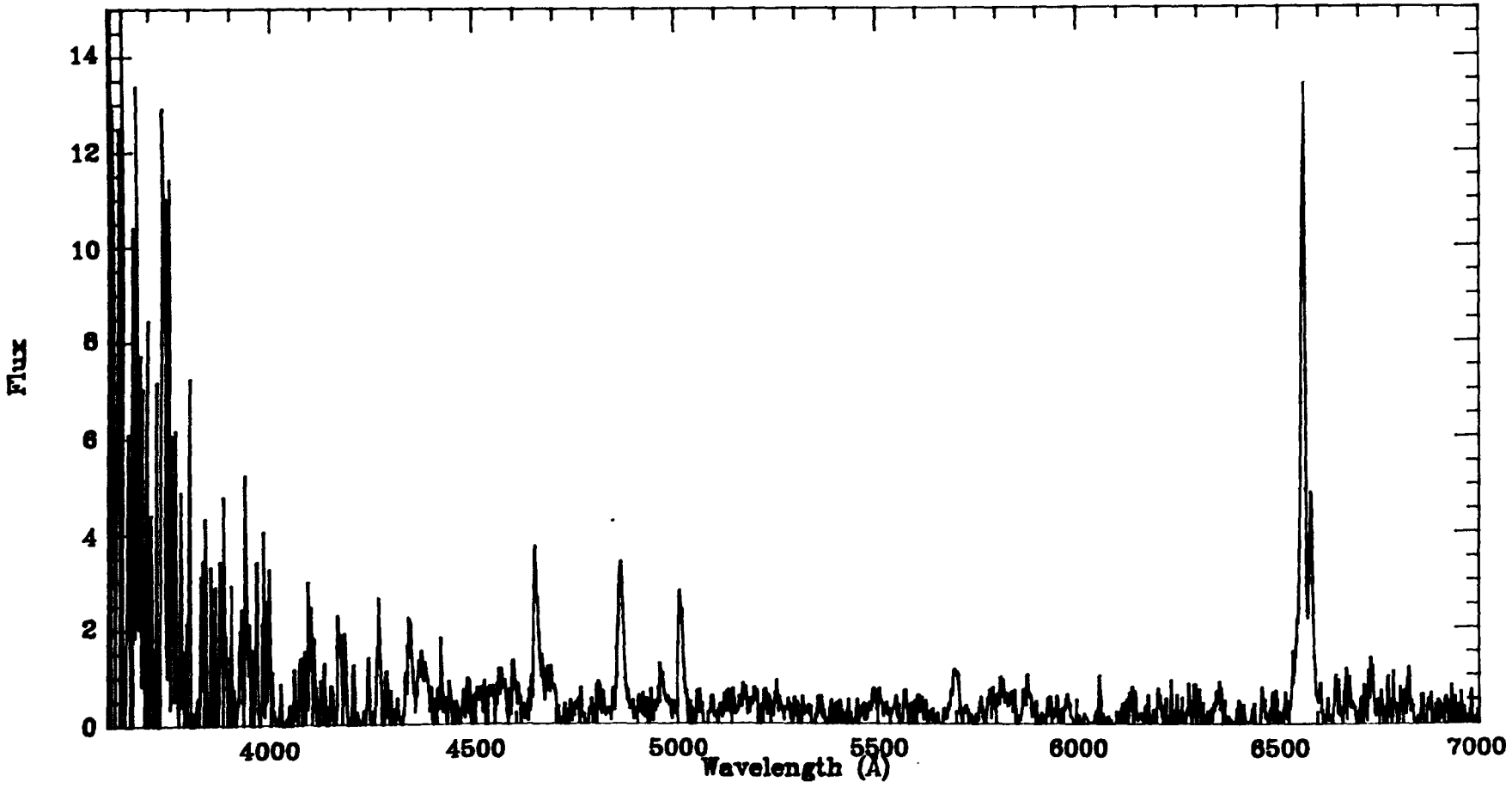

Figure 6.2(b). *IDS medium resolution spectra of SMC VLE's (for continuum level comparison): SMC L302. (Flux units of 10^{-14} ergs cm^{-2} sec^{-1}).*

those of LMC N99, LMC N101, and SMC L302 are all in the range 2000 - 5000 $L_{\odot}$ (§4.4 and Table 4.3 (a) and (b)). The luminosities of LMC N16 and LMC N47 were calculated from IDS Hβ fluxes, and the luminosity of SMC L302 is a lower limit, and they must, therefore, be treated with some caution, although the distinction between the two groups of nebulae is fairly clear.

The stellar H I Zanstra temperatures are all within the range 25000 - 30000 K (§4.4) consistent with H I Zanstra temperatures derived from observations of eight Galactic VLE's (Adams, 1983), and when combined with the stellar luminosity to place the object in the log T_{eff}, log L_* plane of the HR diagram (Fig. 4.3) a clear split in luminosity is again displayed between the MC VLE's. The objects with the lower luminosity fall within the PN evolutionary tracks of Schönberner (1979,1981); the higher luminosity objects, on the other hand, lie well above these tracks. Only two PN , LMC N201 (§4.6) and LMC N25 (Chapter 5), lie near these objects in this diagram. Both of which have significantly higher temperatures (93500 K and 45000 K, respectively) and clearly different spectra to the VLE's, although LMC N25 is a reasonably low excitation object.

Based on this clear separation in luminosity, it is suggested here that the lower luminosity MC VLE's, LMC N99, LMC N101, and SMC L302 are planetary nebulae, and are in a brief, very low excitation, early stage of development. The higher luminosity MC VLE's form a separate class of Population I object, typically compact H II regions with embedded OB type stars.

Further supporting evidence for this distinction comes from Sanduleak and Davis-Philip (1977), who were able to classify SMC L302 and LMC N99 as having 'sharp' [O II]3727 Å lines, and thereby derive an upper limit for the linear diameter of the nebula of <0.5 pc. The [O II]3727 Å line of LMC N16 and LMC N47 was resolved in their observations, and was possibly resolved for SMC N8.

LMC N101 is included within the PN type VLE classification as, although its [O II]3727 Å line intensity is not nearly as strong as the other VLE's, its extremely weak [O III]4959,5007 Å doublet, strong stellar continuum, and 30000 K stellar temperature are all suggestive of a VLE type object. The weak nature of the [O II]3727 Å line could possibly indicate that this object is a member of the 'low-oxygen' group of objects reported in this study (§3.4).

Finally the spectrum of SMC L302 displays features indentified as due to a Wolf-Rayet type central star, the classification of which is discussed in §6.2.

6.2 Wolf-Rayet central stars of MC PN.

It is beyond the scope of this study to give a full review of the Wolf-Rayet star phenomenon, and such a review would cover many areas that are unnecessary for the understanding of the simple classification procedure that is followed in §6.2.2. In §6.2.1, therefore, certain aspects of Wolf-Rayet central stars of PN are highlighted, whilst further detail can be found in de Loore and Willis (1982). Following this brief introduction, the spectral features of 5 MC PN central stars are classified according to the scheme of Torres (1985). In the final subsection, 6.2.3, the relative proportions of PN with Wolf-Rayet central stars in the Galaxy, the LMC, and the SMC are compared and briefly discussed.

6.2.1 Spectral features of Wolf-Rayet central stars of PN.

The typical Wolf-Rayet object is a massive ($\geq$ 10 $M_{\odot}$) star, with an OB like continuum, exhibiting broad spectral features of ionised nitrogen, carbon, and/or oxygen, which are thought to indicate that the star has stripped itself of its outer hydrogen envelope and has a bare stellar core of the remnants of stellar nuclear evolution (Conti, 1982, and references therein). A separate class of Wolf-rayet star, which comprises of $\sim$ 10% of the larger high-mass class, are the low mass ($\sim$ 0.6 $M_{\odot}$), low luminosity, Population II, Wolf-Rayet stars, including the Wolf-Rayet central stars of PN.

The fact that similar broad spectral features are exhibited over such a wide range of masses indicates that the Wolf-Rayet effect is probably due to a stellar atmosphere phenomenon, and is not directly linked to the internal structure or evolutionary phase of the object (although these also play some role in the effect).

The only similarity in the evolution of the two classes of Wolf-Rayet star is that both have lost their outer hydrogen envelope, and now reveal the central core of the star.

Table 6.1 Wolf-Rayet WC spectral classification, from Torres *et al.* (1986).

WC	$\frac{CIII5696}{CIV5801,5812}$	$\frac{CIII5696}{CIII_{or}OV5502}$	Other Criteria
WC9	CIII > CIV	OV weak or absent	CII present
WC8.5	CIII > CIV	OV absent	CII not present
WC8	CIII ~ CIV	OV weak or absent	
WC7	CIII < CIV	CIII ≫ OV	
WC6	CIII ≪ CIV	CIII > OV	
WC5	CIII ≪ CIV	CIII < OV	
WC4	CIV strong, CIII weak or absent	OV moderate	

Only a few PN exhibit the classic Wolf-Rayet spectral features, however, and something more intricate than purely the shedding of the the hydrogen envelope must be the cause of this class of object. Renzini (1982) suggests that the timing of the last helium shell flash is the crucial factor in determining whether a PN will have a Wolf-Rayet central star or not.

The individual classification of all Wolf-Rayet objects is based on their broad spectral features, the strength or absence of which locate the object in one of three subclasses, WC, WN, or WO, for strong carbon, nitrogen, or oxygen emission features, respectively. Each of these classes is further divided into subclasses depending on the strength and breadth of emission features from various ionisation stages of the element is concerned (Heap, 1982). A full list of the classification scheme for the WC subclass is given by Torres *et al.*(1986) and as NPN exhibit only WC (rarely WCN) features, this classification alone is reproduced here, Table 6.1.

For the MC PN classified in §6.2.2, the 5696 Å CIII feature was only measurable as an upper limit, which hindered accurate classification according to the scheme of Table 6.1. However, a separate scheme of Torres (1985) was available to classify these objects based on the flux of the 4650,4686 Å CIII feature and the 5801,5812 Å CIV feature, both of which are reasonably strong in the MC Wolf-Rayet PN spectra. The classification runs from WC4 to WC7, and is given in Table 6.2.

Table 6.2 Wolf-Rayet WC spectral classification, from Torres (1985).

WC	$\frac{CIII\,4650,4686}{CIV\,5801,5812}$ Flux Ratio
WC7	3.50 ± 0.91
WC6	2.85 ± 0.42
WC5	2.13 ± 0.37
WC4	1.82 ± 0.73

6.2.2 Classification of Wolf-Rayet central stars of MC PN.

The Wolf-Rayet spectral features of 5 MC PN are presented in Figs. 6.3 ((a) and (b)) to 6.8 ((a) and (b)), where, in each case, plot (a) covers the wavelength range 4400 Å to 4800 Å , and plot (b) covers the wavelength 5500 Å to 6000 Å . The flux scale varies from plot to plot, to emphasise the features of interest, which cannot therefore be directly compared to each other in terms of strength of emission.

Table 6.3 presents the classification of each object based on the Torres (1985) scheme, and includes a reference to the figure presenting the spectral features of the object.

All 5 objects are consistent with earlier classifications of galactic Wolf-Rayet PN central stars, in as much as they are within the WC group. The low signal to noise on the 4650,4686 Å feature obviously hinders the classification, but it is felt that the flux ratio will give the class to one subdivision. The classification of SMC N6 was derived from both the low resolution and medium resolution IDS spectra, and was found to be WC4 in both cases.

Finally it is noted that the Wolf-Rayet nature of SMC L302 will affect the derived stellar luminosity of its central star, §4.4, as a certain proportion of the stellar energy will be distributed among its stellar emission lines. A recent analysis of an ultraviolet spectrum of this object (Barlow *et al.*, 1986) estimates the ratio of the total stellar flux (including emission features) to the continuum flux to be 1.46, and the derived stellar luminosity of SMC L302, §4.4, was increased by this amount to take account of this effect.

Table 6.3 Wolf-Rayet WC spectral classification for MC PN, based on the Torres (1985) scheme.

Object	$\frac{CIII\,4650,4686}{CIV\,5801,5812}$ Flux Ratio	Class	Figure Reference
LMC N110	1.1	WC4	Fig. 6.3
LMC N133	2.7	WC6	Fig. 6.4
LMC N203	1.1	WC4	Fig. 6.5
SMC N6 low	0.9	WC4	Fig. 6.6
SMC N6 med	0.6	WC4	Fig. 6.7
SMC L302	1.9	WC4	Fig. 6.8

6.2.3 The percentage of PN central stars with Wolf-Rayet features.

In this final subsection the numbers of Wolf-Rayet central stars in the LMC, the SMC, and the Galaxy, as percentages of the sample sizes of PN are compared. For the Galactic PN the PN central star catalogue of Acker *et al.* (1982) is used, giving a sample size of 460 objects. For the LMC and SMC PN the present sample is used although the 'low-oxygen' PN are excluded as they form a larger proportion of the survey than comparable Galactic 'Halo' PN would in the Galactic sample. The sample sizes for the LMC and SMC are therefore 46 and 19 respectively (including PN type VLE's). The percentage of Wolf-Rayet central stars within these samples are 9% , 7% , and 11% for the Galaxy, the LMC, and the SMC respectively.

The uncertainty on these percentages could be quite large, as they are for incomplete and observationally biased samples. However, the three percentages are reasonably close, and certainly show no trend with the metallicity of the galaxies, indicating that the production mechanism for Wolf-Rayet PN is not strongly linked with metallicity. Furthermore, the mean percentage of $9 \pm 2\%$ is in good agreement with the expected 10% of PN that should experience a final thermal pulse after ejection of the nebula (Iben and Renzini, 1983), an evolutionary sequence that has been suggested as being responsible for Wolf-Rayet central stars of PN (Renzini, 1982). These comparisons should, however, be weighed against the errors involved in the sampling of the PN

central stars, and should be further tested with deeper surveys of MC PN to include the fainter objects.

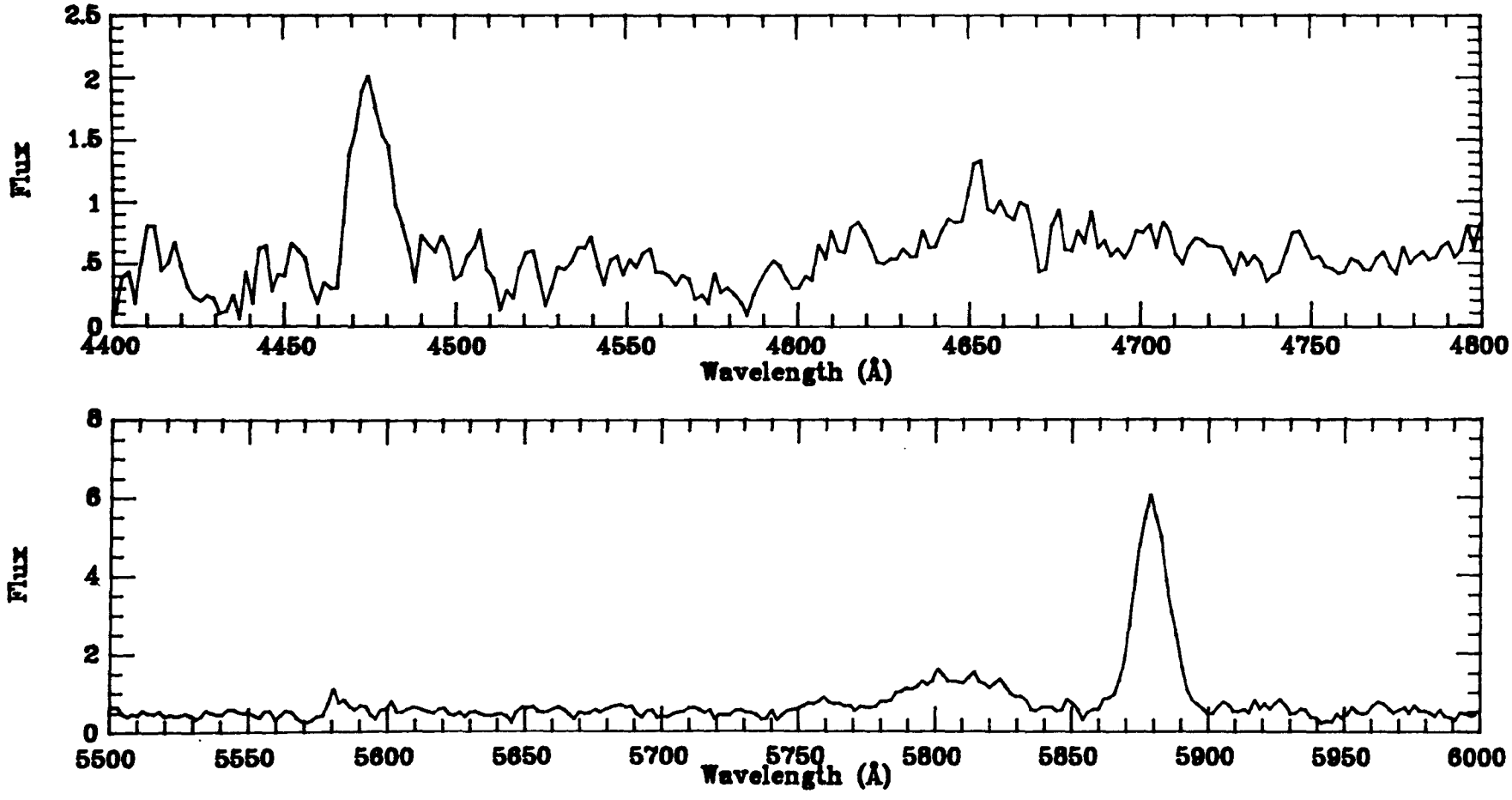

Figure 6.3. *Wolf-Rayet spectral features of LMC N110: (a) 4400 Å to 4800 Å: (b) 5500 Å to 6000 Å: medium resolution. (Top spectrum (a), bottom spectrum (b). Flux units of 10^{-15} ergs cm^{-2} sec^{-1}).*

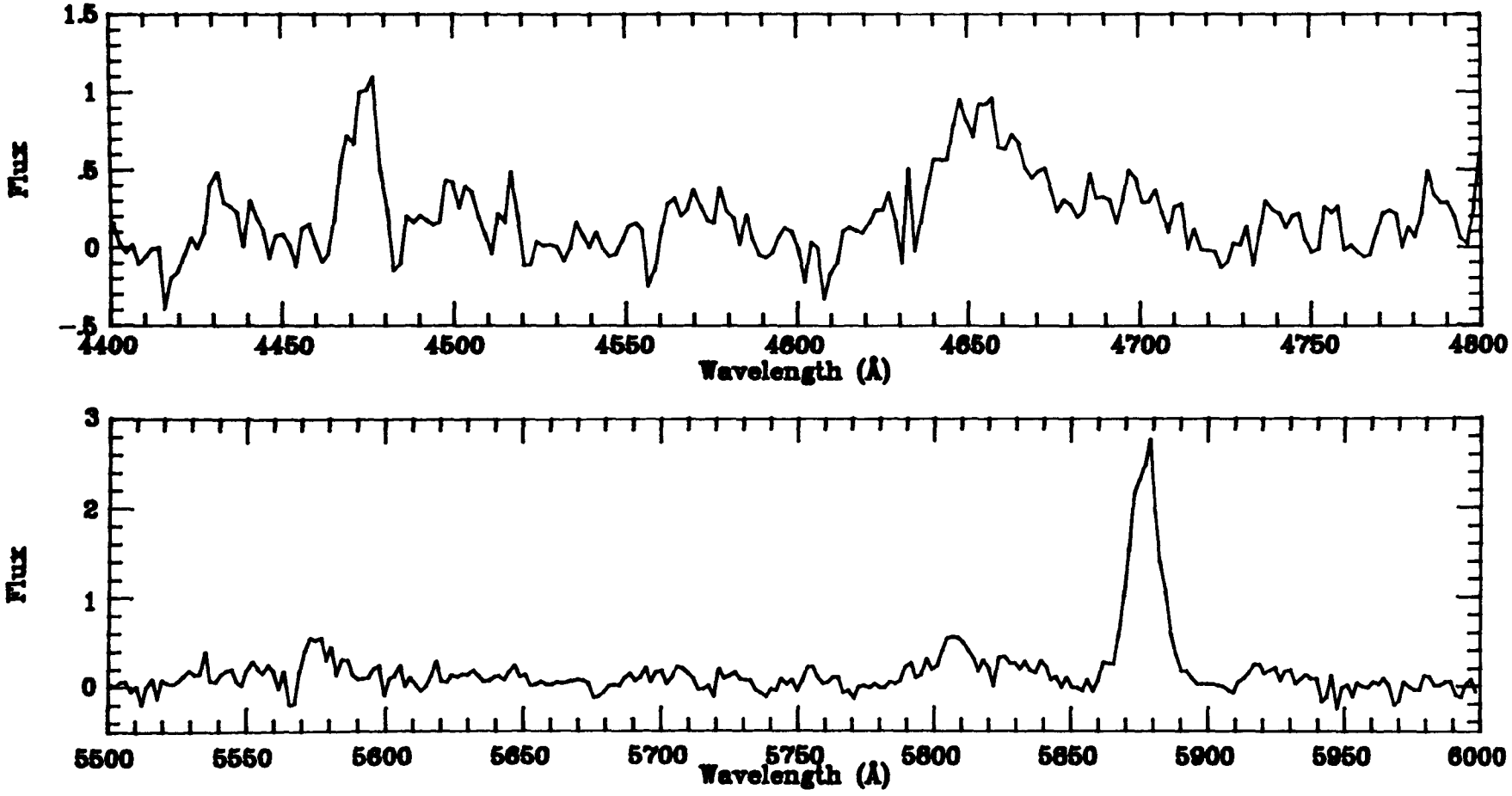

Figure 6.4. *Wolf-Rayet spectral features of LMC N133: (a) 4400 Å to 4800 Å: (b) 5500 Å to 6000 Å: medium resolution. (Top spectrum (a), bottom spectrum (b). Flux units of* 10^{-15} *ergs* cm^{-2} sec^{-1}*).*

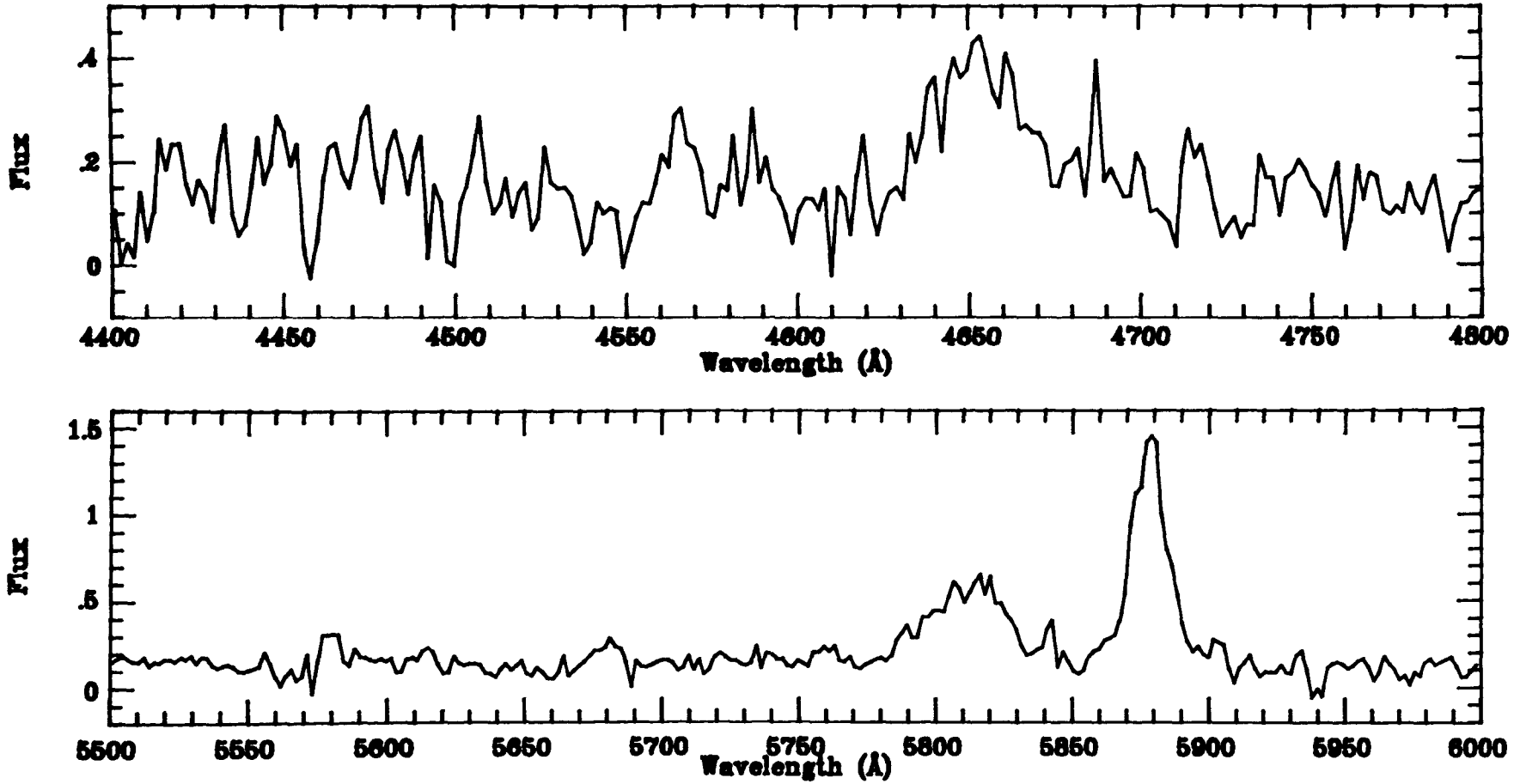

Figure 6.5. *Wolf-Rayet spectral features of LMC N203: (a) 4400 Å to 4800 Å: (b) 5500 Å to 6000 Å: medium resolution. (Top spectrum (a), flux units of 10^{-16} ergs cm^{-2} sec^{-1}). Bottom spectrum (b), flux units of 10^{-15} ergs cm^{-2} sec^{-1}).*

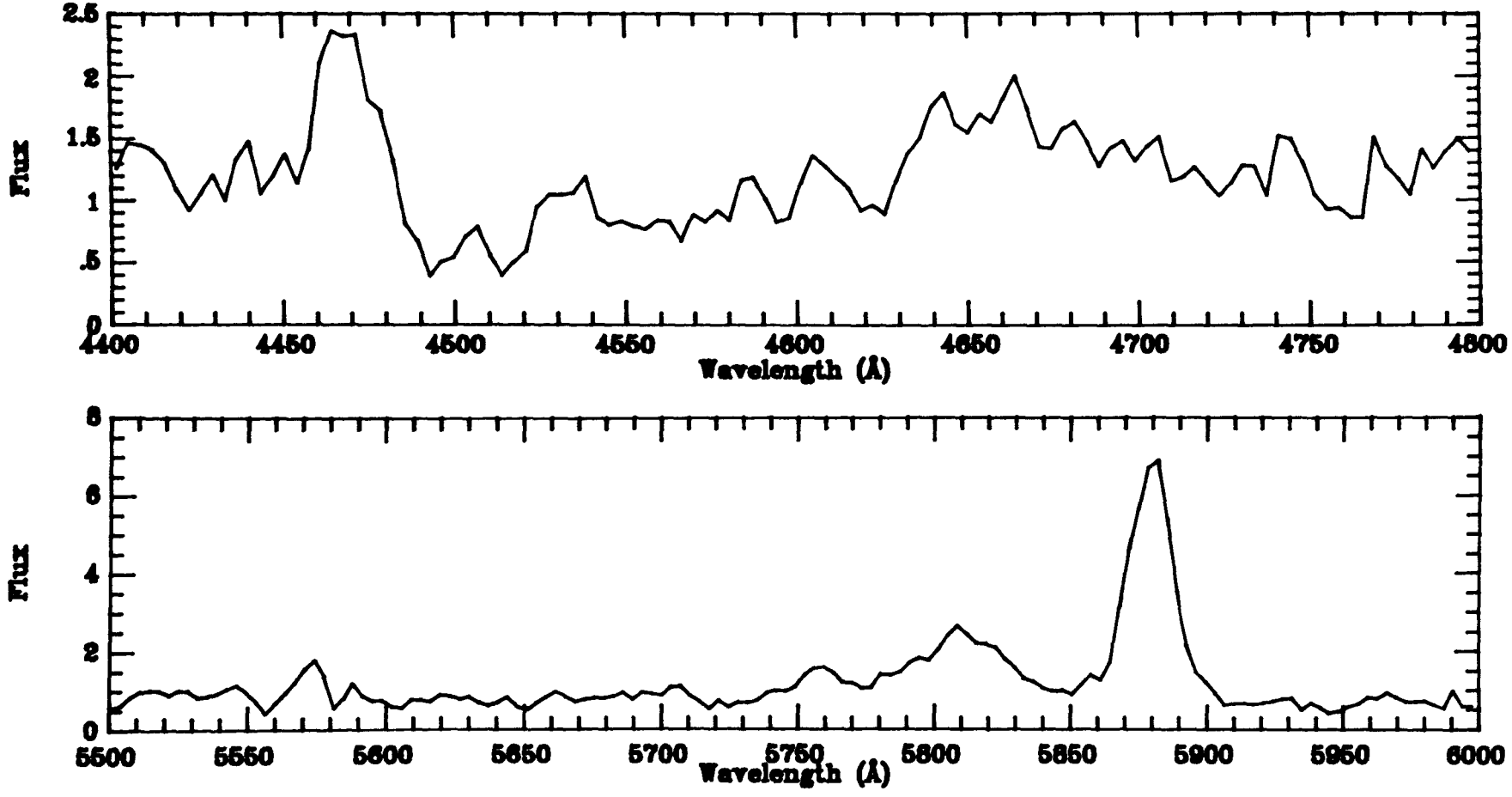

Figure 6.6. *Wolf-Rayet spectral features of SMC N6: (a) 4400 Å to 4800 Å: (b) 5500 Å to 6000 Å: low resolution. (Top spectrum (a), bottom spectrum (b). Flux units of* 10^{-15} *ergs* cm^{-2} sec^{-1}*).*

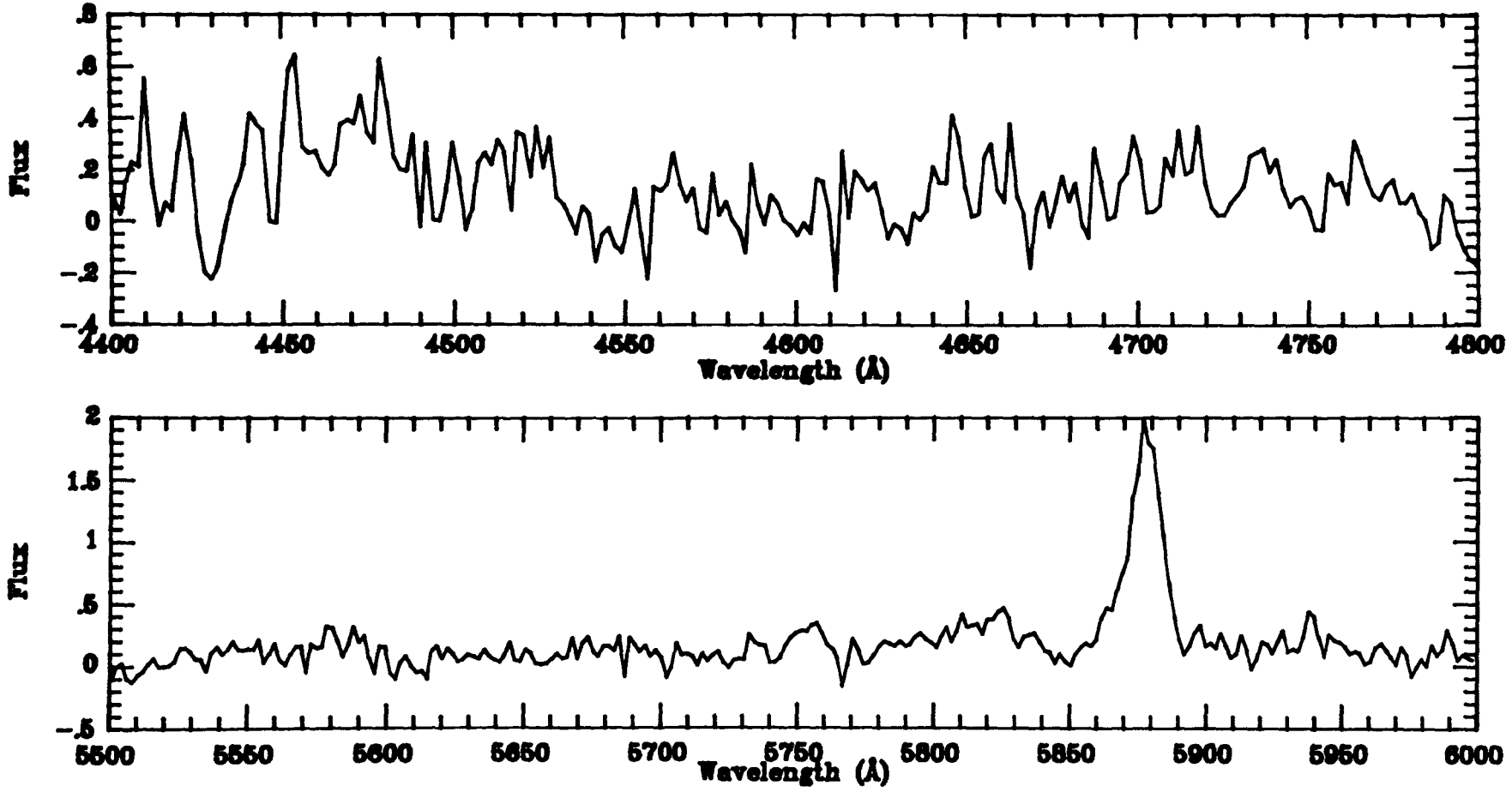

Figure 6.7. *Wolf-Rayet spectral features of SMC N6: (a) 4400 Å to 4800 Å: (b) 5500 Å to 6000 Å: medium resolution. (Top spectrum (a), flux units of 10^{-16} ergs cm^{-2} sec^{-1}). Bottom spectrum (b), flux units of 10^{-15} ergs cm^{-2} sec^{-1}).*

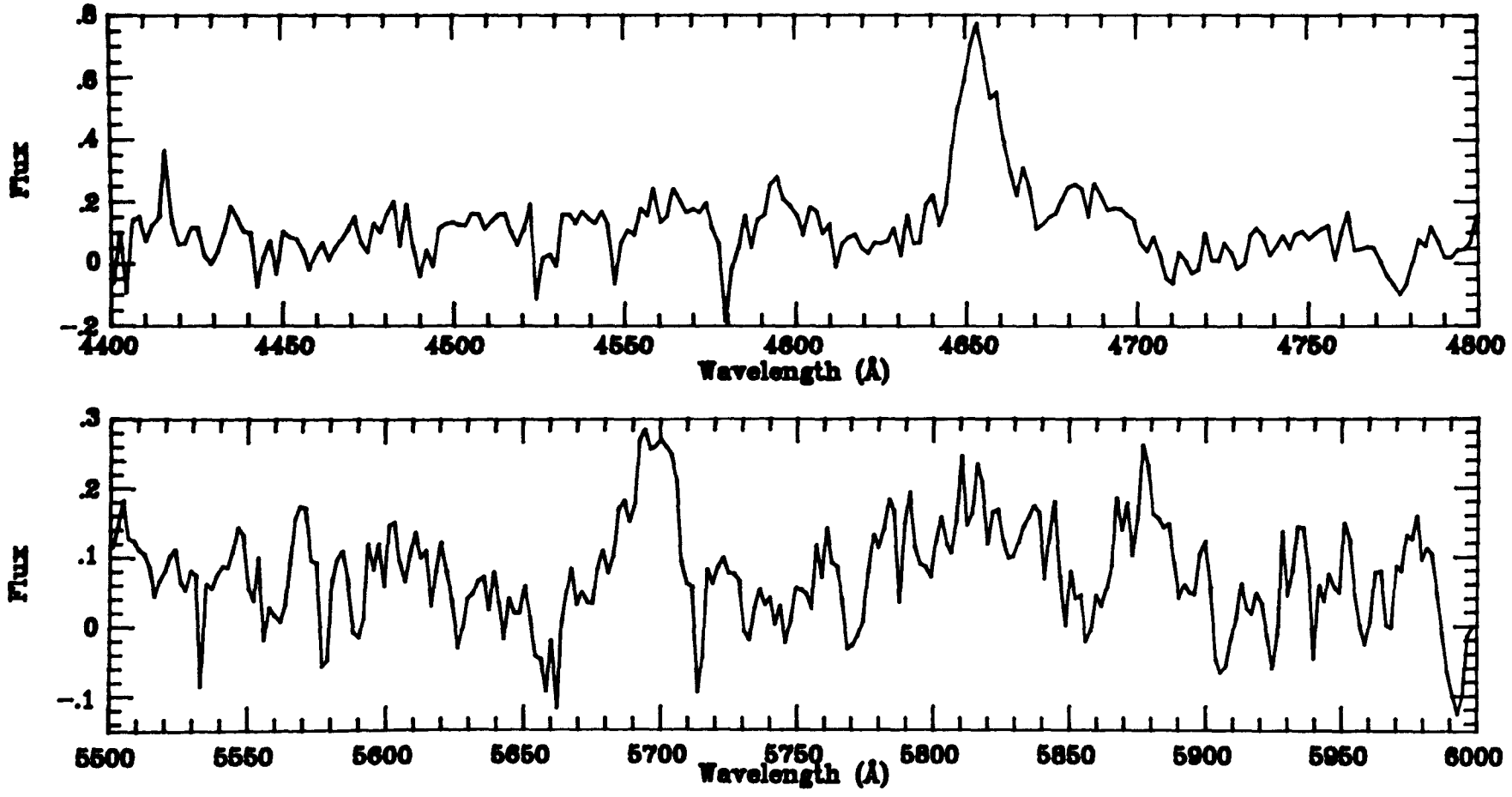

Figure 6.8. *Wolf-Rayet spectral features of SMC L302: (a) 4400 Å to 4800 Å: (b) 5500 Å to 6000 Å: medium resolution. (Top spectrum (a), bottom spectrum (b). Flux units of 10^{-16} ergs cm^{-2} sec^{-1}).*

CHAPTER 7

Summary and Future Work

7.1 Summary

The main findings and accomplishments of this study are summarised as follows:

(1) The intensities of emission lines in the wavelength region 3600 - 7000 Å are presented for a large sample of PN within the Magellanic Clouds.

(2) From the emission line intensities, the electron temperatures in the O^{++} zone and (in some cases) the N^{+} zone of the nebula are derived for the majority of objects studied.

(3) Using the derived electron temperatures (or an assumed value of 10000 K) and the electron densities derived by Barlow (1986) (or an assumed value of 5000 cm^{-3}), the abundances of He, N, O, Ne, and Ar are calculated, where possible, for all objects in the survey.

(4) A comparison of PN and H II region abundances in the Galaxy, the LMC, and the SMC reveals an enhancement of He and N during the PN progenitor stage of the stars life. The nitrogen enhancement from H II region to PN in all three galaxies is remarkably uniform, 0.7 ± 0.2 dex.

(5) The trend of abundances in all three systems is one of lower abundances in the LMC compared to the Galaxy, and lower abundances in the SMC compared to the LMC.

(6) Within the survey analogues of Galactic PN are found; there are 5 (and possibly 10) He and N rich nebulae resembling Peimberts Type I PN, 6 objects with low oxygen abundance, analogous to the Galactic Halo PN, 5 very-low-excitation (VLE) nebulae, and 5 PN with Wolf-Rayet central star features.

(7) The H I Zanstra temperature, and stellar luminosity are calculated for 19 objects within the survey, and are directly compared with the Schönberner (1979,1983) PN evolutionary tracks. Most of the objects are in good agreement with the tracks, although LMC N201 was considerably above them with a derived luminosity of 27502 $L_{\odot}$.

(8) Comparison of the VLE stellar luminosities reveals two distinct groups of objects. The first with luminosities typical of PN central stars, and the second with luminosities far above the typical PN value, *i.e.* $\gg$5000 $L_{\odot}$. The VLE's with the lower luminosities are classed as Planetary Nebulae, and are assumed to be going through an early, low stellar temperature, very low excitation phase of evolution. The higher luminosity VLE's are classed as Population I objetcs.

(9) Five objects within the survey display Wolf-Rayet central star features and are classified within the WC Wolf-Rayet scheme of Torres (1985). The percentage of PN central stars with Wolf-Rayet features is derived for the Galaxy, the LMC, and the SMC. The mean value of $9 \pm 2\%$ is found to be in good agreement with the proportion of PN experiencing a thermal pulse after ejection of the nebula.

(10) For one of the PN with a low oxygen abundance, LMC N25, recent IPCS spectra are analysed which confirm the interesting abundances of the nebula, *i.e.* (log O/H + 12) = 7.62, and He/H = 0.05 ± 0.015. The derived central star H I Zanstra temperature is found to be 45000 ± 5000 K, and the stellar luminosity 12085 $L_{\odot}$.

(11) Although of low ionization the neutral helium content of the nebula of LMC N25 is judged to be small, as the central star temperature is high enough to ionise most of the He^{0}. The ionic helium abundance is therefore adopted as the elemental helium abundance.

(12) Comparison of the derived helium abundance of LMC N25 with primodial abundances and simple Big Bang theory, shows a marked disagreement, with the Big Bang theory unable to encompass the very low derived helium abundance of LMC N25.

7.2 Future Work.

Based on the findings of this survey the following areas would appear to be of importance for future research:

(1) Continuation of large scale surveys of MC PN at higher resolution and sensitivity, to determine the electron temperature, electron density, and elemental abundances with a higher degree of accuracy.

(2) Observation of a wider range of ionisation stages for all elements of interest, to determine elemental abundances less reliant on the accuracy of ionisation correction factors.

(3) Observation of MC PN central stars in the ultraviolet region of the spectrum to determine the stellar luminosity, temperature, and mass for a wide range of MC PN.

(4) Detailed observations of 'low oxygen' MC PN to determine the central star luminosities and temperatures, and the nebular diagnostics and elemental abundances to a higher degree of accuracy.

(5) A more accurate determination of the relationships between nebula ionisation state, central star temperature and nebular neutral helium content, to provide an estimate of the neutral helium content in LMC N25.

(6) The calculation of a full ionisation model for LMC N25.

References

Acker, A., Gleizes, F., Chopinet, M., Marcout, J., Ochsenbein, F., Roques, J. M., 1982,*'Catalogue of the Central Stars of Planetary Nebulae'*, Publ. Spec. du CDS No. 3.

Adams, S. 1983, *Ph.D. Thesis*, University College London.

Aller, L. H., 1983, *Astrophys. J.*, **273**, 590.

Aller, L. H., & Czyzak, S. J., 1983 a, *Astrophys. J. Suppl.*, **51**, 211.

Aller, L. H., & Czyzak, S. J., 1983 b, *Proc. Nat. Acad. Sci.*, **80**, 1764.

Aller, L. H., & Keyes, C. D., 1986. In preparation.

Aller, L. H., Keyes, C. D., Ross, J. E., & O'Mara, B. J., 1981., *Mon. Not. R. astr. Soc.*, **194**, 613.

Auer, L. H., & Mihalas, D., 1972, *Astrophys. J. Suppl.*, **24**, 193.

Baluja, K. L., Burke, P. G., & Kingston, A. E., 1980, *J. Phys. B*, **13**, 829.

Barker, T., 1980, *Astrophys. J.*, **240**, 99.

Barker, T., 1983, *Astrophys. J.*, **267**, 630.

Barker, T., & Cudworth, K. M., 1984, *Astrophys. J.*, **278**, 610.

Barlow, M. J., 1986*Mon. Not. R. astr. Soc.* In Press.

Barlow, M. J., & Adams, S., 1986. In preparation.

Barlow, M. J., Clegg, R. E. S., Monk, D. J., Walker, A. R.,1986. In preparation.

Becker, S. A., & Iben, I., Jnr., 1979, *Astrophys. J.*, **232**, 831.

Beichman, C. A., Neugebauer, G., Habing, H. J., Clegg, P. E., & Chester, T. J., 1984, *IRAS Catalogue Explanatory Supplement*, Publ. Joint IRAS Science Working Group.

Blades, J. C., 1980, *'The RGO Spectrograph'*, Publ. Anglo-Australian Observatory.

Bohlin, R. C., 1975, *Astrophys. J.*, **200**, 402.

Bohlin, R. C., Savage, B. D., & Drake, J. F., 1978, *Astrophys. J.*, **224**, 132.

Boksenburg, A., 1972, In: *Proc. ESO/CERN Conference*, P. 295.

Brocklehurst, M., 1971, *Mon. Not. R. astr. Soc.*, **153**, 471.

Brocklehurst, M., 1972, *Mon. Not. R. astr. Soc.*, **157**, 211.

Burstein, D., & Heiles, C., 1982, *Astrophys. J. Suppl.*, **87**, 8.

Butler, K., & Mendoza, C., 1984, *Mon. Not. R. astr. Soc.*, **208**, 17p.

Caldwell, J. A. R., & Coulson, I. M., 1985, *Mon. Not. R. astr. Soc.*, **212**, 879.

Chopinet, M., & Lortet-Zuckermann, M. C. 1976, *Astr. Astrophys. Suppl.*, **25**, 179.

Clegg, R. E. S., Peimbert, M., Torres-Peimbert, S., 1986*Mon. Not. R. astr. Soc.* In press.

Conti, P. S., 1982, In: *Proc. IAU Symp. 99, p 9,* ed. De Loore, C. W. H., & Willis, A. J., D. Reidel, Dordrecht, Holland.

Davidson, K., & Kinman, T. D., 1984, *Preprint.* .

Dufour, R. J., 1984, In: *Proc. IAU Symp. 108, p 353,* ed. van der Bergh, S., & de Boer, K. S., D. Reidel, Dordrecht, Holland.

Dufour, R. J., & Killen, R. M., 1977, *Astrophys. J.*, **211**, 68.

Dufour, R. J., Shields, G. A., & Talbot, R. J. 1982, *Astrophys. J.*, **252**, 461.

Feast, M. W., 1968, *Mon. Not. R. astr. Soc.*, **140**, 345.

Fitzpatrick, E. L., 1985, *Astrophys. J. Suppl.*, **59**, 77.

Gull, T. R., Maran, S. P., Aller, L. H., Keyes, C. D., Michalitsianos, A. G., & Stecher, T. P., 1986, In: *'New Insights into Astrophysics' Proc. Joint NASA/ESA/SERC Conference,* ESA SP-263.

Harman, R. J., & Seaton, M. J., 1966, *Mon. Not. R. astr. Soc.*, **132**, 15.

Hawley, S. A., & Miller, J. S., 1977, *Astrophys. J.*, **212**, 94.

Heap, S. R., 1982, In: *Proc. IAU Symp. 99, p 423,* ed. De Loore, C. W. H., & Willis, A. J., A. J., D. Reidel, Dordrecht, Holland.

Henize, K. G., 1956, *Astrophys. J. Suppl.*, **2**, 315.

Henize, K. G., & Westerlund, B. E., 1963, *Astrophys. J.*, **137**, 747.

Hindman, J. V., 1967, *Aust. J. Phys*, **20**, 147.

Howarth, I. D., 1983, *Mon. Not. R. astr. Soc.*, **203**, 301.

Howarth, I. D., & Maslen, D., 1984, *Starlink User Note,* No. 50.

Hummer, D. G., & Seaton, M. J., 1963, *Mon. Not. R. astr. Soc.*, **125**, 437.

Hummer, D. G., & Seaton, M. J., 1964, *Mon. Not. R. astr. Soc.*, **127**, 217.

Iben, I., Jr., 1984, In: *Proc. IAU Symp. 105, p 3,* ed Maeder, A., & Renzini, A., D. Reidel, Dordrecht, Holland.

Iben, I. Jr., & Renzini, A., 1983, *Ann. Rev. Astron. Astrophys.*, **21**, 271.

Jacoby, G. H., 1980, *Astrophys. J. Suppl.*, **42**, 1.

Koornneef, J., 1982, *Astr. Astrophys.*, **107**, 247.

Kaler, J. B., 1978, *Astrophys. J.*, **226**, 947.

Kaler, J. B., 1985, *Ann. Rev. Astr. Astrophys.*, **23**, 89.

Koelbloed, D., 1956, *Observatory* , **76**, 894.

Krueger, T. K., & Czyzak S. J., 1970, *Proc. R. Soc. Lon. A*, **318**, 531.

Kunth, D. 1982, *Ph.D. Thesis,* Universitiè Paris VII.

Kunth, D., & Sargent, W. L. W., 1983, *Astrophys. J.*, **273**, 81.

Kurucz, R. L., 1979, *Astrophys. J. Suppl.*, **40**, 1.

Lequeux, J., Peimbert, M., Rayo, J. F., Serrano, A., & Torres-Peimbert, S., 1979, *Astr. Astrophys.*, **80**, 155.

Lindsay, E. M., 1955, *Mon. Not. R. astr. Soc.*, **115**, 248.

Lindsay, E. M., 1956, *Mon. Not. R. astr. Soc.*, **116**, 649.

Lindsay, E. M., 1961, *Astrophys. J.*, **66**, 169.

Lindsay, E. M., & Mullan, D. J., 1963, *Irish A. J.*, **6**, 51.

De Loore, C. W. H., & Willis, A. J., 1982, *Proc. IAU Symp. 99,* Publ. D. Reidel, Dortrecht, Holland.

Maran, S. P., Aller, L. H., Gull, T. R., & Stecher, T. P., 1982, *Astrophys. J. Lett.*, **253**, L43.

Mathewson, D. S., Ford, V. L., & Visvanathan, N., 1986, *Astrophys. J.*, **301**, 664.

Mathis, J. S., Rumpl, W., & Nordsieck, K. H., 1977, *Astrophys. J.*, **217**, 425.

Mendoza, C., 1983, In: *Proc. IAU Symp. 103, p 233,* ed. Flower, D., D. Reidel, Dordrecht, Holland.

Mendoza, C., & Zeippen, C. J., 1982, *Mon. Not. R. astr. Soc.*, **198**, 127.

Mendoza, C., & Zeippen, C. J., 1983, *Mon. Not. R. astr. Soc.*, **202**, 981.

Merrill, P. W., 1932, *Publs. astr. Soc. Pacif.*, **44**, 123.

Morgan, D. H., 1984, *Mon. Not. R. astr. Soc.*, **208**, 633.

Nandy K., 1984, In: *Proc. IAU Symp. 108, p 341,* ed. van der Bergh, S., & de Boer, K. S., D. Reidel, Dordrecht, Holland.

Nandy, K., Morgan, D. H., & Willis, A. J., 1986, In: *'New Insights into Astrophysics' Proc. Joint NASA/ESA/SERC Conference,* ESA SP-263.

Natta, A., & Panagia, N., 1980, *Astrophys. J.*, **242**, 596.

Nussbaumer, H., & Rusca, C., 1979, *Astr. Astrophys.*, **72**, 129.

Nussbaumer, H., & Storey, P. J., 1981, *Astr. Astrophys.*, **99**, 177.

Oke, J. B., 1974, *Astrophys. J. Suppl.*, **27**, 21.

Osmer, P. S., 1976, *Astrophys. J.*, **203**, 352.

Osterbrock, D. E., 1974, *'Atrophysics of Gaseous Nebulae'*, publ. by W. H. Freeman. & Co.

Pagel, B. E. J., 1982, *Phil. Trans. R. Soc. Lond. A*, **307**, 19.

Pagel, B. E. J., Terlevich, R. J., & Melnick, J., 1986, *Publs. astr. Soc. Pacif.* In Press.

Paczyński, B., 1971, *Acta. Astr.*, **21**, 417.

Paczyński, B., 1975, *Astrophys. J.*, **202**, 558.

Peimbert, M., 1978, In: *Proc. IAU Symp. 76, p 215,* ed. Terzian, Y., D. Reidel, Dordrecht, Holland.

Peimbert, M., 1983. In: *Proc. of the ESO Workshop on 'Primordial Helium'*, P. 267.

Peimbert, M., & Torres-Peimbert, S., 1971, *Astrophys. J.*, **168**, 413.

Peimbert, M., & Torres-Peimbert, S., 1983. In: *Proc. IAU Symp. 103, p 233.* ed. Flower, D., D. Reidel, Dordrecht, Holland.

Peimbert, M., Torres-Peimbert, S., & Rayo, J. F., 1978, *Astrophys. J.*, **220**, 516.

Pottasch, S. R., 1983, In: *Proc. IAU Symp. 103, p 391,* ed. Flower, D., D. Reidel, Dordrecht, Holland.

Pradhan, A. K., 1976, *Mon. Not. R. astr. Soc.*, **177**, 31.

Reid, I. N., & Strugnell, P. R., 1986, *Mon. Not. R. astr. Soc.*, **221**, 887.

Renzini, A., 1982, In: *Proc. IAU Symp. 99, p 413,* ed. De Loore, C. W. H., & Willis, A. J., A. J., D. Reidel, Dordrecht, Holland.

Renzini, A., & Voli, M., 1981, *Astr. Astrophys.*, **94**, 175.

Robinson, R. D., 1985, *'The RGO Spectrograph'*, Publ. Anglo-Australian Observatory.

Robinson, L. B., & Wampler, E. J., 1972, *Publ. astr. Soc. Pacific*, **84**, 161.

Rohlfs, K., Kreitschmann, J., Siegman, B. C., & Feitzinger, J. V., 1984, *Astr. Astrophys.*, **137**, 343.

Sanduleak, N., 1984, In: *Proc. IAU Symp. 108, p 341,* ed. van der Bergh, S., & de Boer, K. S., D. Reidel, Dordrecht, Holland.

Sanduleak, N., & Davis-Philip, A. G., 1977, *Publs. astr. Soc. Pacif.*, **89**, 792.

Sanduleak, N., MacConnell, D. J., & Hoover, P. S., 1972, *Nature*, **237**, 28.

Sanduleak, N., MacConnell, D. J., & Davis Philip, A. G., 1978, *Publ. astr. Soc. Pacific*, **90**, 621.

Sanduleak, N., Pesch, P., 1981, *Publs. astr. Soc. Pacif.*, **93**, 431.

Sanduleak, N. & Stephenson, C. B., 1972, *Astrophys. J.*, **178**, 183.

Schönberner, D., 1979, *Astr. Astrophys.*, **79**, 108.

Schönberner, D., 1981, *Astr. Astrophys.*, **103**, 119.

Schönberner, D., 1983, *Astrophys. J.*, **272**, 708.

Searle, L., & Sargent, W. L. W., 1972, *Astrophys. J.*, **173**, 25.

Seaton, M. J., 1975, *Mon. Not. R. astr. Soc.*, **170**, 475.

Seaton, M. J., 1979, *Mon. Not. R. astr. Soc.*, **187**, 785.

Shaver, P. A., McGee, M. X., Newton, L. M., Danks, A. C., & Pottasch, S. R., 1983, *Mon. Not. R. astr. Soc.*, **204**, 53.

Straede, J., 1980, *A.A.O. Preprint,* No. 135.

Smith, M. J., & Weedman, D. W., 1972, *Astrophys. J.*, **177**, 595.

Stecher, T. P., Maran, S. P., Gull, T. E., Aller, L. H., & Savedoff, M. P., 1982, *Astrophys. J. Lett.*, **262**, L41.

Torres, A. N. 1985, *Ph.D. Thesis,* University of Colorado, JILA.

Torres, A. N., Conti, P. S., & Massey, P., 1986, *Astrophys. J.*, **300**, 379.

Torres-Peimbert, S., & Peimbert, M., 1977, *Rev. Mexicana. Astron. Astrof.*, **2**, 181.

Torres-Peimbert, S., Rayo, J. F., Peimbert, M., 1981, *Rev. Mexicana Astron. Astrof.*, **6**, 315.

Tüg, H., White, N. M., & Lockwood, G. W., 1977, *Astr. Astrophys.*, **61**, 679.

Webster, B. E., 1969 a, *Mon. Not. R. astr. Soc.*, **143**, 79.

Webster, B. E., 1969 b, *Mon. Not. R. astr. Soc.*, **143**, 97.

Webster, B. E., 1969 c, *Mon. Not. R. astr. Soc.*, **143**, 113.

Webster, B. E., 1976, *Publ. astr. Soc. Pacific*, **88**, 669.

Webster, B. E., 1978, In: *Proc. IAU Symp. 76, p 215,* ed. Terzian, Y., D. Reidel, Dordrecht, Holland.

Webster, B. E., 1983, *Publ. astr. Soc. Pacific*, **95**, 610.

Westerlund, B. E., & Henize, K. G., 1972, *Astrophys. J. Suppl.*, **14**, 154.

Westerlund, B. E., & Smith, L. F., 1964, *Mon. Not. R. astr. Soc.*, **127**, 449.

Wood, P. R., Bessell, M. S., & Fox, M. W., 1983, *Astrophys. J.*, **272**, 99.

Yang, J., Turner, M. S., Steignman, G., Schramm, D. N., & Olive, K. A., 1984, *Astrophys. J.*, **281**, 493.

Zanstra, H., 1927, *Astrophys. J.*, **65**, 50.

Zeippen, C. 1982, *Mon. Not. R. astr. Soc.*, **198**, 111.